ABSTRACT

Title of Document:	Development of food polymer-based colloidal delivery systems for nutraceuticals
	Yangchao Luo, Doctor of Philosophy, 2012
Directed By:	Assistant Professor Qin Wang Department of Nutrition and Food Science

Colloidal delivery systems have drawn increasing attention in food science area. Biopolymers, i.e. proteins and polysaccharides originated from foods, with low toxicity, high biocompatibility and biodegradability, are the ideal biomaterials to develop delivery systems for nutraceuticals. The present work is dedicated to develop delivery systems for nutraceuticals, using food derived biopolymers, e.g. chitosan and zein. In the first part of this study, different core-shell structured nanoparticles were developed for encapsulating both hydrophilic and hydrophobic nutracetuicals. For chitosan nanoparticles with zein coating, the hydrophilic nutraceutical, selenite, was encapsulated and the physicochemical properties was improved after zein coating. Then, zein nanoparticles with chitosan (CS) or carboxymethyl chitosan (CMCS) coating were developed to encapsulate hydrophobic nutraceuticals, including vitamin E, vitamin D3, indole-3-carbinol and diindolylmethane. The fabrication parameters were systematically studied and the effects of encapsulation on stabilities of nutraceuticals were investigated under different conditions.

Subsequently, a novel approach to prepare CMCS hydrogel beads was developed. CMCS, a water-soluble derivative of CS, was known as unable to form hydrogel beads by itself in aqueous solution due to chain rigidity and inefficient entanglement. In this part, the formation of CMCS hydrogel beads was studied in aqueous-alcohol binary solutions. Chemical crosslinking was required to maintain its integrity upon drying. Different drying methods (i.e. freeze and air drying) were also investigated to understand their effects on swelling and release profile in simulated gastrointestinal conditions. Some possible mechanisms were discussed.

Lastly, cellular evaluation of zein nanoparticles stabilized by caseinate was carried out. The zein-caseinate nanoparticles had a good redispersibility after freeze-drying and were able to maintain original particle size in different cell culture medium and buffer at 37°C over time. The zein-caseinate nanoparticles had no cytotoxicity at concentrations up to 1 mg/ml over 3 days. Then, coumarin 6, a fluorescent marker, was encapsulated into zein-caseinate nanoparticles to investigate their cell uptake and epithelial transport. The cell uptake was clearly visualized by fluorescent microscopy and the uptake mechanisms were investigated. The epithelial transport was investigated on Caco-2 cell monolayers. The results suggested caseinate not only stabilized zein nanoparticles in different buffers, but also improved cell uptake and epithelial transport.

DEVELOPMENT OF FOOD POLYMER-BASED COLLOIDAL DELIVERY SYSTEMS FOR NUTRACEUTICALS

By

YANGCHAO LUO

Dissertation submitted to the Faculty of the Graduate School of the
University of Maryland, College Park, in partial fulfillment
of the requirements for the degree of
Doctor of Philosophy
2012

Advisory Committee:
Professor Qin Wang, Chair
Professor Liangli (Lucy) Yu
Professor David Lei
Professor Srinivasa Raghavan
Professor Jiuzhou Son

Acknowledgements

While this is the last part of my dissertation writing, I deem it the most important part. My Ph.D. study in Department of Nutrition and Food Science at University of Maryland has been an unforgettable period in my life. Without unending help and support from countless individuals, I cannot succeed or even survive during my pursuit of Ph.D. degree.

It is with immense gratitude that I acknowledge the help and support from my advisor, Dr. Qin Wang. She has not only been a great mentor, but also a good friend, who made my graduate life a thoughtful and rewarding journey. Her tremendous knowledge, creative research ideas, and insightful thought have been inspiring and driving me to explore the world of science. Especially, during all these years, I have been appreciating her help and support to accept both me and my wife as her graduate students.

I am also debited to my dissertation committee members, Drs Liangli (Lucy) Yu, David Lei, Srinivasa Raghavan, and Jiuzhou Song. I sincerely appreciate their time and effort in helping me throughout my research. Their support and guidance have been pivotal in shaping this work.

I would also like to thank my labmates, without whom my success could not be possible. I am grateful to each of them: Dr. Boce Zhang, Zi Teng, Yunpeng Wu, and Zhenlei Xiao. They are the people who are nearby whenever I need help. I have been benefiting from them through the thought-provoking discussions during my

experiments and data analysis, as well as constructive comments during my manuscript writing, submission, and publication.

I owe my deepest gratitude to my family for the unselfish and endless love and support during my Ph.D. study at graduate school. I am particularly thankful to my dear wife, Zhenlei Xiao, for her belief and trust in me. I deeply thank my wife for her sacrifice and company with me when I had the dream to pursue my Ph.D. degree in United States three and half years ago. Without her care and belief, it is impossible for me to finish my Ph.D. study in United States. Today, I am even proud of her for the accomplishments and excellences in her research! Also, I am forever in awe of the sacrifices my parents have made to provide me a life that includes more than a decade of higher education.

Last but not least, I also appreciate the entire University of Maryland community for providing such a good academic environment. I sincerely thank graduate school for encouraging and supporting my academic endeavors with great enthusiasm and generosity through Flagship Fellowship program.

Table of Contents

List of Tables

List of Figures

Chapter 1: Literature Review

1.1 Overview of Encapsulation Technology

Encapsulation technology is an emerging technology developed in recent decades. It may be defined as the process to entrap one or several substance within a certain matrix. The substance encapsulated in the matrix is defined as core materials, which could be drug, nutraceuticals, or any bioactive compounds. The matrix is named wall or shell materials, which are usually large molecules, such as polymers. Encapsulation technology has been applied in pharmaceutical and cosmetic industry for decades and become a popular approach in food industry in recent years for improving stability of labile nutraceuticals and flavors and enhancing delivery bioactive compounds. In the majority of cases, encapsulation technology has been studied extensively to package solids, liquids, or gaseous materials in small capsules that are expected to be released at controlled rates over prolonged periods and under specific conditions (Desai & Park, 2005).

Various materials have been studied to fabricate the matrix or shell of these particles, including natural and synthetic polymers. Different from pharmaceutical or cosmetic industry where synthetic materials have been extensively investigated to fabricate nano- or micro-particles to encapsulate drugs, materials used in food industry are more concerned to be natural, edible and non-toxic. The ideal materials used in food industry are biopolymers, especially those originated from foods, such as food proteins and polysaccharides. Meanwhile, the fabrication process of encapsulation applicable to food industry must also be safe and green, without any toxic reagents or intensive conditions as possible. When it comes to food industry, there are bunch of benefits brought by encapsulation technology, and several groups of compounds have already been studied using this novel technology, such as natural ingredients, volatile additives, labile bioactives, polyphenols, enzymes, as well as bacterial in

small capsule. The function of encapsulation include improving their stabilities during long storage periods, protecting nutritional loss during extreme processing environments, and preserving their functionalilities in digestive conditions.

However, we are still facing a lot of problems with encapsulation technology in food industry, such as insufficient protection of nutraceuticals from degrading due to exposure of light, oxygen and heat, fast isomerization of consumed nutrients in gastric fluid, ineffective absorption and delivery of consumed bioactives after encapsulation. Therefore, two or more materials are being explored as a combination to encapsulate substances in recent years. More and more attention has been drawn to use those biopolymer complexes of food proteins and polysaccharides as wall materials to encapsulate nutrients (Cooper, Dubin, Kayitmazer, & Turksen, 2005).

1.2 Food Polymer-Based Nanoparticles for Encapsulation of Nutraceuticals

Nanotechnology is an enabling technology that offers the great potential to revolutionize agricultural and food systems. Due to the unique characteristics of nano-scale materials (10^{-9} m), it provides numerous benefits to food and nutrition applications, such as faster intestinal absorption after oral administration, higher cellular uptake, desired delivery of nutraceuticals to specific site, and maximized in vivo effect. After the first feature research paper in Food Nanotechnology was published in 2003 (Moraru, Panchapakesan, Huang, Takhistov, Liu, & Kokini, 2003), the growing of research interests on this novel area has never ended. As more and more concern is drawn to the application of nanotechnology in food systems, biopolymers have been the most investigated materials used for food nanotechnologies. Because biopolymers are derived from living organisms, especially from edible plants and animals, they are biocompatible, biodegradable, and non-toxic by oral consumption. Proteins and polysaccharides are two large categories of biopolymers with food

origins. Both food protein and polysaccharide have high nutritional value and are generally recognized as safe (GRAS).

In general, protein has various functional groups in the primary sequences of polypeptides and the diverse chain folding structures, and therefore they are able to interact with nutraceutical compounds and encapsulate and protect them. Various food proteins have been studied as wall materials for nutraceuticals delivery systems, including zein, whey protein, egg white, ß-lactoglobulin, gelatin, collagen, casein, albumin, soy glycinin (Chen, Remondetto, & Subirade, 2006). Different methods have been developed to produce micro/nano-particles, films, fibers, and hydrogels based on the properties of protein used. For globular water-soluble protein, thermal treatments, including heat- and cooling- induced gelation, are popular approaches to obtain protein hydrogels. In some cases, ions (Ca^{2+}) are added to the protein suspension to form hydrogel through electrostatic interaction with carboxyl groups on protein molecules. For the water-insoluble protein, such as corn zein and wheat gliadin, phase separation is a unique technique to produce nanoparticles. Due to the simplicity and low cost of phase separation method, water-insoluble food proteins have been attracted much attention in recent years to fabricate nanoparticles. The hydrophobic cores of these proteins could act as reservoirs or microcontainers for various bioactive substances. Therefore, hydrophobic proteins, especially zein, are specifically used to encapsulate lipophilic nutraceuticals due to the strong driving force of hydrophobic interaction between nutraceutical and protein molecules.

Polysaccharides are the polymers of monosaccharides and they are stable, abundant and non-toxic in nature. Among food polysaccharides, there are usually two subgroups: polyelectrolytes and non-polyelectrolytes. Polyelectrolytes are of greater interests because there are charges on their surface, resulting in some unique properties; they can be further divided into positively charged polysaccharides (e.g. chitosan) and negatively charged

polysaccharides (e.g. alginate, hyaluronic acid, pectin, etc). Due to various derivable functional groups on their molecular chains, they can be easily modified to produce various derivatives with desirable properties. In addition, most of them have amino and carboxyl groups which are ready to interact with biological tissues, e.g. mainly epithelia and mucous membrane, to enhance intestinal absorption of nutraceuticals encapsulated (Liu, Jiao, Wang, Zhou, & Zhang, 2008). These properties make food polysaccharides promising biopolymers to prepare nanoparticles as delivery systems of nutraceuticals, without issues of safety, toxicity and availability. In recent years, numerous studies have been conducted on food polysaccharides, especially polyelectrolytes, due to the simplicity of nanoparticles fabrication via electrostatic interaction.

1.3 Chitosan (CS) and its Derivatives

1.3.1 Chitin and CS

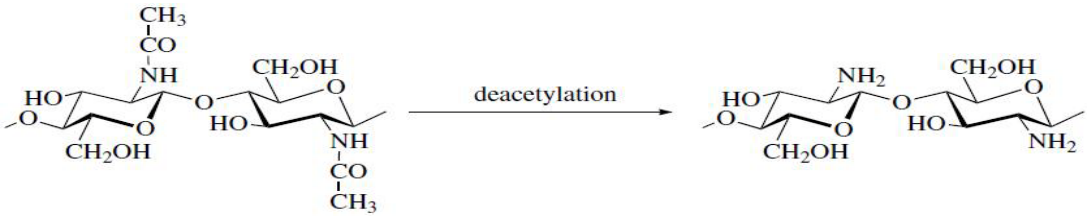

Fig. 1.1. Preparation of chitosan from chitin by deacetylation process (Il'ina & Varlamov, 2005).

Chitin, as a natural polysaccharide, is mostly found in the exoskeleton of crustaceans, insects, and fungi. It is ubiquitous in nature, being the second most abundant biopolymer, next to cellulose. Chitosan (CS), the N-deacetylation product of chitin, is a linear polysaccharide, composed of glucosamine and N-acteyl glucosamine units via ß(1-4) linkage, randomly or block distributed throughout the biopolymer chain, depending on the preparation method to derive CS from chitin (**Fig. 1.1**). The deacetylation degree is defined as the ratio of glucosamine to N-acetyl glucosamine, an important parameter determining its properties and

applications. After deacetylation process, CS could be dissolved in acidic medium and become the only polysaccharide in nature that possesses high density of positive surface charge, due to the protanation of amino groups on its backbone. Besides this unique characteristic, CS has been proved to have many other intrinsic properties, such as non-toxicity, biocompatibility and biodegradability (Kean & Thanou, 2010). Therefore, CS has been received significant scientific interests and become one of the hottest topics in this decade, especially for its medical and pharmaceutical applications, including drug delivery (Bhattarai, Gunn & Zhang, 2010; Hejazi & Amiji, 2003) and tissue engineering (Di Martino, Sittinger, & Risbud, 2005; Thein-Han, Kitiyanant, & Misra, 2008).

1.3.2 CS Applications in Food Science

CS has been widely used as a food additive in Japan and Korea since 1983 and 1995, respectively (KFDA, 1995; Weiner, 1992). The biological safety data were firstly established in 1990 using animal trials (Hirano, Itakura, Seino, Akiyama, Nonaka, Kanbara, et al., 1990). Since then numerous studies have been conducted to explore CS applications in food industry, and various functional properties of CS have been discovered. In 2005, the US FDA approved a shrimp-derived CS as a GRAS (generally recognized as safe) for its general applications in food industry.

1.3.2.1 Antimicrobial Activity and Film Forming Property

The antimicrobial activity of CS has been attracted notable attention as a potent food preservative of natural origin. CS has been proved to be a wide-spectrum antimicrobial, including foodborne filamentous fungi, yeast, and bacteria (Rabea, Badawy, Stevens, Smagghe, & Steurbaut, 2003). Recently, edible coating on fresh-produce or minimally processed fruits is a hot topic in food industry and CS is one of the popular biopolymers that have been extensively studied in this area, thanks to its excellent capability to form biodegradable film (Valencia-Chamorro, Palou, del Río, & Pérez-Gago, 2011). For instance,

a recent study reveals that CS coating on fresh-cut strawberries can significantly improve shelf life and product quality by providing excellent inhibitory effect on the growth of microorganisms during storage under different temperatures (Campaniello, Bevilacqua, Sinigaglia, & Corbo, 2008). The combination of CS and other antimicrobial agent is a novel approach to maximize the antimicrobial effects and quality improvement. The CS coating enriched with thyme oil on mushrooms showed a better efficacy than thyme oil or CS coating itself, in terms of maintaining postharvest quality and extending shelf life by inhibiting microorganism growth (Jiang, Feng, & Zheng, 2011). The combination of CS and sodium chlorite coating on fresh-cut pears also exhibited enhanced antimicrobial effects (Xiao, Luo, & Wang, 2011). CS film incorporating with green tea extract has been recently demonstrated to not only inhibit microbial growth, reduce lipid oxidation, but also improve the qualities and prolong shelf life of refrigerator stored pork sausages (Siripatrawan & Noipha, 2012).

The antimicrobial efficacy of CS, however, varies with the species of microbial as well as the types of foods. For instance, Simpson and co-workers reported that the different cultures of bacteria had significant different susceptibilities to CS, e.g. CS bactericidal concentration of 0.02% for Bacillus cereus, 0.0075% for *Escherichia coli* and *Proteus vulgaris* (Simpson, Gagne, Ashie, & Noroozi, 1997). Some other studies also suggested different efficacy of CS to *B. cereus* (Chang, Cho, Gao, & Choe, 1989). The discrepancy in studies may be partly due to the reason that a lot of factors may affect CS antimicrobial effects. One of the major mechanisms of antimicrobial activity of CS is that the positive surface charge of CS molecules can interact with negatively charged microbial cell membranes, resulting in the leakage of proteinaceous and other intracellular constituents (No, Meyers, Prinyawiwatkul, & Xu, 2007). The molecular weight and deacetylation degree of CS may significantly affect its surface charge density, which will in turn influence its antimicrobial activity remarkably (Zheng & Zhu, 2003). Another possible reason is that

different foods contains different compositions, such as the salt concentration, pH, textures, etc., all of which will determine the protonation of CS molecules. Last but not least, the technique used to test antimicrobial activity may also contribute to large variations of the biocide properties of CS (Fernandez-Saiz, Lagaron, & Ocio, 2009).

1.3.2.2 Food Emulsion Stabilizer and Quality Enhancer

CS, as a food polysaccharide, is a well-known amphiphilic polyelectrolyte and thus possesses both the electrosteric and stabilizing properties. CS has been widely used to stabilize and improve overall quality of mutilple-layer emulsions. Both of the molecular weight and decacetylation degree will influence the particle size and stability of CS-stabilized emulsions. The higher molecular weight and lower decacetylation degree produced more stable emulsion with smaller particle size (Mun, Decker, & McClements, 2006). Recently, maillard reaction is applied to conjugate CS and other polymers in order to produce the complex emulsifier with better properties, since the reaction may bring the products with combined beneficial properties with two or more biopolymers. The maillard production of lactoglobulin and CS exhibited enhanced bactericidal activity against E. coli than their individual effects (Mun, Decker, & McClements, 2006). The CS-glucose maillard product has been recently developed using gamma radiation method, to improve the rheological properties and enhance the stability of β-carotenen against oxidation during storage (Rao, Chawla, Chander, & Sharma, 2011).

1.3.2.3 Nutritional Properties and Biological Activities

In addition to the applications of CS as food additives and stabilizers, considerable attention has also been attracted by its nutritional properties and biological activities, namely, hypocholesterolemic, immunity-enhancing, anticancer effects, accelerating mineral absorption, etc. (Xia, Liu, Zhang, & Chen, 2011). Similar as physicochemical properties of CS, both decacetylation degree and molecular weight play important roles in its biological

activities. However, the majority studies of nutritional properties of CS are focused on low molecular weight CS, which is proven to be more effective using in vivo animal models than high molecular weight CS. For instance, the CS with low molecular weight has shown significantly better hypolipidemic activity in rats through increasing serum and liver lipoprotein lipase activity, than the CS with high molecular weight (Zhang, Zhang, Mamadouba, & Xia, 2012). CS not only improve lipid metabolism but also helps with kidney functions. A new study reported that the oral administration of low molecular weight CS to mice can effectively reverse aristolochic acid-induced renal lesions by suppressing the elevation of urinary and blood nitrogen concentration (Chang, Chang, Huang, Chen, Lee, & Chung, 2011). The CS oligosaccharides have also been shown to exhibit excellent therapeutic effects against mase cell-mediated allergic inflammatory responses and airway inflammation in allergic inflammatory diseases, including asthma (Chung, Park, & Park, 2012).

1.3.3 Applications of CS Particulate Systems in Nutraceutical Delivery

Due to the unique physicochemeical properties of CS, including mucoadhesive, positive surface charge, low toxicity, biodegradable, etc., it has been extensively studied for encapsulation and delivery of drug/nutraceuticals in various fields. Many types of delivery systems can be easily developed from CS by various methods, such as tables, nano/micro particles, hydrogels, beads, emulsions, and films. Some of the popular types of CS-based particulate delivery systems widely used in food science field are discussed below.

1.3.3.1 Nano- / Micro- Particles of CS

Many reports are available on the fabrication and evaluation of CS particulate delivery systems. The particles are simply prepared via electrostatic interactions between positively charged CS and negative charged molecules. The negatively charged polyelectrolytes can be small molecules, such as sodium tripolyphosphate, and macromolecules, such as polysaccharides and proteins. Generally, ionic gelation of CS

nanoparticles offers simple and mild preparation conditions as well clear processing window for manipulation of physicochemical properties of the nanoparticles, such as size and surface charge (Gan & Wang, 2007). Because of these beneficial characteristics, increasing attention has been drawn to the applications of CS-based micro and nanoparticles in the pharmaceutical and nutraceutical fields (Grenha, Seijo, & Remuñán-López, 2005; Kockisch, Rees, Young, Tsibouklis, & Smart, 2003; Shah, Pal, Kaushik, & Devi, 2009). Among various polyanions, tripolyphosphate (TPP) is the most investigated one due to its quick gelling capability and non-toxic property. CS/TPP nanoparticles have been proved to be excellent carriers for drug and nutrient in therapeutic and nutritional applications, such as providing efficient and target delivery of shRNA sequence (Wang, Yao, Guo, Dong, Li, Gu, et al., 2009), lowering toxicity of therapeutic antisense oligonucleiotide (Dung, Lee, Han, Kim, Ju, Kim, et al., 2007), increasing bioavailability of nutraceuticals (Dudhani & Kosaraju, 2010; Hu, Pan, Sun, Hou, Ye, & Zeng, 2008; Zhang, Yang, Tang, Hu, & Zou, 2008), as well as achieving long term controlled release of protein, e.g., bovine serum albumin (Gan & Wang, 2007) and unstable drugs, e.g., venlafaxin hydrochloride (Shah, Pal, Kaushik, & Devi, 2009).

In addition to small anionic molecules, CS can form nano/microparticles with macromolecules which carry negative surface charges, including both natural and synthetic polymers (Hamman, 2010). The particles formed with macromolecules are generally defined as polyelectrolyte complexes (PECs). Among the natural polymers that can form PECs with CS, alginate, carrageenan, pectin, and hyaluronic acid are the most investigated ones. Generally speaking, the PECs demonstrated some superior properties over the particles formed by CS and small molecules.

1.3.3.3 CS Hydrogel Beads

Hydrogels are the crosslinked polymer networks that hold a large amount of water. The polymers used to prepare hydrogels normally consist of a large portion of hydrophilic

groups and the formed networks are prevented from dissolving due to the chemical or physical bonds between the polymer chains. Water can penetrate into the networks, resulting in the swelling of the hydrogels. Based on different fabrication parameters, the dimensions of hydrogels can vary widely, from nanometer to centimeters in width. The CS hydrogels are prepared with various approaches to produce different shapes, geometries, including liquid gels, films, capsules, sponges, microparticles, composites, beads, etc. The hydrogels discussed in this study are the hydrogel beads, whose dimension are generally from hundreds of micrometers to several millimeters. Compared to other delivery systems, hydrogel beads have some unique features depending on the polymer used, including slow release profile due to physical or chemical crosslinking, enhanced drug residence time and tissue permeability, mucoadhesive characteristics, survival against gastrointestinal tract and colon delivery, etc (Bhattarai, Gunn, & Zhang, 2010). Further, for food industry, hydrogel beads may be more feasible to achieve and industrialize, due to the low cost and controllable preparation parameters, and scalable procedures, compared with nano/microparticles delivery systems in food industry.

The crosslinking approaches are normally adopted to prepare CS hydrogel beads, physical crosslinking via ionic gelation with anionic molecules, and irreversible chemical crosslinking. While physical crosslinking is more preferred due to low toxicity and higher biocompatibility, it has certain limitations, such as hard to control pore size, fast degradation or dissolution, quick release of encapsulated nutraceuticals, compared with chemical crosslinking. Both approaches have been extensively studied for their drug delivery applications in food and/or pharmaceutical areas in recent decades.

For instance, CS hydrogel beads by physically crosslinked with TPP was developed as a pH-sensitive drug release system to encapsulate glipizide, an insulin stimulating drug. The hydrogel beads were proposed to release the encapsulated drug slowly upon

subcutaneous injection, with good tolerability and prolonged half life (Sun, Li, Li, Wei, & Tian, 2011). Many other drugs/nutraceuticals were also encapsulated into CS-based pH-sensitive hydrogel beads for oral or injection delivery recently (Dai, Li, Zhang, Wang, & Wei, 2008; Elzatahry, Eldin, Soliman, & Hassan, 2009; Meng, Li, Wei, & Zhang, 2011; J. Yang, Chen, Pan, Wan, & Wang, 2012). In food science area, another major application of CS-based hydrogel beads is the enzyme immobilizations for various applications. During last decade, numerous CS-based hydrogel beads have been developed to immobilize hundreds of enzymes for multiple applications in food and agricultural industries, such as organic compounds removal from wastewaters, measurement of environmental pollutants, metabolite control, and so on (Krajewska, 2004).

1.3.4 Carboxylmethyl Chitosan (CMCS) and its Application in Drug Delivery

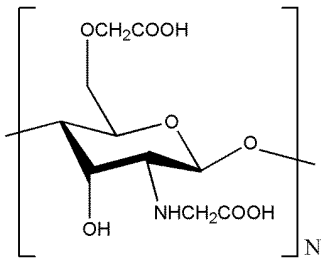

Fig. 1.2 Molecular structure of carboxymethyl chitosan (CMCS)

In addition to native CS, its derivatives have also been extensively studied in drug delivery. The presence of functional groups, such as $–NH_2$ group at the C-2 position or –OH groups at C-3 and C-6 positions, offers great opportunities for chemical modification, leading to various applications that native CS cannot achieve. CS derivatives include quaternized CS, carboxyalkyl CS, thiolated CS, sugar-bearing CS, cyclodextrin-linked CS, etc. The chemical modifications of CS are designed to provide specific properties to improve its special applications. Carboxylmethyl CS (CMCS, **Fig. 1.2**) is one of the most investigated derivatives to improve CS solubility in neutral pH, and it is widely used for biomedical

applications, including wound dressings, artificial bone and skin, bacteriostatic agents and blood anticoagulants (Sahoo, Sahoo, Mohanty, Sasmal, & Nayak, 2009). It is soluble in neutral aqueous solution, and it has been shown that negatively charged CMCS is able to form nanoparticles spontaneously with positively charged ions (Shi, Du, Yang, Zhang, & Sun, 2006). Several bioactive compounds have already been successfully encapsulated into CMCS nanoparticles to achieve controlled release and target delivery properties (Anitha, Maya, Deepa, Chennazhi, Nair, Tamura, et al., 2011; Kim, Jeong, Choi, Roh, Kang, Jang, et al., 2006). CMCS has also been modified by cholesterol to form self-assembled nanoparticles able to deliver anticancer drugs with higher targeting efficiency and longer retention time in the liver than those of pure drug solution (Wang, Jiang, Li, Liu, Zhang, & Zhao, 2008). In addition, it is newly elucidated that negatively charged CMCS nanoparticles with particle size around 150 nm had a better in vitro cellular uptake and more efficient in vivo targeting delivery of entrapped drug to tumor (He, Hu, Yin, Tang, & Yin, 2010).

1.4 Zein

1.4.1 Introduction of Zein

Zein is a maize prolamine protein with three-fourths lipophilic and one-fourth hydrophilic amino acid residues, leading to its unique aqueous-alcohol solubility and film forming properties. Due to the poor solubility in water and the imbalanced essential amino acid profile, zein isolate is not used directly for human consumption. Since 1990s, a lot of research was focused on the extraction of zein from corn to lower the cost of manufacturing zein (Shukla & Cheryan, 2001). After the first U.S. patent of the application of zein for encapsulation was published in 1992, more interests have been gradually drawn to explore the novel applications of zein as a biodegradable biopolymer and many patents about the encapsulation technological application of zein have been published (Shukla & Cheryan,

2001). During last decade, more and more research interests have been focused on the applications of zein in food, pharmaceutical and biodegradable plastic industries (Anderson & Lamsal, 2011).

1.4.2 Zein Application for Encapsualtion of Nutraceuticals

1.4.2.1 Zein Nanoparticles: Preparation and Application

Liquid-liquid phase separation is the widely used method to produce zein nano/micro particles, due to the unique solubility of zein. So far, several methodologies were developed by different researchers. In a simple method, zein microspheres and the hydrophobic drugs were first dissolved in aqueous-alcohol solution together, then water was added into the zein solutions (Hurtado-López & Murdan, 2006; X. Liu, Sun, Wang, Zhang, & Wang, 2005). Upon the decrease of alcohol concentrations, the zein became not dissolvable and co-precipitated with the hydrophobic drug. Another approach was to shear zein aqueous-alcohol solution into a bulk water phase. This method has been used to produce zein nanoparticles to encapsulate essential oils (Parris, Cooke, & Hicks, 2005). A recent study reported the variables during the production of zein nanoparticles using this method (Zhong & Jin, 2009a). The report suggested that this method was simple and scalable for food industries, and the particle size and viscosity could be easily modulated by controlling fabrication parameters, such as shearing rate, alcohol and zein concentrations. The liquid-liquid phase separation method has been widely applied in recent years to encapsulate various nutraceuticals or drugs (Lai & Guo, 2011; Lau, Johnson, Mikkelsen, Halley, & Steadman, 2012; Podaralla & Perumal, 2010; Wu, Luo, & Wang, 2012; Zou, Li, Percival, Bonard, & Gu, 2011). While many literatures have been reported on the preparation and encapsulation of drugs or nutraceuticals of zein nanoparticles, so far, only a few literatures studied the bioavailability and efficacy of zein nanoparticles as delivery systems. Zein nanoparticles have been reported to accumulate in liver after intravenous injection to mice and prolong blood residence time of

5-fluorouracil (Lai & Guo, 2011). Another study showed that zein nanoparticles encapsulating cranberry procyanidins decreased the cytotoxicity compared to free cranberry procyanidins to human promyelocytic leukemia HL-60 cells, partly attributed to the encapsulation and controlled release properties (Zou, Li, Percival, Bonard, & Gu, 2011).

In addition to liquid-liquid phase separation method, spray drying was also developed to produce zein microparticles in recent years, especially for encapsulation of antimicrobials. For instance, it has been reported that lysozyme (Jin, Davidson, Zivanovic, & Zhong, 2009; Zhong & Jin, 2009b), flax oil (Quispe-Condori, Saldaña, & Temelli, 2011), nisin (Xiao & Zhong, 2011), and thymol (Xiao, Davidson, & Zhong, 2011) are successfully encapsulated into zein microparticles by spray drying. The release profiles of the antimicrobials from zein microparticles were significantly dependent on the preparation parameters, including the mass ratio of zein/antimicrobials, surfactant, inlet temperatures, as well as the pH value of the release medium. The antimicrobials-encapsulated zein microparticles by spray drying demonstrated better antilisterial properties than free antimicrials in fat milk, especially when glycerol was added as plasticizer during the preparation (Xiao, Davidson, & Zhong, 2011). However, more work needs to be done to further improve the antimicrobial efficacy and release profiles in various food systems.

1.4.2.2 Zein Fiber by Electrospinning

Electrospinning is novel method developed in recent years to prepare ultrathin fiber networks by using high electrostatic potentials from biomaterials. This process involves use of strong electrostatic field by high voltage to produce ultrathin fiber. Zein is becoming a popular protein to produce nanofibers by electrospinning during this decade, and fabrication variables during the electrospinning process have been extensively investigated and physicochemical properties of electrospun zein fiber have also been fully characterized in recent years (Miyoshi, Toyohara, & Minematsu, 2005; Neo, Ray, Easteal, Nikolaidis, & Quek,

2012; Torres-Giner, Gimenez, & Lagaron, 2008; Yao, Li, & Song, 2006). Jiang and Yang reported a new method to modify electrospun zein fiber by crosslinking with citric acid (Jiang & Yang, 2011). The crosslinking process could remarkably enhance its both dry and wet tensile strength, and the crosslinked zein fiber was able to maintain fibrous structure for 15 days in PBS at 37°C.

In recent years, the increasing attention has been drawn to the applications of zein electrospun fiber in encapsulation and controlled delivery, as well as stabilization sensitive antioxidants in food area. The light sensitive antioxidant, β-carotene has been successfully encapsulated into untrafine zein fiber by electrospinning (Fernandez, Torres-Giner, & Lagaron, 2009). The study demonstrated that the dimension of electrospun zein fiber was in the range of micro- and nanoscale in the cross-section. The β-carotene was shown to be stable and widely dispersed inside the zein fibers and its light stability was significantly improved when exposed to UV-vis irradiation, compared with unencapsulated β-carotene. Ultrafine zein fibers were also tested for encapsulation of green tea polyphenol, epigallocatechin gallate to improve its stability (Li, Lim, & Kakuda, 2009). The study suggested that aging at 0% relative humidity for at least 1 d was required for better protection and recovery of polyphenol, compared with freshly spun fibers. Many other nutrients were also encapsulated into electrospun zein fibers to improve their stabilities with controlled release (Neo, Ray, Jin, Gizdavic-Nikolaidis, Nieuwoudt, Liu, et al., 2012; Yang, Zha, Yu, & Liu, 2012).

1.4.2.3 Zein Film

Film forming properties of zein has been well documented since 1970s, and the coatings of zein films appear to be one of the most promising applications in industries, including food, pharmaceutics, and cosmetics (Shukla & Cheryan, 2001). The recent development of zein film applications have been further expanded into more areas in various

industries. Several most recent literatures on zein film application in food science areas are discussed below.

Food safety is one of the hottest areas of zein film applications, with aim to improve fresh produce, including minimally process and fresh-cut foods, and ready-to-eat foods which are the most susceptible of microbial contaminations. Several antimicrobials have been encapsulated into zein films for edible coating applications. For instance, Janes and others investigated the effect of nisin encapsulated in zein film coatings on ready-to-eat chicken against *L. monocytogenes* (Janes, Kooshesh, & Johnson, 2006). Their results showed that adding nisin into zein films coating significantly inhibited the growth of *L. monocytogenes* from day 0 to day 24 at 8°C, and even maintain its level as undetectable at 4°C. The mutilayers of zein-based films loaded with spelt bran and thymol has been recently developed as an effective packaging material to control the thymol release rate with sustained antimicrobial efficacy (Mastromatteo, Barbuzzi, Conte, & Del Nobile, 2009).

In addition to food safety, another top area of zein film applications is the food quality improvement, such as food packaging. Zein is considered as a novel biodegradable material for modified atmosphere packaging, but sometimes plasticization or modification may be needed to enhance its efficacy. The zein films plasticized with oleic acid have been shown to possess better water vapor and gas barrier propties, compared with untreated zein films (Rakotonirainy, Wang, & Padua, 2001). This modified zein films have been tested as modified atmosphere package for fresh broccoli florets to maintain their original firmness and color. Zein edible film is also reported as an effective coating to improve the quality of dried tomatoes to inhibit microbial growth and preserve original color (Baysal, Ersus, & Apaydın, 2009). The study demonstrated that addition of potassium sorbate into zein film coating could further decrease total aerobic mesophilic bacterial on tomatoes during the long term storage.

1.5 Biopolymer Complex in Encapsulation of Nutraceuticals

Several studies reported that encapsulation of nutraceuticals into the nanoparticles formed by single polymer (single layer) may not be effective to protect the encapsulated nutraceutical under simulated gastric fluid, because highly water-soluble proteins undergo quick degradation by enzymatic hydrolysis in stomach with presence of pepsin. In this scenario, many researchers began to coat the protein nanoparticles with a second polymer to form double layer. Therefore, more and more studies have been carried out to investigate the preparation, characterization, and application of micro-/nanocomplexes formed by two or more polymers (Berger, Reist, Mayer, Felt, Peppas, & Gurny, 2004; Wang & Uludag, 2008).

Polysaccharides are the popular candidates to coat protein nanoparticles, because protein and polysaccharide can be easily associated via physical interactions upon mixing together. The non-covalent interactions include electrostatic and hydrophobic interactions, steric exclusion, hydrogen bonding, etc. Due to the polysaccharide coatings on the protein, the digestive enzymes may need longer time to pass through polysaccharide coating and hydrolyze protein molecules, resulting in the retarded controlled release of encapsulated nutraceuticals in stomach. Furthermore, higher encapsulation efficiency could be achieved by the coating of polysaccharide on protein particles. For instance, several studies reported the coating of different polysaccharides, i.e. CS and alginate, on ß-lactoglobulin nanoparticles could signicantly improve physicochemical properties (Chen & Subirade, 2005; Somchue, Sermsri, Shiowatana, & Siripinyanond, 2009).

1.6 Call for Encapsulation of Nutraceuticals – Significance & Benefits

Nutraceuticals are the bioactive compounds from foods and provide health-promoting effects, including prevention and treatment against diseases. They may have different forms in the market, including pills, powders, capsules, vials, etc. However, the application of nutraceuticals as diet supplementation is restricted by their stability. During the

manufacturing or storage of the commercial products, nutraceuticals are often subjected to thermal, oxidative, acidic, basic, humidity, and light (both UV and visible) stress, resulting in degradation or iosermerization and thus loss their beneficiary efficacy. In addition to process and storage conditions, the food-related factors also demonstrated great impact on the stability of nutraceuticals, including moisture content, water activity, lipid oxidation, alkaline media, small amounts of transition metals, as well as the interactions with other ingredients present in food products. For example, vitamins, especially lipophilic vitamins (A, D, E, & K), are the most sensitive nutraceuticals, they must be protected from pro-oxidant elements which could greatly impact their chemical integrity and efficacy (Gonnet, Lethuaut, & Boury, 2010). For instance, the contents of vitamin E in milk-based infant formula decreased by more than 50% during 17-month storage time (Miquel, Alegría, Barberá, Farré, & Clemente, 2004). Therefore, encapsulation technology constitutes a promising approach to preserve sensitive nutraceuticals from various conditions, as the nutraceuticals are buried in the core structure with a protection barrier of a polymer-based shell structure. The call for encapsulation of nutraceuticals is recently becoming more and more significant and numerous studies are being carried out in this fast-growing area. In this dissertation, one hydrophilic nutraceutical (selenite) and four hydrophobic nutraceuticals (vitamin E, vitamin D3, indole-3-carbinol and diindolymethane) were studied and discussed in detail in the following chapters.

Chapter 2: Preparation, Characterization and Evaluation of Selenite-loaded Chitosan/TPP Nanoparticles with or without Zein Coating

Luo, Y., Zhang, B., Cheng, W-H., Wang, Q. Carbohydrate Polymers, 82 (3), 942-951.

2.1 Abstract

The selenite-loaded chitosan (CS) nanoparticles using tripolyphosphate (TPP) as a crosslinking agent with or without zein coating were prepared to obtain selenite supplement formulations with low toxicity and improved antioxidant property. Scanning electron microscopy observation showed selenite-loaded CS/TPP nanoparticles had a spherical shape with uniform diameter. The results demonstrated that particle size, surface charge, encapsulation efficiency, and release profile could be modulated by fabricating conditions. After zein coating, the particle size maintained nano-scale while encapsulation efficiency increased from 60% to 95%. The release profile was also prominently improved with zein coating, the released selenite reduced from 85% to 30% within 4 hours in PBS. In simulated gastrointestinal condition with enzymes, 93% of selenite released from non-coated CS/TPP nanoparticles into gastric fluid, however, the releasing rate decreased to 46% after coated with zein. Moreover, due to high antioxidant activity of CS, the in vitro antioxidant properties of selenite-loaded CS/TPP nanoparticles were significantly enhanced, compared with pure selenite.

2.2 Introduction

Selenium is an essential trace element in human nutrition closely associated with the population health. It plays an important role to prevent various diseases, such as

hypercholesterolemia, (Navas-Acien, Bley, & Guallar, 2008), cardiovascular disease (Thomson, 2004; Ray et al., 2006), and certain cancers (Ferguson, Philpott, & Karunasinghe, 2006). Although food and vegetables can be the major source of selenium intake, selenium supplementation is still needed in the low selenium areas (Navarro-Alarcon, & Cabrera-Vique, 2008). Available dietary supplement of selenium mainly consists of two inorganic forms, selenite and selenate, both of them are considered toxic if consumed in large quantity. Sodium selenite has been used in the selenium-fortified milk formula, especially for infants, however, many studies reported that 50-90% of consumed selenite was lost and excreted in urine due to the short retention time in gastrointestinal tract (Zachara, Gromadzinska, Wasowizc, & Zbrog, 2006; Dael, Davidsson, Munoz-Box, Ray, & Barclay, 2001). It has been also evidenced that supplementation of selenite to mice and cells may cause various adverse effects due to its pro-oxidant property, which depends on the concentration and other factors (Cheng, 2009; Shimizu, Ueno, Okuno, Sakazaki, & Nakamuro, 2009; Xiang, Zhao, & Zhong, 2009; Björkhem-Bergman et al., 2002; Moak, & Christensen, 2000). Therefore, how to provide efficient and safe application of dietary selenite supplementation has become a challenge topic in recent years.

Chitosan (CS), the N-deacetylation form of chitin mostly found in the exoskeleton of crustacean, insects, and fungi, is a natural polysaccharide. CS is not only non-toxic and biodegradable with low immunogenicity, but also possesses a high density of positive charge in an acid solution attributed to the glucosamine group on its backbone. Because of these beneficial characteristics, increasing attention has been drawn to the applications of CS-based micro- and nanoparticles in the pharmaceutical and nutraceutical field (Shah, Pal, Kaushik, & Devi, 2009; Grenha, Seijo, & Remuñán-López, 2005; Khlifi, EI Hachimi, Khalil, Es-Safi, & EI Abbouyi, 2005; Kockisch, Ress, Young, Tsibouklis, & Smart, 2003). Ionic gelation is the most studied and widely used method for fabricating CS nanoparticles, in which cationic CS

and multivalent polyanions interact to form CS nanoparticles under simple and mild conditions. Among various polyanions, tripolyphosphate (TPP) is the most investigated due to its quick gelling capability and non-toxic property. CS/TPP nanoparticles have been proved to be excellent carriers for drug and nutrient in therapeutic and nutritional applications, such as providing efficient and target delivery of shRNA sequence (Wang et al., 2009), lowering toxicity of therapeutic antisense oligonucleiotide (Dung et al., 2007), increasing bioavailability of nutraceuticals (Dudhani, & Kosaraju, 2010; Hu, Pan, Hou, Ye, Hu, & Zeng, 2008; Zhang, Yang, Tang, Hu, & Zou, 2008), as well as achieving long term controlled release of protein, e.g., bovine serum albumin (Gan, & Wang, 2007) and unstable drugs, e.g., venlafaxin hydrochloride (Shah et al., 2009).

In the last decade, CS has already been introduced to decrease toxic effects and enhance beneficial properties of therapeutic treatment of selenium compounds. CS hydrogen selenite was prepared by the reaction between CS and selenous acid (Qin, Xiao, Du, & Gao, 2002). It was found that CS hydrogen selenite inhibited the growth against sarcoma 180 solid tumor cell with lower acute toxicity, comparing to sodium selenite. Seleno-short chain CS is a newly developed CS derivative modified by introducing selenic acid groups (–SeO3) to amino positions of CS (Patent Number CN1600793A), and proved to possess a therapeutic potential in human treatment with improved efficacy (Liu, Song, Cao, Liu, & Jia, 2008). In this study, CS/TPP was chosen to form nanoparticles with sodium selenite to decrease the toxicity (personal communication with Dr. Wen-Hsing Cheng) and enhance the antioxidant property of selenite dietary supplement. The ionic gelation method was used to prepare CS/TPP nanoparticles to encapsulate sodium selenite. Different fabricating conditions were evaluated in terms of their effects on physicochemical properties of selenite-loaded CS/TPP nanoparticles, including morphology, particles size, surface charge, the encapsulation efficiency, and release profile, as well as the antioxidant properties. Furthermore, zein, a

water insoluble corn protein, was chosen as a coating material to achieve better encapsulation efficiency and controlled release profiles of selenite loaded CS/TPP nanoparticles.

2.3 Materials and Methods

2.3.1 Materials

Low molecular weight CS with 92% deacytelation degree (Batch No.: MKBB4232), TPP, sodium selenite, 2,3-diaminonaphthalene (DAN), linoleic acid, 1,10-phenanthroline, and pepsin were purchased from Sigma-Aldrich Chemical Co. Ltd (St. Louis, MO). Disodium salt of ethylenediaminetetraacetic acid (EDTA) solution (5 M) was obtained from Boston Bioproducts Incorporation (Boston, MA). Phosphate butter saline (PBS) was purchased from EMD Chemicals Incorporation (Gibbstown, NJ). Simulated gastric fluid without pepsin (SGF) and simulated intestinal fluid with pancreatin (SIF) were purchased from RICCA chemical company (Arlington, TX). All other reagents, including FeSO4 and H2O2, were of analytical grade. DAN was dissolved in 0.1 M hydrochloric acid to prepare a 0.1% solution; once dissolved, it was extracted with cyclohexane three times to remove impurities.

2.3.2 Preparation of Selenite-Loaded CS/TPP Nanoparticles

CS solution (5 mg/ml) was prepared by dissolving CS in 1% (w/v) acetic acid solution under stirring overnight at room temperature. The CS solution was diluted with deionized water (refer to water thereafter) to produce different concentrations. CS/TPP nanoparticles were prepared according to the ionotropic gelation process. In brief, TPP aqueous solution (0.5 mg/ml) was added dropwise to the CS solution and stirred (600 rpm) for 30 minutes at room temperature to obtain blank nanoparticles. For preparation of selenite-loaded CS/TPP nanoparticles, the selenite solution with various concentrations was added

slowly to CS solution with mild stirring (600 rpm) for 30 minutes at room temperature, and then TPP solution was added dropwise to the mixture with mild stirring (600 rpm) for another 30 minutes. The CS/TPP weight ratio used throughout this study was 5:1, which was obtained from the results of several trials.

2.3.3 Fourier transform infrared spectroscopy (FTIR)

FTIR was used to measure changes in chemical structure of the CS, blank nanoparticles, and selenite-loaded nanoparticle samples. The samples were first lyophilized (RVT 4104-115, Refrigerated Vapor Trap, Thermo Savant, Waltham, MA), and then ground into homogeneous powders. The spectra were acquired at 600-4000 cm-1 wavenumbers with a 4 cm-1 resolution utilizing a NEXUS 670 FTIR spectrophotometer (Thermo Nicolet Corp. Madison, WI) equipped with a diamond ATR cell.

2.3.4 Morphology Mbservation

Morphological structures of TPP, selenite, CS, CS/TPP and selenite-loaded CS/TPP nanoparticles were obtained by a scanning electron microscopy (SEM, Hitachi SU-70 Pleasanton, CA). Samples were first cast-dried on an aluminum pan before cutting into an appropriate size, and then adhered to conductive carbon tapes (Electron Microscopy Sciences, Ft. Washington, PA). Subsequently, they were mounted on specimen stubs, and coated with a thin (<20 nm) conductive gold and platinum layer using a sputter coater (Hummer XP, Anatech, CA). Representative SEM images were reported in the result section.

2.3.5 Particle Size and Surface Charge

Hydrodynamic diameter of selenite-loaded CS/TPP nanoparticles was measured by a dynamic light scattering instrument (DLS, BI-200SM, Brookhaven Instruments Corporation, Holtsville, NY). DLS is equipped with a 35 mW HeNe laser beam at a wavelength of 637 nm. All DLS measurements were performed at 25°C. Reflective index and viscosity of water

were 1.590 and 0.8904 centipoise, respectively, which were used for calculating effective diameter from autocorrelation. Surface charges of the nanoparticles were measured by a laser Doppler velocimetry (Zetasizer Nano ZS90, Malvern, UK), using a fold capillary cuvette (Folded Capillary Cell-DTS1060, Malvern, UK). The freshly prepared solutions of nanoparticles were used for particle size and surface charge measurement. All measurements were conducted in triplicate.

2.3.6 Encapsulation Efficiency

The encapsulation efficiency (EE) of the nanoparticles was defined as the drug content that is entrapped into nanoparticles (Shah et al., 2009; Hu et al., 2008), and calculated as follows:

$$\text{EE (\%)} = \frac{\text{Total selenite amount} - \text{Free selenite amount}}{\text{Total selenite amount}} \times 100$$

The total selenite amount was the added selenite. Amount of free selenite molecules were obtained using a membrane separation method. First, free selenite were separated from nanoparticles using an Ultra-15 centrifugal filter device (Millipore corp., Ann Arbor, MI) with 10 kDa molecular weight cut off, according to the previously reported method (Hu et al., 2008). Being centrifuged at 4,000*g* for 30 min, free selenite molecules would penetrate into the filtrate receiver, and the CS nanoparticles would stay in the filter unit. The separated nanoparticles were then lyophilized for further characterization. The free selenite content in the filtrate was measured using the method of Veiga, Rivero-Huguet, and Huertas (2008) with modifications. In brief, nanoparticles solution was diluted with water, and then 5 ml sample solution was poured into a test tube, followed by adding 2 ml 0.05 M EDTA and 2 ml 0.1% DAN solution. The tubes were warmed at 60^{o}C for 30 min. The formed piaselenol was extracted by 4 ml cyclohexane. The absorbance in the cyclohexane layer was measured at 378 nm by a spectrophotometer (Beckman Coulter, DU-730, Fullerton, CA). The amount of selenite was calculated by appropriate calibration curve of free selenite (R^2 = 0.9979), and

each measurement was conducted in triplicate. And the content of selenite entrapped in the CS/TPP matrix was measured right after the separation using the same method to confirm that the addition of free selenite and encapsulated selenite equaled to the total content of added selenite.

2.3.7 In vitro Release

In vitro release study of selenite from nanoparticles was carried out in PBS medium, according to a reported procedure (Shah et al., 2009). Certain amount (5-10 mg) of nanoparticles were resuspended in PBS with pH 7.4 and placed in a dialysis membrane bag with molecular weight cut off at 10 kDa. The membrane bag was placed in 50 ml PBS. The entire system was then kept at 37°C with mild and continuous stirring. At certain time intervals, 5 ml release medium was collected and 5 ml fresh PBS was replaced into release system. The release of selenite from nanoparticles were also investigated under simulated gastrointestinal tract (GI tract), according to the reported method (Somchue, Sermsri, Shiowatana, & Siripinyanond, 2009). The nanoparticles with or without coating were first incubated in 10 ml of SGF with 0.1% pepsin (w/v) at 37°C under mild stirring for 2 hours. The supernatant was separated by centrifugation for determination of selenite content. The swollen aggregates were collected and subsequently incubated in SIF with 1.0% pancreatin (w/v) at 37°C under mild stirring for 4 hours. The supernatant was separated by centrifugation for determination of selenite content. The content of selenite was measured at 378 nm absorbance by the method described in section 1.1.6.

2.3.8 Antioxidative Properties

Two methods, hydroxyl radical scavenging effect and inhibitory effect against lipid peroxidation, were used to evaluate the antioxidant properties of selenite and selenite loaded CS/TPP nanoparticles.

Hydroxyl radical scavenging effect (HRSE): The hydroxyl radical-scavenging experiment was carried out using the method described by Tian et al. (2009) with some modifications. In brief, 1,10-phenanthroline (1 ml, 0.93 mM), the selenite, CS, or selenite-loaded nanoparticles sample (1 ml), and an acetate buffer (1 ml, 0.3 M, pH=3.6) were added to a screw-capped tube orderly and mixed thoroughly. Then, $FeSO_4 \cdot 7H_2O$ (1 ml, 0.93 mM) was pipetted to the mixture. The reaction was initiated by adding H_2O_2 (1 ml, 0.025% v/v). The mixture was incubated at 37°C for 60 min, and the absorbance was measured at 509 nm against reagent blank. The negative control was prepared by replacing 1 ml sample with water, and the blank control was prepared by replacing 1 ml H_2O_2 with 1 ml water. The HRSE was calculated using the following formula:

$$HRSE\,(\%) = \frac{A_S - A_N}{A_B - A_N} \times 100\%$$

where A_B, A_N and A_B were the absorbance values of the sample, negative control, and blank control, respectively. Determination of each sample was performed in triplicate.

Inhibitory effect against lipid peroxidation (IEALP): The inhibitory effect of selenite, CS, and selenite-loaded nanoparticles against lipid peroxidation was evaluated by the formation of conjugated dienes in linoleic acid emulsion system, according to the procedure prescribed by Khlifi et al. (2005), with minor modification. In brief, a 100 µl sample was added to 2.0 ml of 10 mM linoleic acid in phosphate buffer (pH 7.0, 10 mM) emulsified with Tween 20. The mixture was incubated in darkness at 37°C to accelerate oxidation. The control was prepared by replacing 100 µl sample with 100 µl water. After incubation for 15 h, the absorbance was measured at 234 nm against reagent blank with a spectrophotometer (Beckman Coulter, DU-730, Fullerton, CA). The IEALP was calculated with the following equation:

$$IEAPL(\%) = \frac{A_C - A_S}{A_C} \times 100\%$$

where A_C and A_S were the absorbance of the control and sample, respectively.

2.3.9 Improved Nanoparticle Formulation with Zein Coating

To prepare zein-coated selenite-loaded CS/TPP nanoparticles, the selenite-loaded CS/TPP nanoparticles was first prepared (CS concentration, 1.5 mg/ml; selenite loading concentration, 0.6 mg/ml) and then mixed with proper volume of ethanol. Then, the appropriate concentration of zein was dropwise added to above solution under mild stirring for 30 min. The mass ratio of CS to zein was 1:1 and 1:3. The particle size, encapsulation efficiency and release profile were further evaluated and compared with nanoparticles without zein coating.

2.3.10 Statistical Analysis

All the experiments were conducted in triplicate with data reported as mean ± standard error. Experimental statistics were performed using the SAS software (Version 9.2, SAS Institute Inc., Cary, NC). The student's *t* test was used to compare the treatment means of antioxidant activities between nanoparticles and selenite or CS. The analysis of variance (ANOVA) Tukey's multiple comparison tests was used in analysis of differences between physicochemical properties of nanoparticles with and without zein coating. The significance level (*P*) was set at 0.05.

2.4 Results and Discussion

2.4.1 Physicochemical Characterization

The molecular structures of selenite, TPP, and CS are shown in **Fig. 2.1**. CS is a cationic polyelectrolyte polysaccharide due to the protonation of amino groups in acidic solution. Each selenite and TPP molecule carries a maximum of two and five negative charges, respectively.

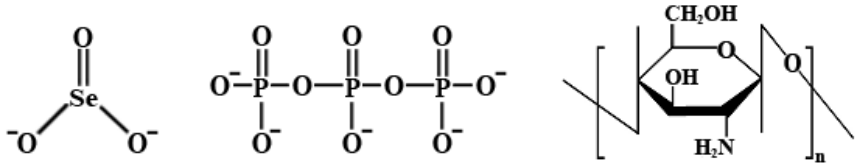

Fig. 2.1 Molecular structure of selenite, TPP and CS.

2.4.1.1 FTIR study

The intermolecular interaction of nanoparticles was characterized by FTIR (**Fig. 2.2**). Six characterization peaks, observed in CS (**Fig. 2.2A**) at 3358.52, 1648.61, 1586.59, 1418.88, 1375.24, and 1025.94 cm^{-1}, were thought to be O–H stretch, C=O stretching from amide I, N–H bending and C-N stretching from amide II, $–CH_2$ bending, $–CH_3$ symmetrical deformation, and skeletal vibration of C–O stretching, respectively (Shah et al., 2009; Lawrie, keen, Drew, Chandle-Temple, Rintoul, & Fredericks, 2007). It was observed that the spectrum of CS/TPP nanoparticles was different from that of CS matrix (**Fig. 2.2B**), highlighted in the wavenumber range from 1400 to 1650 cm^{-1}. The peak of 3358.52 cm^{-1} became wider and flatter, indicating that hydrogen bonding was enhanced (Wu, Yang, Wang, Hu, & Fu, 2005). The peaks of amide I and amide II in CS/TPP nanoparticles shifted to 1635.52 and 1558.23 cm^{-1}, respectively, due to the electrostatic interaction between phosphoric groups of TPP and amino groups of CS in nanoparticles. These observations were consistent with the results reported previously (Shah et al., 2009; Hu et al., 2008; Wu et al.,

2005). Compared with the spectrum of CS/TPP nanoparticles, the electrostatic interaction between selenite and amino groups was confirmed by the shift of absorption peaks of amide II from 1558.23 to 1539.41 in the spectrum of selenite-loaded CS/TPP nanoparticles (**Fig. 2.2C**). This phenomenon was further confirmed by surface charge results presented in section 1.2.3.

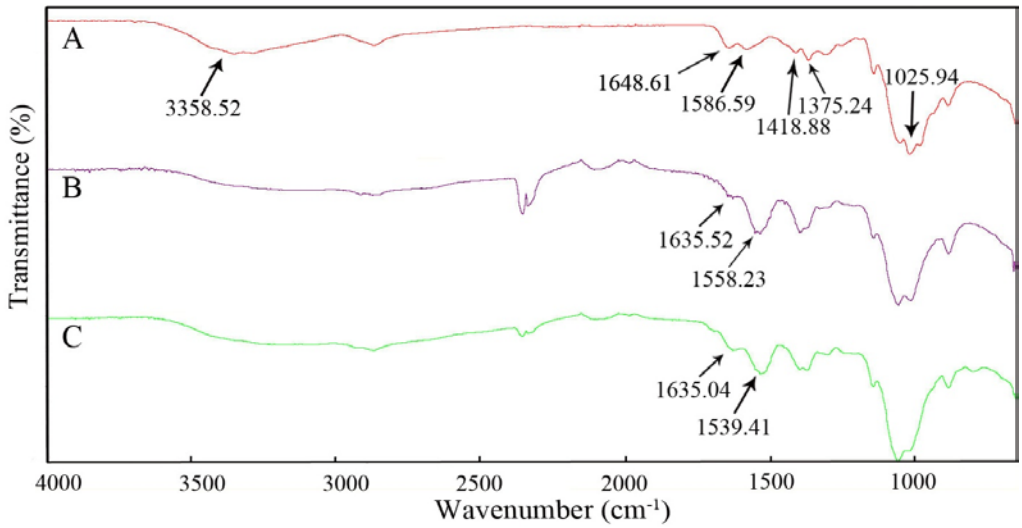

Fig. 2.2. FTIR spectra of individual components and nanoparticles. A, CS; B, CS/TPP nanoparticles; and C, selenite-CS/TPP nanoparticles.

2.4.1.2 Morphological Observation

The morphological changes of each ingredient and nanoparticles after cast drying on an aluminum surface were observed with a SEM, as shown in **Fig. 2.3**. Positively charged pure CS exhibited rough membrane structures (**Fig. 2.3A**) due to its ability to form films by cast drying (Picker-Freyer & Brink, 2006), while the negatively charged TPP formed smooth film (**Fig. 2.3B**). As an inorganic molecule, sodium selenite crystallized into a needle-shaped structure with a diameter of 1-2 μm (**Fig. 2.3C**). When mixing CS and TPP together with or without selenite, spherical particles with uniform particle size in the nanoscale formed, ranging from 200 to 300 nm (**Fig. 2.3D and E**). The aggregates, usually having a rod shape, as observed in the SEM photos were probably formed during the drying process. The particle

size of nanoparticles obtained after cast drying was in good agreement with that measured in an acidic aqueous system presented in the next section.

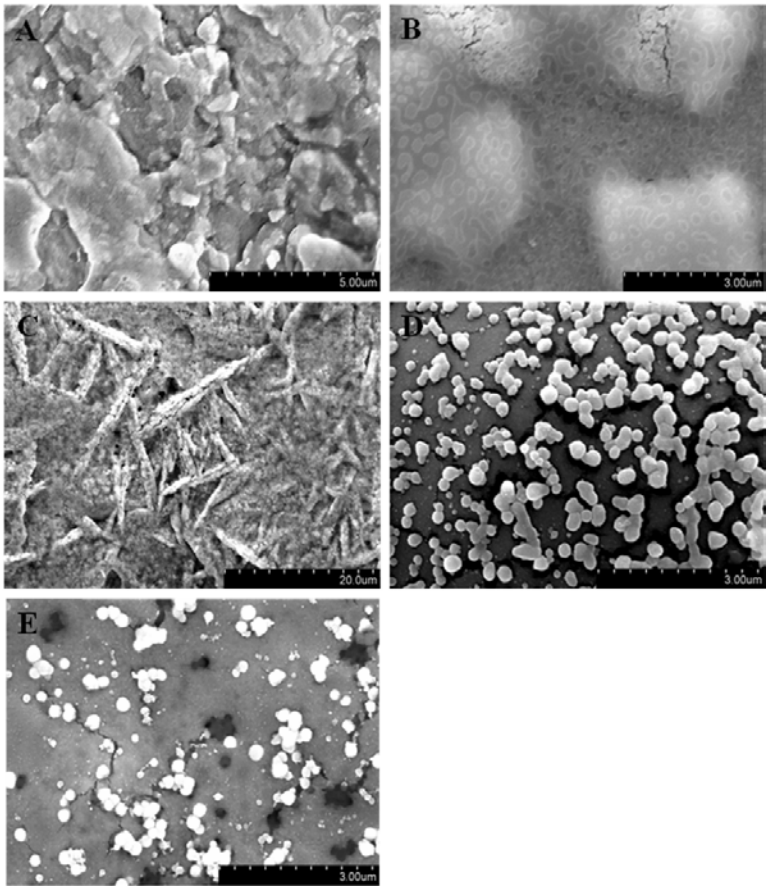

Fig. 2.3. Scanning electron microscopy (SEM) photographs of individual components and nanoparticles. A, CS; B, TPP; C, selenite; D, CS/TPP nanoparticles, and E, selenite-loaded CS/TPP nanoparticles.

2.4.2 Effect of Formulations on Particle Size

The effects of CS concentration and selenite loading concentration on particle size and polydispersity index (PDI) of selenite-loaded CS/TPP nanoparticles were summarized in **Table 2.1**. The particle size increased linearly from 120 to 300 nm with the increase of CS concentration in the range of 0.5-2.5 mg/ml (R^2 = 0.9528). These trends were in accordance with previously reported results (Hu et al., 2008; Gan, Wang, Cochrane, & McCarron, 2005). However, when the selenite concentration increased from 0.2 to 1.0 mg/ml, the particle size

decreased slightly from 300 to 200 nm, showing a linearly negative correlation between selenite loading concentration and CS concentration ($R^2 = 0.9597$). This result is expected since selenite carried negative charges and electrostatically interacted with CS, which would promote formation of nanoparticles through ionic cross-linking. All formulations of selenite-loaded nanoparticles had a small polydispersity, and increased slightly with increasing of chitosan concentrations (**Table 2.1**).

Table 2.1 The particle size and PDI of different formulations

Nanoparticles	Particle size	PDI	Nanoparticles	Particle size	PDI
A1	124.27 ± 4.39	0.16 ± 0.03	B1	302.63 ± 6.23	0.21 ± 0.05
A2	203.53 ± 4.93	0.18 ± 0.03	B2	276.00 ± 4.5	0.19 ± 0.05
A3	233.05 ± 9.86	0.18 ± 0.03	B3	233.05 ± 9.86	0.18 ± 0.03
A4	254.55 ± 9.67	0.29 ± 0.01	B4	229.20 ± 5.31	0.23 ± 0.02
A5	304.20 ± 9.11	0.28 ± 0.01	B5	214.43 ± 11.64	0.28 ± 0.01

PDI, Polydispersity index. A1, A2, A3, A4, and A5 were the nanoparticle samples with CS concentrations of 0.5, 1.0, 1.5, 2.0, and 2.5 mg/ml, respectively, while the selenite loading concentration and CS-TPP mass ratio are fixed at 0.6 mg/ml and 5:1, respectively. B1, B2, B3, B4, and B5 were the nanoparticles samples with selenite loading concentrations of 0.2, 0.4, 0.6, 0.8, and 1.0 mg/ml, respectively, while the CS concentration and CS-TPP mass ratio were fixed at 1.5 mg/ml and 5:1, respectively.

Particle size is one of the most important parameters determining biocompatibilities and bioactivities of micro and nanoparticles. Small nanoparticles have a higher intracellular uptake than large ones. Desai, Labhasetwar, Amidon, and Levy (1996) reported that the gastrointestinal uptake of particles of 100 nm was 15-250 fold greater than larger size microparticles. In another study, they also pointed out that the uptake mechanism of biodegradable microparticles in Caco-2 cells was largely dependent on particle sizes, as the cell uptakes of particles with 100 nm diameter was 2.5 and 6 times greater than those with 1 μm and 10 μm, respectively (Desai, Labhasetwar, Walter, & Levy, 1997). Since particle size plays a vital role in mucosal and epithelial tissue uptake and intracellular trafficking of

nanoparticles (Gan et al., 2005), it is possible to enhance the mucoadhesive properties of CS nanoparticles by decreasing its particle size, and thus to improve mucosal uptake of selenium from selenite.

2.4.3 Effect of Formulations on Surface Charge

As soon as CS and TPP were mixed together in an acetic acid, the nanoparticles were formed spontaneously with a significant positive surface charge obtained by the zeta potential measurement (37 to 50 mV, **Fig. 2.4**). Since CS/TPP nanoparticles were formed by the interaction between protonized $–NH_3^+$ in CS and the polyanionic phosphate groups in TPP, the zeta potential of nanoparticles increased linearly due to a more available protonized $–NH_3^+$ on the surface of nanoparticles formed with higher CS concentration (**Fig.2. 4A**). However, zeta potential decreased slightly with the increase of selenite concentration (**Fig. 2.4B**), owing to an electrostatic interaction between protonized $–NH_3^+$ of CS and selenite that resulted in reduced surface charge.

Zeta potential is another key parameter contributing to various nutritional properties of CS nanoparticles. It has been well documented that CS possesses mucoadhesive properties (Sinha, Singla, Wadlhawan, Kaushik, & Kumria, 2004; Kockisch et al., 2003; Shimoda, Onishi, & Machida, 2001) due to molecular attractive forces formed by an electrostatic interaction between positively charged CS and negatively charged mucosal surfaces. Since most tumor cell membranes are negatively charged, CS nanoparticles have recently been studied to develop tumor-specific delivery of anticancer drugs. For example, encapsulation of paclitaxel using CS-modified nanoparticles could significantly increase lung tumor-specific distribution and enhance the uptake across the endothelial cells of the lung tumor capillary (Yang et al., 2009). Thus, it is possible that encapsulation of selenite into CS/TPP nanoparticles may contribute to the increased efficiency of targeted delivery to tumors and lower its toxicity to normal cells and tissues.

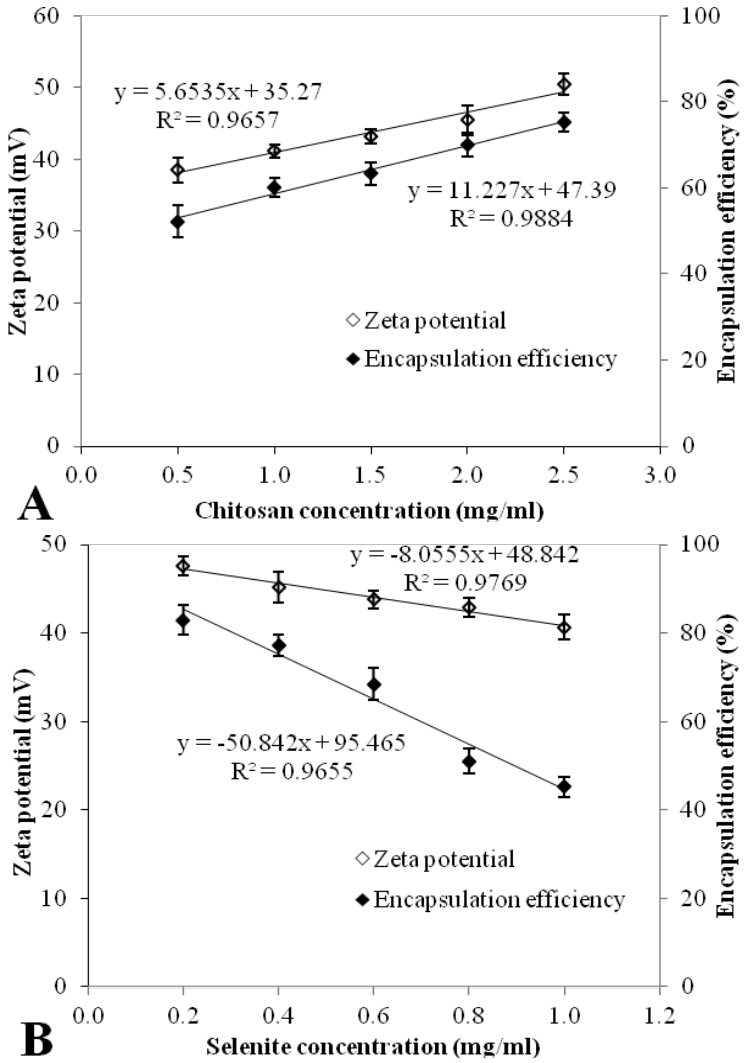

Fig. 2.4. Effect of nanoparticle formulations on zeta potential and encapsulation efficiency.

(A) Effect of CS concentrations (selenite loading concentration = 0.6 mg/ml, CS-TPP mass ratio = 5:1). (B) Effect of selenite loading concentration (CS concentration = 1.5 mg/ml, CS-TPP mass ratio = 5:1). Values were expressed as mean ± standard error.

2.4.4 Effect of Formulations on Encapsulation Efficiency

Encapsulation efficiency is defined as percentage of selenite loading content that can be entrapped into CS/TPP nanoparticles. The effects of CS concentration and selenite loading concentration on encapsulation efficiency are demonstrated in **Fig. 2.4A and 2.4B**, respectively. With the increase of initial CS concentration during the encapsulation process,

more protonized CS ($–NH_3^+$) were available in the system, evidenced by increased surface charge, leading to a stronger electrostatic attraction between selenite and CS. Thus, the encapsulation efficiency of selenite increased linearly with the increase of CS concentration (**Fig. 2.4A**). This observation was accordance with the previous studies, showing the encapsulation efficiency of catechins was positively associated with CS initial concentration (Hu et al., 2008). As shown in **Fig. 2.4B**, encapsulation efficiency was affected by the initial concentration of selenite in a CS solution. A dramatic decrease of encapsulation efficiency from 85% to 42% was observed when loading concentration of selenite increased from 0.2 to 1.0 mg/mL. A reversed linear correlation was obtained between encapsulation efficiency and selenite loading concentration. As the selenite loading concentration increased, more selenite molecules were just electrostatically adsorbed onto the surface of CS and were easily separated from CS-nanoparticles by centrifugation. Similar results were also reported by Wu et al. (2005) showing that encapsulation efficiency of ammonium glycyrrhizinate in CS/TPP nanoparticles decreased with increasing drug loading concentration.

2.4.5 Effect of Formulations on Release Profile

Fig. 2.5 presented the *in vitro* release profiles of selenite from CS/TPP nanoparticles, with respect to different CS concentration (**Fig. 2.5A**) and different selenite loading concentration (**Fig. 2.5B**). Analyses of selenite release showed a very rapid initial burst (0 to 60 minutes), followed by a very slow release in all samples. Accumulative release at 240 minutes was reduced from 98% to 85% with CS concentration increased from 0.5 to 2.5 mg/ml, and the initial burst effect also reduced slightly. These results indicated that the higher the CS concentration was (**Fig. 2.5A**), the lower the release rate would be. Similar results were also reported in other studies (Hu et al., 2008; Ko, Park, Hwang, Park, & Lee, 2002). This phenomenon was attributed to that the increased viscosity at higher CS concentration would result in formation of the denser selenite-loaded CS particles upon interaction with

TPP, and thus the greater cross-linking density and less swelling ability (Shah et al., 2009). In addition, increasing CS concentration would lower the membrane permeability of CS nanoparticles, leading to increased chain packing and rigidity, as well as interchain bonding.

Selenite release from the nanoparticles was also dependent on selenite loading concentration (**Fig. 2.5B**). As the selenite loading concentration increased from 0.2 to 1.0 mg/ml, greater initial burst effect was observed at higher selenite loading concentration. Almost 85% selenite was released from nanoparticles at 1.0 mg/ml selenite loading concentration within 30 min, whereas the amount of selenite released from nanoparticles decreased to 60% when 0.2 mg/ml selenite loading concentration was used.

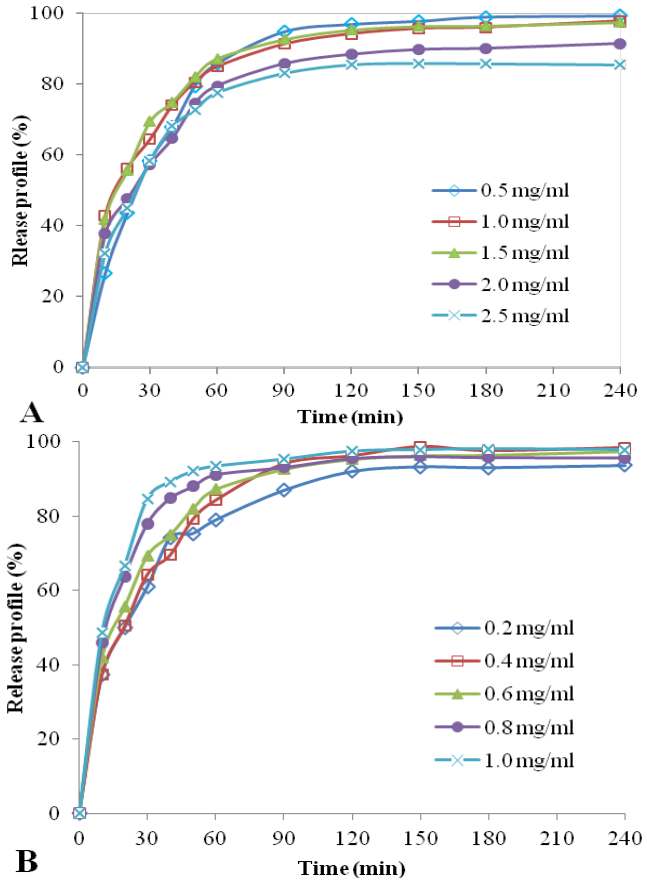

Fig. 2.5. Kinetic release profile of selenite from nanoparticles in different formulations. (A) Effect of CS concentrations on release profile of selenite-loaded CS/TPP nanoparticles (selenite loading concentration = 0.6 mg/ml, CS-TPP mass ratio = 5:1). (B) Effect of selenite loading concentrations on release profile of selenite-loaded CS/TPP nanoparticles (CS concentration = 1.5 mg/ml, CS-TPP mass ratio = 5:1). Values were expressed as mean ± standard error.

Drug molecules diffusion and polymer matrix degradation have been suggested as mechanisms of release profile from nanoparticles and microspheres (Zhou et al., 2001). By studying ammonium glycyrrhizinate loaded CS nanoparticles, Wu et al. (2005) proposed that drug molecule diffusion played a predominant role in release profile when the size of encapsulated drug molecule was much smaller than the formed nanoparticles. Thus, as demonstrated by the release profiles, due to the much smaller size of selenite used in this study, the selenite could diffuse very easily through the surface or the pore of nanoparticles in a very short period of time. Since the formulated selenite loaded CS/TPP nanoparticles had fast releasing property that is hard to achieve the controlled release purpose, zein was further formulated as a hydrophobic material to coat the nanoparticles to obtain better encapsulation efficiency and release profile and the results were presented in section 2.4.7.

2.4.6 Evaluation of Antioxidative Properties

2.4.6.1. Hydroxyl Radical Scavenging Effect (HRSE)

Results presented in **Fig. 2.6** demonstrated the scavenging effect of selenite-loaded nanoparticles, CS (**Fig. 2.6A**) and selenite (**Fig. 2.6B**) on hydroxyl radicals. From **Fig. 2.6A**, it was observed that HRSE of nanoparticles increased from 34.1 to 42.5% as the CS concentration increased from 0.5 to 2.5 mg/ml, and that there was no significant difference between HRSE of CS and that of selenite-loaded CS nanoparticles at higher CS concentrations. From **Fig. 2.6B**, it was found that HRSE of nanoparticles was also slightly enhanced with an increase in selenite loading concentration. However, the HRSE of nanoparticles was 2 to 13 times greater than that of sodium selenite at the equivalent selenite concentrations ($P < 0.05$).

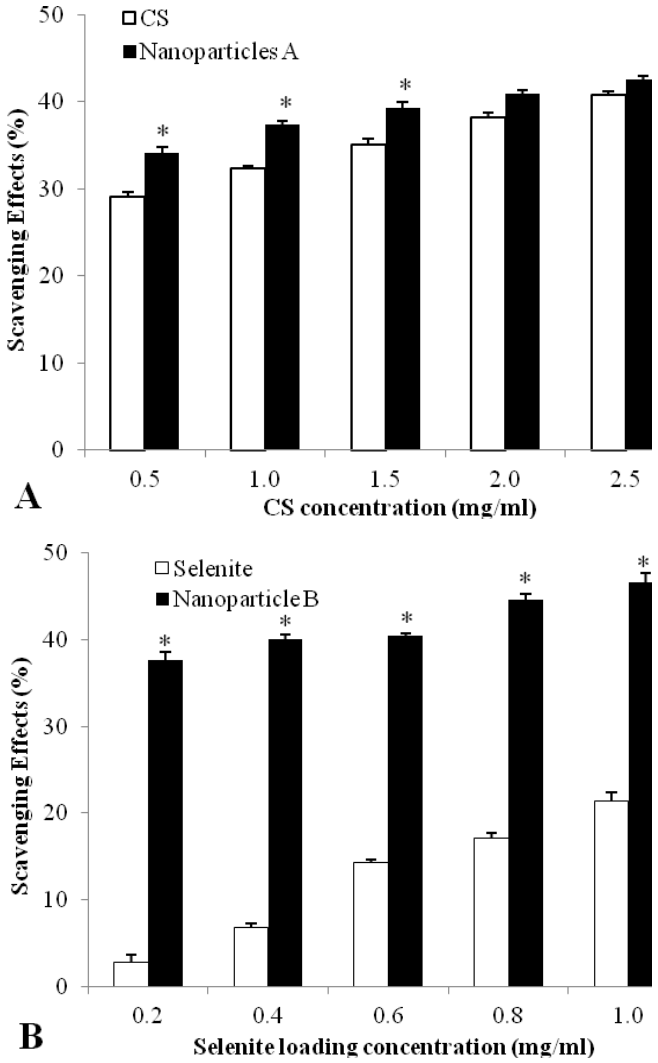

Fig. 2.6. Hydroxyl radical scavenging effect of selenited-loaded nanoparticles.
(A) Effect of CS concentrations on scavenging effect of selenite-loaded CS/TPP nanoparticles against hydroxyl radicals (selenite loading concentration = 0.6 mg/ml, CS-TPP mass ratio = 5:1). (B) Effects of selenite loading concentrations on scavenging effect of nanoparticles against hydroxyl radicals (CS concentration = 1.5 mg/ml, CS-TPP mass ratio = 5:1). Values were expressed as mean ± standard error. (*) $P < 0.05$, compared with CS (A) or selenite (B) at the equivalent concentration.

1.4.6.2. Inhibitory Effect against Lipid Peroxidation (IEALP)

The inhibitory effect of selenite-loaded nanoparticles, CS and selenite against lipid peroxidation in linoleic acid system were presented in **Fig. 2.7**. CS possessed higher IEALP in higher concentrations, while that selenite-loaded nanoparticles had a similar trend on IEALP which increased from 44 to 87% with increase of CS concentration in formulations

(**Fig. 2.7A**). No significant difference was observed between IEALP of CS and that of nanoparticles at higher CS concentration. The IEALP of nanoparticles slightly increased from 79 to 88% as the selenite loading concentration increased from 0.2 to 1.0 mg/ml. The IEALP of nanoparticles were significantly improved ($P < 0.05$), compared with selenite at equivalent concentrations (**Fig. 2.7B**). Although the IEALP of selenite was stronger at higher concentration reaching 58% at 1.0 mg/ml, when considering the decreased encapsulation efficiency of selenite (45%) at 1.0 mg/ml (**Fig. 2.4B**), the increase of selenite loading concentration would not efficiently enhance the antioxidant activities of nanoparticles.

It was reported that when the gold nanoparticles were prepared using CS as a stabilizer, the catalytic activity of gold nanoparticles upon elimination of hydroxyl radicals was remarkably elevated, which was 80-fold higher than that of nanoparticles stabilized by an ascorbic acid (Esumi, Takei, & Yoshimura, 2003). Recently, fungal CS and crab CS have been discovered to possess potent antioxidant properties, including scavenging ability on hydroxyl radicals and inhibitory effect against linoleic acid oxidation (Yen et al., 2007, 2008). Based on our results, it is suggested that although both selenite and CS contributed to the antioxidant properties of the nanoparticles, the contribution of CS was much greater than that of selenite. The encapsulation of selenite into CS nanoparticles could significantly improve the antioxidant profile of selenite supplementation *in vitro*; however, the *in vivo* evaluation of selenite-loaded CS nanoparticles deserves further studies.

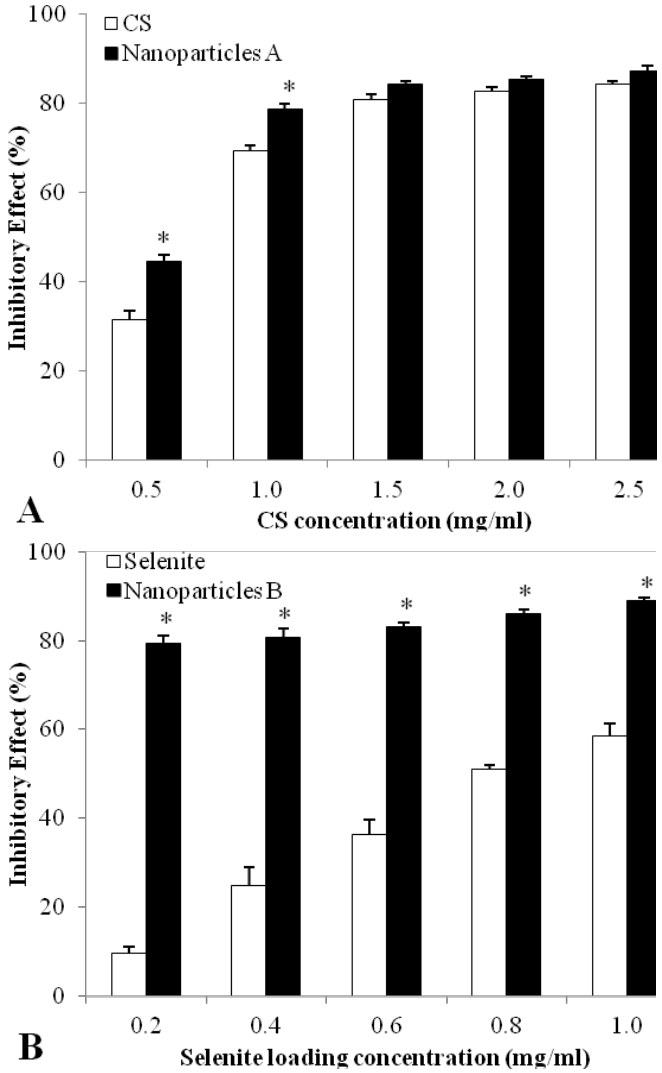

Fig. 2.7. Inhibitory effect against lipid peroxidation of selenite-loaded nanoparticles (A) Effect of CS concentrations on inhibitory effect of selenite-loaded CS/TPP nanoparticles against lipid peroxidation (selenite loading concentration = 0.6 mg/ml, CS-TPP mass ratio = 5:1). (B) Effects of selenite loading concentrations on inhibitory effect of selenite loaded CS/TPP nanoparticles against lipid peroxidation (CS concentration = 1.5 mg/ml, CS-TPP mass ratio = 5:1). Values were expressed as mean ± standard error. (*) $P < 0.05$, compared with pure ingredient at the equivalent concentration.

2.4.7 Zein Coating on Nanoparticles

Studies have shown that a large portion of dietary supplements of selenite cannot be effectively absorbed because of short retention time in gastrointestinal tract (Zachara et al., 2006; Dael et al., 2001). Considering that selenite is best absorbed in intestine for further

utilization in the body, selenite needs to be protected in the encapsulated nanoparticles until it reaches the target site, the intestine. However, all formulations of selenite-loaded CS/TPP nanoparticles had fast release effect in PBS and the selenite contents dropped to ~10% within 4 hours (**Fig. 2.5**). Therefore, zein was proposed as a hydrophobic coating material for the prepared nanoparticles and it could be considered as water barrier to inhibit CS swelling and strengthen the polymer matrix through hydrogen bond with CS.

Table 2.2. Effects of zein coating on physicochemical properties of selenite-loaded CS/TPP nanoparticles

Formulations	Particle size (nm)	PDI	EE (%)	Stimulated GI tract Release (%)	
				SGF (2h)	SIF (4h)
Without zein coating	233.05 ± 9.86[a]	0.18 ± 0.03	63.34 ± 2.54[a]	93.37 ± 2.25[a]	
Coated with zein (CS to Zein 1:1)	236.93 ± 22.14[a]	0.21 ± 0.06	96.16 ± 3.80[b]	49.06 ± 4.35[b]	50.43 ± 5.72
Coated with zein (CS to Zein 1:3)	454.13 ± 21.15[b]	0.28 ± 0.06	95.71 ± 2.10[b]	45.94 ± 3.33[b]	53. 39 ± 4.47

Note: The selenite-loaded CS/TPP nanoparticles without zein coating: CS concenctration, 1.5 mg/ml; selenite loading concentration, 0.6 mg/ml; CS-TPP mass ratio, 5:1. EE, encapsulation efficiency; SGF, simulated gastric fluid; SIF, simulated intestinal fluid. Values were expressed as mean ± standard error. The values with different letter in the same column were significantly different at $P < 0.05$.

As shown in **Table 2.2**, after coating with zein, the encapsulation efficiency of selenite was significantly improved from 60 to 95%. Particle size of zein coated nanoparticles increased with zein concentration, and reached 450 nm when the mass ratio of CS to zein was 1:3. Interestingly, as the mass ratio of CS to zein was 1:1, the particle size of coated nanoparticles maintained around 260 nm, similar to that of the uncoated nanoparticles, whereas the encapsulation efficiency achieved 96%. Thus, nanoparticles with mass ratio of CS to zein as 1:1 might be the optimal formulation to obtain both small particle size and high encapsulation efficiency. Zein has been proved to possess film-forming ability when treated in acidic system (Wang, Yin, & Padua, 2008), including acetic acid (Shi, Kokini, & Huang, 2009) which was used as a common medium to prepare CS/TPP nanoparticles. In our study,

zein can form a coating film around the nanoparticles (**Fig. 2.8A and 2.8B**), and with higher concentration of zein, the coating was denser and thicker, resulting in increased diameter tested by DLS.

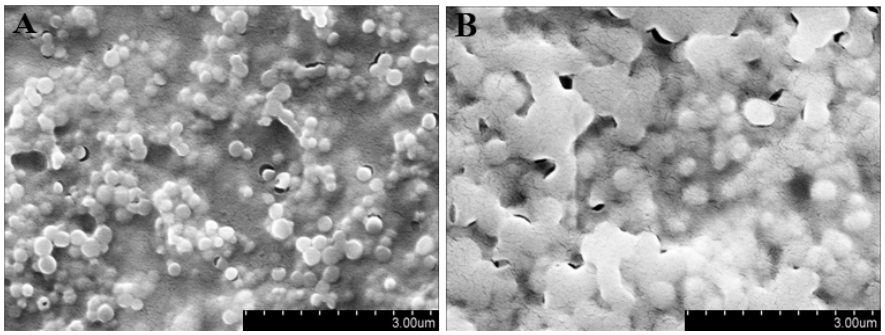

Fig. 2.8. Scanning electron microscopy (SEM) photographs of selenite-loaded CS/TPP nanoparticles with zein coating.
(A), CS : zein = 1:1; (B), CS : zein = 1:3.

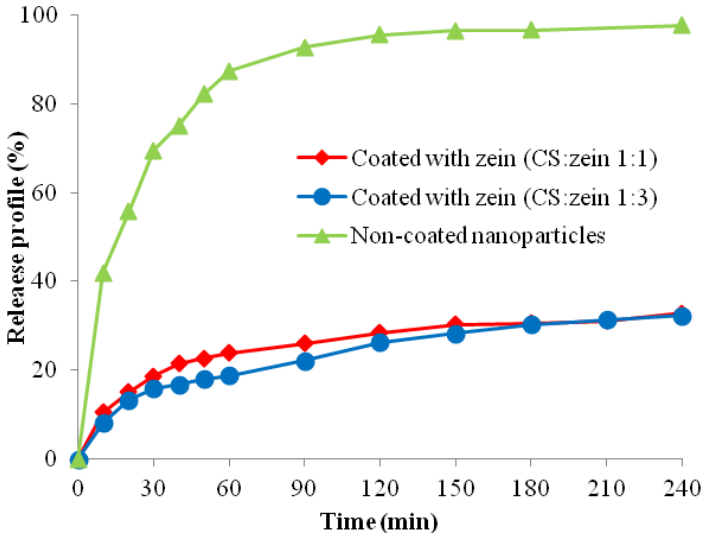

Fig. 2.9. Effects of zein coating on selenite release profile from nanoparticles.
CS concentration = 1.5 mg/ml, selenite loading concentration = 0.6 mg/ml, CS-TPP mass ratio = 5:1. Values were expressed as mean ± standard error. The values with different letter were significantly different at $P < 0.05$.

The release profile of zein-coated nanoparticles in PBS medium was illustrated in **Fig. 2.9**. Comparing to selenite loaded CS/TPP nanoparticles without coating, both the burst effect and accumulative release were greatly improved. Burst effect for the coated nanoparticles occurred at 30 minutes and only 20% of encapsulated selenite released from

matrix, while burst effect for the non-coated nanoparticles occurred at 60 minutes and more than 85% of selenite released out. The accumulative release of selenite within 4 hours decreased dramatically from 98% for non-coated nanoparticles to 32% for coated ones. To further investigate the protective effect of zein coating on selenite release, the release profile was examined under simulated gastric fluid (SGF) and simulated intestinal fluid (SIF) digestion conditions with the presence of enzymes (pepsin and pancreatin, respectively). **Table 2.2** showed the selenite encapsulated in CS/TPP nanoparticles without zein coating almost completely released in SGF (93.37 ± 2.25%) in 2 hours. However, after coated with zein, the selenite release was greatly prolonged and nanoparticles was well-protected against gastric condition, showing that only about 50% of encapsulated selenite released in SGF. The release of the remaining selenite completed after 4 hours of incubation in SIF for both coated samples. No significant difference was observed between the two experimented concentrations of zein coating. Coating the particles with another polymer has been proposed as an effective approach to prolong the controlled release of encapsulated nutraceuticals. Somchue et al. (2009) found after α-tocopherol encapsulated protein-based delivery particles were coated with alginate, the release profile of delivery was retarded prominently. From our study, the release of selenite as well as encapsulation efficiency of CS/TPP nanoparticles was dramatically improved by zein coatings.

2.5 Conclusion

The present study demonstrated that selenite-loaded CS/TPP nanoparticles can be successfully prepared under mild conditions via ionic gelation method. Physicochemical properties, such as particle size, surface charge, encapsulation efficiency, and controlled release can be modulated by controlling critical fabricating parameters including the CS and selenite loading concentrations. The encapsulation of selenite into CS can significantly

improve the *in vitro* antioxidant properties, compared with free selenite. After coated with zein, the encapsulation efficiency was greatly increased and release profile was dramatically retarded, indicating that zein-coated selenite CS/TPP nanoparticles possess a high potential to be developed as an alternative to traditional selenium treatment or supplementation. Moreover, the i*n vitro* cytotoxicity evaluation of selenite encapsulated nanoparticle formulations are being studied in Dr. Cheng's lab, which would give further information on cellular Se retention, toxicity as well as DNA response of selenite-loaded CS/TPP nanoparticles.

Chapter 3: Preparation, Characterization of Zein/Chitosan Complex for Encapsulation of α-Tocopherol and in vitro Controlled Release Study

Luo, Y., Zhang, B., Whent, M., Yu L., Wang, Q. Colloids and Surfaces B: Biointerfaces, 85 (2), 145-152

3.1 Abstract

Chitosan (CS) nanoparticles coated with zein has been newly demonstrated as a promising encapsulation and delivery system for hydrophilic nutrient with enhanced bioactivities in our previous study. In this study, a hydrophobic nutrient, α-tocopherol (TOC), was successfully encapsulated into zein/CS complex. The fabrication parameters, including zein concentration, zein/CS weight ratio, and TOC loading percentage, were systematically investigated. The physicochemical structure analysis showed that the electrostatic interactions and hydrogen bonds were major forces responsible for complex formation. The scanning electron microscopy study revealed the spherical nature with smooth surface of complex. TOC encapsulation was also evidenced by differential scanning calorimetry. The particle size and zeta potential of complex varied from 200 to 800 nm and +22.8 to +40.9 mV, respectively. The kinetic release profile of TOC showed burst effect followed by slow release. Compared with zein nanoparticles, zein/CS complex could provide better protection of TOC release against gastrointestinal conditions, due to CS coatings. Zein/CS complex is believed to be a promising delivery system for supplementation or treatment of hydrophobic nutrients or drugs.

3.2 Introduction

Vitamin E is the main dietary fat-soluble antioxidant, playing important roles in the body. It is a family of four tocopherols (α, β, γ, and δ) and four corresponding tocotrienols (α, β, γ, and δ), of which α-tocopherol (TOC) has the highest biological activity. Vitamin E acts as a chain-breaking antioxidant preventing the propagation of free radical reactions, and thus consumption of vitamin E has been widely considered to help reduce risk of many chronic diseases, such as cardiovascular diseases (Herrera & Barbas, 2001; Tucker & Townsend, 2005). Although the overt deficiency of vitamin E is rare in humans, the marginal vitamin E deficiency could lead to increased susceptibility to free radical damage, especially in premature infants and hypercholesterolemic subjects, resulting in neuromuscular abnormalities, myophthies, and other neurological diseases (Brigelius-Flohe & Traber, 1998; Simon, Paul, Atger, Simon, & Moatti, 1998). Therefore, supplementation of vitamin E is required in aforementioned cases. However, like other lipophilic nutraceuticals, TOC is poorly soluble in water and biologically unstable when exposed to environmental factors, such as light, temperature, and oxygen (Miquel, Algeria, Barbera, Farre, & Clemente, 2004; Sabliov, Fronczek, Astete, Khachaturyan, Khachatryan, & Leonardi, 2009).

In order to overcome the susceptibility and improve the stability of bioactive compounds during processing and storage, the emerging technology of nano-/micro-encapsulation has been recently applied in food and nutraceutical industries. Besides protecting them from the harsh processing conditions and adverse storage environment, the encapsulations of bioactive compounds can also achieve targeted delivery and controlled release of entrapped nutrients to the specific site. TOC has been early encapsulated into gliadin, a plant protein from wheat gluten, to form microparticles around 900 nm, however, the controlled release was only performed in organic medium (decane) at 25 oC, which is hard to simulate release of TOC in vivo environment (Duclairoir, Orecchioni, Depraetere, &

Nakache, 2002). The controlled release of TOC in simulated gastric fluid (SGF) and simulated intestinal fluid (SIF) without enzymes could be achieved by microencapsulation of TOC in calcium-alginate gels (Yoo, Song, Chang, & Lee, 2006) and calcium-pectinate microcapsules (Song, Lee, & Lee, 2009). The in vivo study also revealed that encapsulation of TOC in calsium-pectinate microcapsules could provide sustained release of TOC in plasma and thus improve the bioavailability of TOC through oral administration. A new study showed that free TOC decomposed rapidly when it was incubated in simulated gastrointestinal tract (SGI) with presence of enzymes, however, its stability was dramatically improved after encapsulated into ß-lactoglobulin emulsion gels (Liang, Line, Remondetto, & Subirade, 2010). Therefore, encapsulation of TOC by polymer-based delivery systems could not only improve the stability and controlled release of TOC in vivo but also enhance the bioavailability of TOC in vivo. To the best of our knowledge, however, most delivery systems of TOC with controlled release are at micro-scale beads or gels; the encapsulation and delivery systems at nano-scale have not been fully developed and characterized.

Zein is considered as generally recognized as safe (GRAS) and food-grade ingredient by the Food and Drug Administration (FDA). It contains three quarter of lipophilic and one quarter of hydrophilic amino acid residues. Because of its high hydrophobicity, zein has been successfully applied as a promising carrier for encapsulation and controlled release of fat-soluble compounds (e.g. gitoxin, fish oil, etc.) in the pharmacuetical and food areas (Muthuselvi & Dhathathreyan, 2006; Zhong, Tian, & Zivanovic, 2009). Chitosan (CS) is a linear polysaccharide consisting of randomly distributed N-acetyl-D-glucosamine and ß-(1-4)-linked D-glucosamine units. CS has been widely considered as a versatile polymer used in pharmaceutical and nutraceutical areas as wall materials for development of delivery systems, due to its favorable biological properties such as biodegradability, biocompatibility, and low toxicity (Sahoo, Sahoo, Mohanty, Sasmal, & Nayak, 2009). Compared with other delivery

systems, nano- or micro-particles prepared by CS have a special feature of being able to adhere to mucosal surface and transiently open tight junction between epithelial cells, due to its positive surface charge of CS molecules. In recent years, CS has been involved in delivery systems of TOC. For instance, CS has been used as a wall material to coat TOC encapsulated liposome nanoparticles, resulting in a great improvement of TOC stability, compared with non-coated liposome nanoparticles (Liu & Park, 2009). Also, it has recently been shown that TOC encapsulated CS nanoparticles can be successfully prepared by ultrasound (Naghibzadeh, Amani, Amini, Esmaeilzadeh, Mottaghi-Dastjerdi, & Faramarzi, 2010). However, it has been shown that CS-tripolyphosphate (CS-TPP) nanoparticles might not provide adequate protection and sustained release of small molecular drugs encapsulated in gastrointestinal environment, due to the high solubility of CS in aqueous acidic conditions resulting in the fast release of encapsulated drugs (Yoksan, Jirawutthiwongchai, & Arpo, 2010; Luo, Zhang, Cheng, & Wang, 2010). Therefore, in order to overcome these obstacles, it would be helpful to introduce a second polymer to form stronger polymeric complex with CS.

Recently, many studies have been carried out to investigate the preparation, characterization, and application of micro-/nanocomplexes formed by two or more polymers (Berger, Reist, Mayer, Felt, Peppas, & Gurny, 2004; Wang, & Uludag, 2008). Zein and CS complexes have been newly developed to form antimicrobial ultrathin fiber structure by electrospinning (Torres-Giner, Ocio, & Lagaron, 2009; Song, Yao, & Li, 2010). However, the investigation of polymeric complexes of zein and CS through their self-assembly properties is still lacking in the literature. A CS/zein nano-delivery system has been successfully developed in our lab to encapsulate hydrophilic nutrient with high bioactivities, and the release profile of hydrophilic nutrient from CS nanoparticles can be greatly improved after the nanoparticles are coated by zein protein (Luo et al., 2010). In present study, a novel nano-scale delivery system of TOC using zein/CS complex was developed in order to provide

protection of TOC against gastrointestinal conditions and controlled release. The various formulations with different zein concentrations, ratios of zein/CS, and loading concentrations of TOC were investigated. Characterization was carried out by evaluating the particle size, zeta potential, and encapsulation efficiency of TOC/zein-CS complexes. The molecular interactions were investigated by Fourier transform Infrared spectroscopy (FTIR) and differential scanning calorimetry (DSC). The controlled release of encapsulated TOC in different media with or without presence of enzymes was also studied.

3.3 Materials and Methods

3.3.1 Materials

Low molecular weight CS with 92% deacytelation degree (Batch No.: MKBB4232), vitamin E (TOC, Fluka >= 97%), Tween-20 (Tw), and pepsin were obtained from Sigma-Aldrich Chemical Co. Ltd. (St. Louis, MO). Zein sample with a minimum protein content of 97% was provided by Showa Sangyo (Tokyo, Japan). Phosphate buffer saline (PBS) was purchased from EMD Chemicals Incorporation (Gibbstown, NJ). Simulated gastric fluid without pepsin (SGF) and simulated intestinal fluid with pancreatin (SIF) were purchased from RICCA chemical company (Arlington, TX). All other reagents were of analytical grade.

3.3.2 Preparation of TOC-Encapsulated Zein-CS (TOC/Zein-CS) Complex

Different amount of TOC was first encapsulated into zein by adding TOC (dissolved in pure ethanol) dropwise to zein (dissolved in 75% ethanol) solutions with magnetic stirring at 600 rpm for 60 min. CS with different concentrations dissolved in 1% acetic acid was then added to the above solution dropwise with magnetic stirring for 60 min, followed by adding Tw solution (1% in ethanol) dropwise with magnetic stirring for another 60 min. The final concentration of Tw was 0.44%. The different formulations prepared in this study were shown in **Table 3.1**. The freshly prepared nanoparticle solutions were subjected to particle

size, zeta potential, and encapsulation efficiency measurements. Samples for release profile measurements were freeze-dried right away after ethanol was removed under nitrogen stream using a nitrogen evaporator (N-EVAP 111, Organomation Associates, Inc., MA), and stored at -20 ^{o}C for further assay. TOC-encapsulated zein nanoparticle without CS coating (TOC/zein) was prepared as control nanoparticles, zein-CS complex without TOC was prepared as blank complex.

Table 3.1. Different formulations of complex developed in this study

Samples	Zein (mg/ml)	TOC loading percentage	Weight ratio of zein/CS
A1	5	20%	10/1
A2	10		
A3	15		
A4	20		
B1	10	20%	No chitosan
B2			20/1
B3			10/1
B4			5/1
C1	10	10%	10/1
C2		20%	
C3		30%	

3.3.3 Fourier Transform Infrared Spectroscopy (FTIR) and Differential Scanning Calorimetry (DSC)

The chemical structure of zein, CS, TOC, Tw, TOC/zein nanoparticles, and TOC/zein-CS complex were monitored by FTIR of Jasco 4100 series with an attenuated total reflection (ATR) cell (Jasco Inc. Easton, MO). Samples were first cast-dried on an aluminum

tray for 24 h, and then mounted onto ATR crystal directly. The spectra were acquired at 550-4000 cm^{-1} wavenumbers with a 4 cm^{-1} resolution.

DSC analysis of pure zein, CS, zein-CS physical mixture, TOC/zein nanoparticles, TOC/zein-CS complex were performed using Differential Scanning Calorimeter (Pyris-1, Perkin-Elmer, Waltham, MA), calibrated with indium. Each sample (5 mg) was placed onto a standard aluminum pan, crimped and heated from room temperature to 250 ^{o}C, with constant heating rate 10 ^{o}C/min under continuous purging of nitrogen (20 ml/min). An empty sealed aluminum pan was applied as baseline.

3.3.4 Morphology Observation

Morphological structures of zein, CS, TOC/zein nanoparticles and TOC/zein-CS complex were obtained by a scanning electron microscopy (SEM, Hitachi SU-70 Pleasanton, CA). Samples were first cast-dried on an aluminum pan before cutting into an appropriate size, and then adhered to conductive carbon tapes (Electron Microscopy Sciences, Ft. Washington, PA). Subsequently, they were mounted on specimen stubs and coated with a thin (<20 nm) conductive gold and platinum layer using a sputter coater (Hummer XP, Anatech, CA). Representative SEM images were reported.

2.3.5 Particle Size and Surface Charge

The freshly prepared complex samples at pH range of 5.3–5.5, TOC (4 mg/ml) dissolved in pure ethanol solution at pH 5.9, and zein solutions (10 mg/ml) dissolved in 75% ethanol solution at pH 5.8 were used for particle size and zeta potential measurement. Hydrodynamic diameters of different treatments were measured by a dynamic light scattering instrument (DLS, BI-200SM, Brookhaven Instruments Corp., Holtsville, NY). DLS is equipped with a 35mW HeNe laser beam at a wavelength of 637 nm. All DLS measurements were performed at 25 $^{\circ}$C. Zeta potential of different samples were measured by a laser

Doppler velocimetry (Zetasizer Nano ZS90, Malvern, UK), using a fold capillary cuvette (Folded Capillary Cell - DTS1060, Malvern, UK). Zeta potential was expressed by zeta potential, which was converted from the measured electrophoretic mobility using the Smoluchowski theory. All the measurements were performed in three replicates.

3.3.6 Encapsulation Efficiency (EE)

The encapsulation efficiency was defined as the drug content that is entrapped into polymeric matrix and calculated as follows:

$$EE\,(\%) = \frac{Total\ TOC\ amount - Free\ TOC\ amount}{Total\ TOC\ amount} \times 100\%$$

The total TOC amount was the added TOC. The free TOC was obtained using a membrane separation method with an Ultra-15 centrifugal filter device (Millipore Corp., Ann Arbor, MI), as described in previous studies (Luo et al., 2010; Hu, Pan, Sun, Hou, Ye, Hu, & Zeng, 2008). Being centrifuged at 4000 × g for 30 min, free TOC would penetrate into the filtrate receiver, and the TOC encapsulated in zein nanoparticles or TOC/zein-CS complex would stay in the filter unit. Free TOC obtained in the filtrate was first dried by nitrogen stream to remove ethanol and extracted by hexane to appropriate concentration, and then vortexed thoroughly. The absorbance at 297 nm was measured with a UV/vis spectrophotometer (Beckman Coulter, DU-730, Fullerton, CA) (Somchue, Sermsri, Shiowatana, & Siripinyanond, 2009). The amount of TOC was calculated by appropriate calibration curve of free TOC in hexane (R^2=0.9994). The encapsulated TOC retaining in the filter unit were then lyophilized for further characterization. All measurements were performed in three replicates.

3.3.7 In vitro Release

After removal of free TOC by membrane separation, the complex samples were then freeze-dried and subjected for *in vitro* release profile test to investigate the effect of CS coating. Certain amount of complex samples with or without CS coatings were incubated in 30 ml PBS (pH 7.4) containing Tw (0.5% w/v) to increase TOC solubility, at 37°C. Release medium from each sample was periodically removed and replaced with fresh PBS (pH 7.4) containing Tw. The removed medium was first dried under nitrogen stream and then TOC was extracted by hexane. The resultant extract was analyzed using an UV-visible to measure TOC content as described in section 2.3.6. The accumulative release was plotted as a function of incubation time (up to 6.5 h). Each experiment was carried out in three replicates. The kinetic release profile of TOC in PBS medium was reported.

The release profile of TOC in simulated gastrointestinal (SGI) tract containing enzymes was also evaluated, using the method as previously reported (Liu, Sun, Wang, Zhang, & Wang, 2005). The treatment of SGI tract conditions refers to dissolution carried out in SGF for 0.5 h followed by SIF for 6 h. The complex samples were first incubated in 30 ml SGF with 0.1% pepsin (w/v) at 37°C under mild stirring for 0.5 h. The digestion was stopped by raising pH to 7.5 with NaOH. The supernatant was separated from the swollen aggregates by centrifugation. The released TOC content was analyzed as aforementioned. Subsequently, the swollen aggregate was then digested by 30 ml of SIF with 1.0% pancreatin (w/v) at 37°C under mild stirring for 6 h. The release medium was periodically withdrawn and fresh SIF was replaced to release system. TOC content was analyzed and accumulative percentage of released TOC in SGF and SIF was reported. All measurements were performed in three replicates.

3.4 Results and Discussion

3.4.1 Physicochemical Characterization

2.4.1.1. FTIR Study

FTIR was applied to characterize the intermolecular interactions of complex. The representative spectra of each component and their composites were shown in **Fig. 3.1**. In the original spectra of zein (**Fig. 3.1A**), CS (**Fig. 3.1B**), and TOC (**Fig. 3.1C**), the bands of hydrogen bonds were at 3312, 3368, and 3477 cm^{-1}, respectively. However, after formation of complex, shift of hydrogen bands occurred, and the peaks were at 3312, 3309, 3315 cm^{-1} in the spectra of TOC/zein nanoparticles, zein-CS blank complex, TOC/zein-CS complex, respectively. Hydrogen bonds can be formed between amide groups of glutamine in zein and hydroxyl groups in TOC. CS has both amide and hydroxyl groups, thus the hydrogen bonds can be easily formed between CS and TOC, CS and zein. Particularly, the hydrogen bonds of TOC at 3477 cm^{-1} disappeared and merged into the intensifier vibration at 3312 and 3315 cm^{-1} in TOC/zein nanoparticles and TOC/zein-CS complex, respectively, showing that strong hydrogen bonds formed between TOC and zein or zein/CS complex systems. Additionally, as both TOC and zein are hydrophobic compounds, the hydrophobic attraction could be another force involved during the formation of TOC/zein nanoparticles.

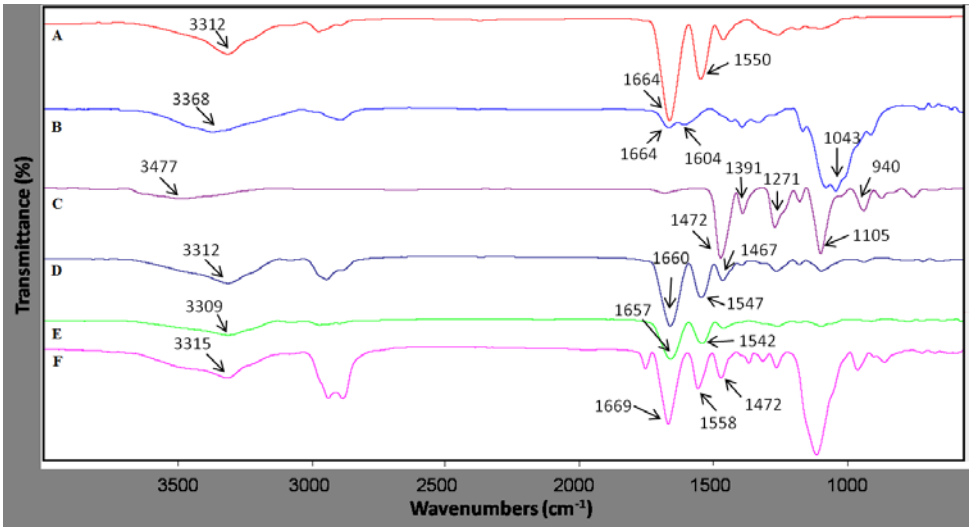

Fig. 3.1. FTIR spectra of individual components and their complex samples.
A, zein, powder; B, α-tocopherol, original oil droplets; C, CS, powder; D, TOC/zein nanoparticles, sample B1; E, zein-CS blank complex, sample B3 without TOC; F, TOC/zein-CS complex, sample B3. Refer to **Table 3.1** for the abbreviation of each formulation.

Another peak area of interest was between 1500 to 1700 cm^{-1}, representing amide I and amide II groups. Comparing the spectra of zein with TOC/zein nanoparticles, the bands of amide I and amide II groups shifted from 1664 and 1550 to 1660 and 1547 cm^{-1}, respectively, suggesting that the electrostatic interactions be another intermolecular force between TOC and zein. Compared with zein , the bands of amide I and amide II groups shifted to 1657 and 1542 cm^{-1} (**Fig. 3.1E**), respectively, in zein-CS blank complex, indicating the electrostatic interactions between zein and CS. Further shift of these bands occurred after TOC was encapsulated into complex, as shown in **Fig. 3.1F**. The electrostatic interactions among zein, CS, and TOC were further confirmed by zeta-potential measurement in the following section.

3.4.1.2 DSC Thermal Analysis

DSC thermograms of zein (**Fig. 3.2A**) and CS (**Fig. 3.2B**) showed characteristic endothermic peaks at 73.2 and 91.2 ^{o}C, respectively. These endotherms for zein and CS could be associated with evaporation of bound water. Similar phenomena have been reported by

other studies indicating the strong affinity between polymer and water (Dudhani & Kosaraju, 2005; Parveen, Mitra, Krishnakumar, & Sahoo, 2010). Compared with CS, the first endotherms of TOC/zein nanoparticles (**Fig. 3.2D**) and TOC/zein-CS complexes (**Fig. 3.2E**) shifted to lower temperature, indicating lower affinity with water, perhaps due to the encapsulation of hydrophobic molecules. It was reported that the shift of endothermic peak in CS and CS derivatives was associated with the strength of water-polymer interactions as well as water holding capacity (Kittur, Prashanth, Sankar, & Tharanathan, 2002). Therefore, the presence of hydrophilic group could increase the bindings of water molecules to polymer network and consequently increase the content of bound water; whereas the presence of hydrophobic groups could thus decrease the content of bound water. Similar observation was also reported that the encapsulation of essential oil into chitosan/cashew gum beads resulted in the shift of endothermic peak to lower temperature (Paula, Sombra, Cavalcante, Abreu, & de Paula, 2011).

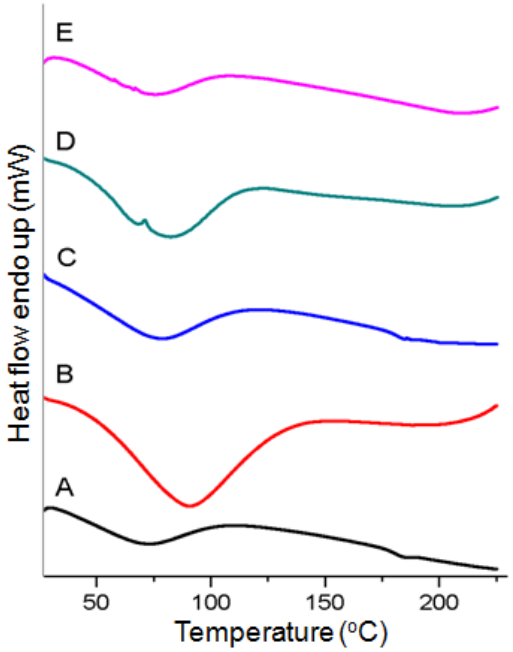

Fig. 3.2. DSC thermograms of pure polymers and their complex samples.
A, Zein, powder; B, CS, powder; C, Zein-CS physical mixture, powder; D, TOC/zein nanoparticles, sample B1; E, TOC/zein-CS complex, sample B3.

3.4.2 Morphological Observation

The morphological observation of zein, CS, TOC/zein nanoparticles and TOC/zein-CS complex were performed by SEM after samples were cast dried on an aluminum surface. The representative photographs were shown in **Fig. 3.3**. The self-assembled zein nanoparticles with diameter around 500 nm formed by cast drying (**Fig. 3.3A**). This observation was consistent with our previous study (Zhang, Luo, & Wang, 2011). As shown in **Fig. 3.3B**, a rough membrane structure was observed after CS was cast dried, indicating the film-forming ability of pure CS and its potential to be applied as a coating material. TOC/zein nanoparticles exhibited nanospheres with smooth surface (**Fig. 3.3C**), however the diameter was not homogenous varying from 300 to 1000 nm. Furthermore, TOC/zein nanoparticles formed the dark core and bright shell structure under SEM observation. The color contrast might be caused by evaporation of TOC, an oil molecule, under vacuum condition of SEM. This similar structure was also reported by other studies of oil-encapsulated micro-/nanoparticles (Naghibzadeh, et al., 2010; Klaypradit, & Huang, 2008). As shown in **Fig. 3.3D**, TOC/zein-CS complex formed sphere nanoparticles with smooth surface and much smaller and more homogeneous diameter (around 400-500 nm), compared with TOC/zein nanoparticles. The reduced particle size might be contributed by the electrostatic interactions between TOC/zein nanoparticles and CS molecules. CS molecules carried high positive surface charge, which could interact with TOC/zein nanoparticles carrying small negative charges, thus facilitate a thin membrane coated at the surface of TOC/zein nanoparticles and consequently dispersed them into smaller nanospheres through electronic repulsions.

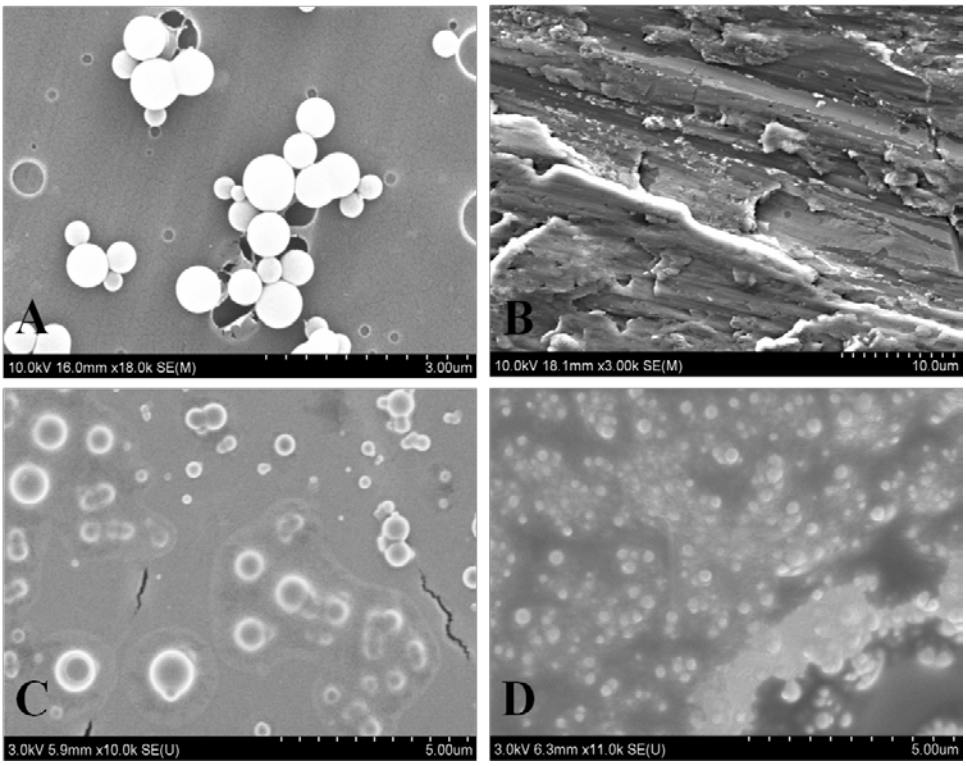

Fig. 3.3. Scanning electron microscopy (SEM) of single ingredients and their complex samples.
A, Zein, 10 mg/ml; B, CS, 1.0 mg/ml; C, TOC/zein nanoparticles, sample B1; D, TOC/zein-CS complex, sample B3.

3.4.2 Effect of Formulations on Particle Size

The effects of different formulations on particle size and polydispersity index (PDI) of complex were summarized in **Table 3.2**. As zein concentration increased from 5 to 15 mg/ml, particle size of TOC/zein nanoparticles decreased from 444.6 to 351.0 nm. However, particle size increased to 537.2 nm as zein concentration increased to 20 mg/ml. At low concentration of zein with low TOC loading and CS concentrations, the oil molecules might mainly deposit on the surfaces of zein spheres leading to the large hydrodynamic size of complex. As further increase of TOC content and CS concentration, TOC might migrate to the internal parts of the complex resulting in a decrease of hydrodynamic diameter. However, when the concentration of zein increased to 20 mg/ml, particle size of complex began to

increase due to the formation of larger self-assembled nanospheres. This interesting phenomenon has also been reported by Naghibzadeh et al. (2010), demonstrating that particle size of TOC-loaded CS nanoparticles decreased with increase of TOC content in the formulation. With the increase of CS concentrations and TOC loading percentage, particle size of TOC/zein-CS complex increased from around 200 to 800 nm, indicating denser complex formed at greater concentrations. All samples had a small PDI less than 0.3 except for TOC/zein nanoparticle which had a greater PDI of 0.45. This indicated that the particle size of TOC/zein nanoparticles was not as homogenous as other formulations, which was consistent with the SEM results (**Fig. 3.3**).

Table 3.2 Particle size, surface charge, and encapsulation efficiency of different samples

Samples[a]	Particle size (nm)	PDI	Zeta potential	Encapsulation Efficiency
A1	444.6 ± 7.9	0.24 ± 0.01	37.7 ± 1.4	76.6 ± 1.2
A2	364.1 ± 9.2	0.21 ± 0.02	30.8 ± 0.5	82.3 ± 0.5
A3	351.0 ± 11.2	0.31 ± 0.04	35.6 ± 1.0	84.3 ± 0.6
A4	537.2 ± 10.0	0.25 ± 0.02	33.6 ± 1.4	86.5 ± 0.3
B1	795.9 ± 8.4	0.45 ± 0.02	-2.8 ± 0.5	82.5 ± 2.6
B2	211.3 ± 19.1	0.20 ± 0.01	22.8 ± 2.2	81.3 ± 1.7
B3	364.1 ± 9.2	0.21 ± 0.01	30.8 ± 1.0	82.3 ± 0.5
B4	862.1 ± 29.0	0.38 ± 0.02	40.9 ± 1.0	85.0 ± 1.3
C1	294.9 ± 9.7	0.14 ± 0.04	28.3 ± 0.9	87.7 ± 0.9
C2	364.1 ± 9.2	0.19 ± 0.03	30.8 ± 1.0	82.3 ± 0.5
C3	811.4 ± 17.3	0.15 ± 0.05	32.7 ± 1.1	81.3 ± 0.7

Note: [a] Refer to **Table 3.1** for the abbreviation of each formulation. Values are expressed as mean ± standard error (n=3).

Interestingly, the particle size of TOC/zein nanoparticles without CS coating was around 800 nm; however, particle size decreased to around 364 nm after coating with CS, at the equivalent zein concentration (10 mg/ml) and TOC loading percentage (20%). This reduction of particle size was consistent with SEM observation, indicating the interactions of

TOC/zein nanoparticles and CS. As the increase of CS concentration or TOC loading percentage, the particle size of complex incremented gradually to around 800 nm (sample B4 and C3), which might be caused by the excess of CS and TOC concentration. Similar observations were also reported by other studies, showing that CS concentration as well as CS molecular weight could greatly affect the particle size (Hu et al., 2008; Gan & Wang, 2007). It is well known that reducing the particle size of encapsulated delivery system could improve the uptake of encapsulated drug from nano-/microparticles in cells. As reported in a recent study, encapsulation of vitamin E into polyethylene glycol-based nanospheres improved the efficacy of vitamin E against oxidative stress, compared with unencapsulated vitamin E (Shea, Ortiz, Nicolosi, Kumar, & Watterson, 2005). Thus, it was proposed that coating TOC/zein nanoparticles with CS might contribute to better absorption and enhanced efficacy than uncoated TOC/zein nanoparticles. Further study needs to be conducted to confirm this expectation.

3.4.3 Effect of Formulations on Zeta Potential

Opposite surface charge of two compounds is one of the major forces when they are mixing together to form nanoparticles or complex. Surface charge, as expressed by zeta potential, of each formulation and pure ingredient was shown in **Table 3.2**. The TOC/zein nanoparticle (B1) was found to be slight negatively charged with zeta potential of -2.8 mV. Although the driving force between TOC and zein was considered as hydrophobic interactions, the electrostatic interactions might also contribute to the encapsulation of TOC into zein Because it was found that TOC and zein carried opposite charge, although the charge density of each was not high (+13.1 and -2.8 mV, respectively). After TOC /zein nanoparticles were coated by CS, the zeta potential of complex became highly positive in the range of +22.8 to +40.9 mV. These observations confirmed that CS was successfully coated on the surface of TOC/zein nanoparticles by electrostatic interactions. Interestingly, the zeta

potential of the complex samples slightly augmented with the increase of TOC loading percentage, which evidenced the electrostatic interactions between TOC and zein. The similar observation was also revealed in other studies (Naghibzadeh et al., 2010; Hatanka, Chikamori, Sato, Uchida, Debari, Onoue, & Yamada, 2010). By studying on the encapsulation of TOC in negatively charged polymeric systems (i.e. water soluble CS nanoparticles and lecithin nano-emulsion), it was found in their studies that the increase of TOC content in nanoparticles could interact and offset the negative charges, and consequently change the zeta potential to a less negative value.

High positive zeta potential demonstrated the potentiality of TOC-zein/CS complex as a promising targeted delivery system of TOC in vivo, due to the interactions with negatively charged biological membranes with improved stability in the presence of biological cations. The mucoadhesive ability of CS nanoparticles could improve the adsorption/bioavailability of drugs or nutrients with poor absorption characteristics. For example, selenite-loaded CS nanoparticles has been demonstrated to have better efficacy of delivering selenium into cells and also to provide better protection of cells against selenium-induced DNA damage response, compared with free selenium (Zhang, Luo, Zeng, Wang, Tian, Song, & Cheng, 2011). Duan and cowkers studied the synthesis of CS-coated curcumin nanoparticles with high positive zeta potential and also the in vivo evaluation of CS-coated nanoparticles using animal model (Duan, Zhang, Han, Chen, Li, Liao, et al., 2010). Higher plasma concentration of curcumin was discovered in animals treated with intravenous injection of CS-coated nanoparticles, compared with uncoated nanoparticles. Because the positive surface charge on nanoparticles could prolong the retention of drug in the blood compartment as well as provide sustained release of the drug.

3.4.4 Effect of Formulationson EE

The encapsulation efficiency of different formulations was also demonstrated in **Table 3.2**. It was observed that the higher zein concentration or CS content in the formulation, the greater encapsulation efficiency of TOC, in the range of 76.5 to 86.5%. As TOC loading percentage increased from 10 to 30%, encapsulation efficiency of TOC in zein/CS complex slightly decreased from 87.7 to 81.3%, which might be due to the excessive loading of TOC. This phenomenon was also observed in other polymeric matrices that over-loading of encapsulated material will cause a decrease of encapsulation efficiency (Liu et al., 2009; Shah, Pal, Kaushik, Devi, & 2009). It was found that there was no significant difference between the encapsulation efficiency of TOC/zein nanoparticles and TOC/zein-CS complex. This result suggested that CS coating did not affect the encapsulation efficiency of TOC/zein nanoparticles, maybe because TOC had been encapsulated into zein nanospheres before CS coating was applied.

3.4.5 Release Profile

3.4.5.1 Kinetic Release Profile of TOC in PBS medium

The kinetic release profiles of complex with different formulations were investigated in PBS medium, and results were shown in **Fig. 3.4**. The kinetic release profile of TOC from complex can be described as a two-step biphasic process, i.e., an initial burst effect followed by subsequent slower release. **Fig. 3.4A** presented the kinetic release profile as a function of zein concentration, which was found to be concentration dependent. At low concentration of zein (5 mg/ml), burst effect occurred within 1.5 h and more than 85% encapsulated TOC released from the complex. As zein concentration increased, the burst effect was dramatically alleviated and the accumulative release after 6.5 h was reduced from 93 to 55%, as zein concentration reached 20 mg/ml.

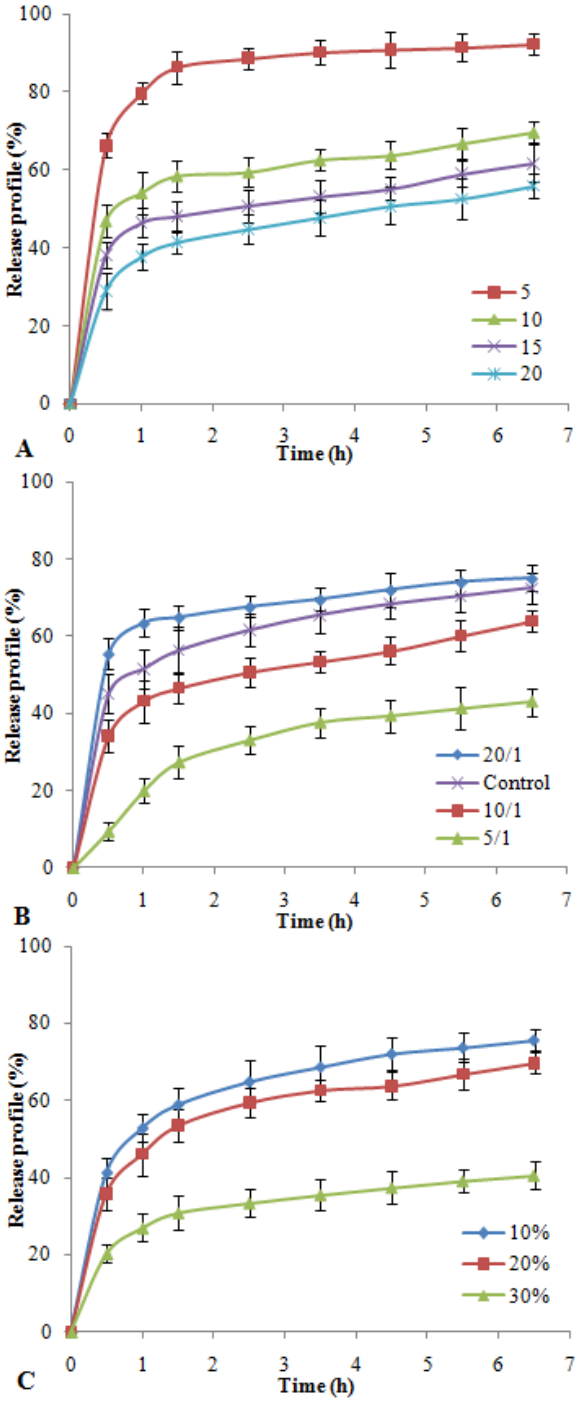

Fig. 3.4. Kinetic release profiles of TOC from zein/CS complex in PBS medium.
A, effect of zein concentration (mg/ml); B, effect of weight ratio of zein/CS; C, effect of TOC loading percentage. Values were expressed as mean ± standard error (n=3).

Fig. 3.4B demonstrated kinetic release profile of TOC with different weight ratio of zein/CS. Free TOC content released due to burst effect was gradually reduced as the weight

ratio of zein/CS decreased, and only about 30% of TOC released out due to burst effect in the formulation with lowest zein/CS weight ratio as 5/1. The accumulative release was also greatly reduced as increase of CS content in the formulation. However, in the formulation with highest zein/CS weight ratio, the burst effect was even greater than TOC/zein nanoparticles without CS coating, although their accumulative release of TOC after 6.5 h was similar. This could be mainly attributed to the particle size of these two formulations. Complex with smaller particle size would have greater surface-to-volume ratio, thus may result in fast release of TOC adsorbed on the surface. Another possible reason was that the electrostatic and hydrogen bond interactions between zein and CS were not strong enough to act as a barrier against hydrophilic environment due to the low concentration and hydrophilic property of CS. But when the zein/CS weight ratio decreased further to 10/1 and 5/1, TOC/zein-CS complex was able to improve the kinetic release profiles compared with TOC/zein nanoparticles without CS coatings.

The kinetic release profile of TOC/zein-CS complex with different TOC loading percentage was shown in **Fig. 3.4C**. With increase of TOC loading percentage, both burst effect and accumulative release of TOC were improved. When loading percentage was 30%, TOC content released due to burst effect and accumulative release was less than 30% and 40%, respectively. Zein, as a protein, possessed the ability to capture the oil molecule and formed a film structure to wrap it. As more oil molecules exist in the system, zein protein would form thicker film to capture them, resulting in augment of particle size (**Table 3.2**) and thicker and denser complex with slow release profile.

3.4.5.2 Accumulative Release Profile in SGI

To speculate release profile of TOC from complex in vivo, all formulations were subjected to release measurement in SGI tract with presence of pepsin and pancreatin for 6.5 h. The results were displayed in **Fig. 3.5**, with respect to different zein concentration (**Fig.**

3.5A), weight ratio of zein/CS (**Fig. 3.5B**), and TOC loading percentage (**Fig. 3.5C**). The release in SGF was mainly due to the enzymatic breakdown of zein resulting in the collapse of complex and the solubility of CS at low pH value. With increase of zein concentration or decrease of zein/CS weight ratio, the accumulative release of TOC in SGF reduced gradually (**Fig. 3.5A and 3.5B**). In the formulation with the smallest zein/CS weight ratio of 5/1, the release of TOC in SGF was only 30%. With thicker CS coating, it took longer for pepsin to pass through CS coating and hydrolyze zein, thus encapsulated TOC diffused from complex more slowly. The slow release may also be attributed to greater particle size of this formulation. The similar observation was also reported by Somchue et al. (2009), pointing out that by coating with a polysaccharide the release of TOC from protein-based delivery particles could be significantly retarded, and higher concentration of coating material showed better protection effect against SGI conditions. In particular, it was also reported that the hydrophilic shell may prevent aggregation and enzymatic degradation of the protein in biological fluids and consequently provide better protection of encapsulated ingredients (Kim, Chae, Jin, Sivasubramanian, Son, Choi, et al., 2010). The difference of release profile in SGF between TOC/zein nanoparticles and TOC/zein-CS complex at equivalent zein concentration and TOC loading percentage (**Fig. 3.5B**) was similar with kinetic release profile (**Fig. 3.4B**) in PBS as discussed above. The release in SGF was also reversely dependent on TOC loading percentage (**Fig 3.5C**).

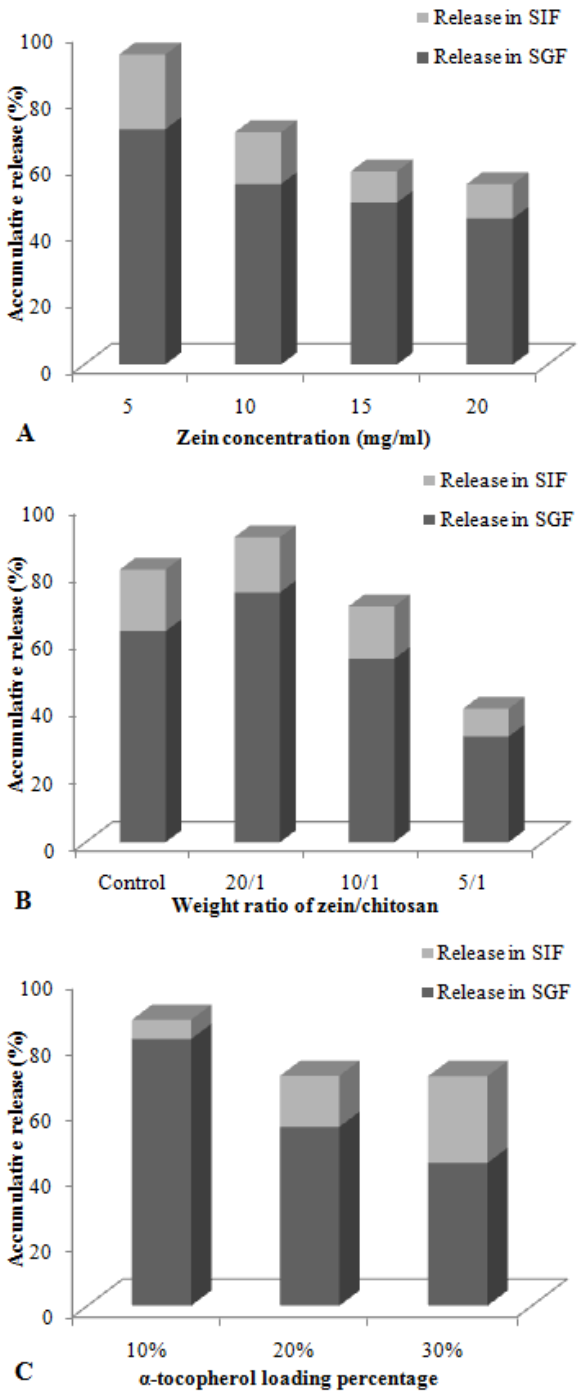

Fig. 3.5. Accumulative release profiles of TOC from TOC/zein-CS complex with different formulations in SGI with presence of enzymes.

A, effect of zein concentration; B, effect of weight ratio of zein/CS; C, effect of TOC loading percentage. (The standard error of each measurement was within 10% of the mean, n=3). The treatment of SGI tract conditions refers to dissolution carried out in SGF with 0.1% pepsin (w/v) for 0.5 h followed by SIF with 1.0% pancreatin (w/v) for 6 h.

After incubation in SGF for 0.5 h, all samples were further subjected to incubation in SIF with pancreatin for 6 h. The effects of zein concentrations and weight ratio of zein/CS on accumulative release of TOC in SIF were similar with their effects in SGF. However, as increase of TOC loading percentage, there was an increase of TOC content released in SIF. This could be attributed to that as the polymeric matrix was hydrolyzed or eroded by enzymes, TOC in the inner part of matrix was exposed and more ready for release. Compared with TOC content released in SGF, it was found that much less TOC content released in SIF. According to a study of Liang et al. (2010), it was found that releasing rate of TOC from ß-lactoglobulin emulsion gels was rather slow in SIF, compared with SGF. They proposed that the products of partial hydrolysis of ß-lactoglobulin formed after digestion in SGF may act as an emulsifier and adsorb to the oil droplet surfaces and thereby increase the resistance to be digested in SIF. Thus, the slow release profile of TOC from zein/CS complex observed in this study may also be explained by a similar mechanism that the hydrolytes of zein may adsorb to TOC droplet and therefore retard the release of TOC in SGF.

3.4.6 Schematic Illustration

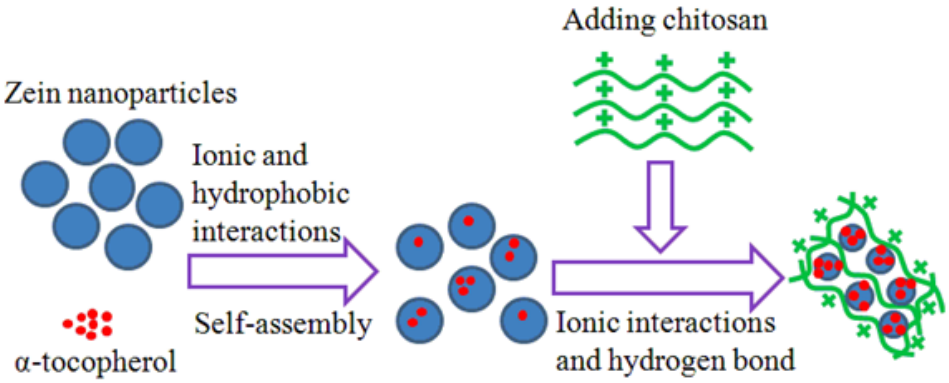

Fig. 3.6. Schematic illustration of formation of zein/chitosan complex for encapsulation of TOC.

Recently, polymer complexes or composites have drawn increasing interests. Due to cationic properties of CS, many anionic natural polymers have been intensively investigated to form polyelectrolyte complexes with CS to develop novel drug delivery systems, including

alginate, carrageenan, pecin, xanthan gum, hyaluronic acid, etc (Hamman, 2010; Saether, Holme, Maurstald, Smidsrod, & Stokke, 2008). In this study, although zein only carried a few negative charges, the prepared zein/CS complex might still be considered as a polyelectrolyte complex based on our results. Herein, a schematic illustration for the formation of TOC encapsulated zein-CS complex was proposed and shown in **Fig. 3.6**. As TOC was added to zein solutions, zein molecules would wrap up TOC to form a thin film on its surface, and the forces of hydrogen bonds and hydrophobic attraction between two molecules could induce the formation of TOC encapsulated nanoparticles with relatively large particle size about 800 nm. As soon as CS solution was added to the system, the positively charged CS would interact with negatively charged TOC/zein nanoparticles; CS coating around the surface of TOC/zein nanoparticles would then be formed and consequently disperse them into uniform and smaller size nanoparticles with diameter about 200-300 nm. At the same time, with the formation of smaller complex, some of TOC would become only adsorbed to the surface of complex resulting in fast release, which can be compromised by thicker CS coatings.

3.5 Conclusion

In the present study, TOC/zein-CS complex was successfully prepared under mild conditions. Physicochemical analyses suggested that electrostatic interactions, hydrogen bond, and hydrophobic interactions are the main forces in TOC/zein-CS complex. By coating TOC/zein nanoparticles with CS, particle size was dramatically reduced and zeta potential was increased to be highly positive, depending on different formulations. CS coating did not affect the encapsulation efficiency but greatly improved the controlled release of TOC in both PBS and SGI conditions, indicating that TOC/zein-CS complex can be developed as a novel TOC supplementation or treatment. In near future, the *in vitro* and *in vivo* evaluation of TOC/zein-CS complex in different cell lines and animal models will be studied.

Chapter 4: Development of Zein Nanoparticles Coated with Carboxymethyl Chitosan for Encapsulation and Controlled Release of vitamin D3

Luo, Y., Teng, Z., Wang, Q. Journal of agricultural and food chemistry, 60 (3), 836-843

4.1 Abstract

In this study, zein nanoparticles coated with carboxymethyl chitosan (CMCS) were prepared to encapsulate vitamin D3 (VD3). VD3 was first encapsulated into zein nanoparticles using a low-energy phase separation method, and coated with CMCS simultaneously. Then, calcium was added to crosslink CMCS to achieve thicker and denser coatings. The nanoparticles with CMCS coatings had a spherical structure with particle size from 86–200 nm. The encapsulation efficiency was greatly improved up to 87.9% after CMCS coating, compared with 52.2% of that using zein as a single encapsulant. The physicochemical properties were characterized by differential scanning calorimetry and Fourier transform infrared spectroscopy. Nanoparticles with coatings provided better controlled release of VD3 in both PBS medium and simulated gastrointestinal tract. The photostability against UV-light was significantly improved after encapsulation. Encapsulating of hydrophobic nutrients in zein nanoparticles with CMCS coatings is a promising approach to enhance chemical stability and controlled release property.

4.2 Introduction

Vitamin D (VD) is an essential nutrient to human health. It is one of the fat soluble vitamins and consists of two major physiologically forms, vitamin D2 (ergocalciferol) (VD2) and vitamin D3 (cholecalciferol) (VD3). VD is a prohormone and can be synthesized from a precursor in the skin under sunlight exposure. Dietary source of VD3 is very limited, and only fish are found to be the abundant source (Picciano, 2010). Recently, VD has been intensively investigated to be not only important for calcium absorption and homeostasis regulation, but also essential for many other chronic diseases, such as type 2 diabetes, hypertension, cardiovascular disease, etc (Picciano, 2010; Pittas, Chung, Trikalinos, Mitri, Brendel, Patel, et al., 2010). It was found that for the elderly people in chronic disease and those with insufficient exposure to sunlight, VD deficiency is very frequent, especially in the US and Europe where 30-60% populations have been diagnosed as VD deficiency (Ginter & Simko, 2009). Furthermore, based on the data drawn from National Health and Nutrition Examination Surveys (NHANES), it has been shown that the mean serum VD status in the year of 2000 – 2004 was significantly lower than that in the year of 1988 – 1994 (Looker, Pefeiffer, Lacher, Schleicher, Picciano, & Yetley, 2008). As a result, FDA encouraged the addition of VD to milk and cereals to prevent rickets in children and osteoporosis in adults. Also, the Recommended Daily Allowance of VD in Dietary Guideline for Americans newly released by USDA in 2010 has increased to 600 IU per day for children and 800 IU per day for most adults who have minimal sun exposure (Dietary guidelines for Americans, 2010). A large

number of evidence has demonstrated that the increasing attention and importance have been given to improve VD status.

As a lipophilic vitamin, VD is not soluble in water and very sensitive to various environmental factors. For example, light, heat, and oxygen could rapidly induce isomerization or oxidation of VD3, and then adversely affect its chemical structure and physiological benefits (Nelson, Ballard, Zhu, & Seburg, 2007). In recent development in food and nutraceutical industries, encapsulation of lipophilic bioactive compounds has received tremendous interests as this technology is able to constitute an appropriate mean to increase their stability and preserve health-promoting properties during processing and storage (Huang, Yu, & Ru, 2010). Another benefit of encapsulation is that it might further provide target delivery and controlled release of nutraceuticals, thus enhancing bioactivity and diminishing side-effects of potential hypervitaminosis due to high administration dose (Gonnet, Lethuaut, & Boury, 2010). Although the encapsulation of VD has been reported since 1998 (Delaurent, Siouffi, Pepe, 1998), many disadvantages still exist, inhibiting further application and industrialization of VD supplementation. For instance, encapsulation of VD3 into cyclodextrin involved high temperature (50oC) during the preparation which would cause loss of VD3 (Delaurent, 1998). Microencapsulation of VD2 has been later developed using chitosan/ethylcellulose complex microcapsule by Shi and Tan (2002). In their study, although high encapsulation efficiency (>95%) and controlled release were achieved, the toxic solvents were used, such as tetrachloride and petroleum ether, which would pose potential side effects to final products due to residue of these solvents. A new study reported a novel method to

encapsulate VD2 into a natural nano-capsular vehicle prepared with bovine casein micelle (Semo, Kesselman, Danino, & Livney, 2007). However, it was found that the loading capacity (vitamin/protein ratio) was as low as 0.05% which means large amount of protein is needed to encapsulate a few amount of vitamin, and only around 27.5% of VD2 was incorporated into micelles and the rest of vitamin was only bound to the surface of casein molecules, resulting in little protection against UV exposure.

Zein is a maize prolamine protein with three quarter of lipophilic and one quarter of hydrophilic amino acid residues, leading to its unique aqueous-alcohol solubility and film forming property. Zein has been extensively investigated for its capability to form self-assemble nanoparticles encapsulating bioactive compounds in food and pharmaceutical applications, such as fish oil (Zhong, Tian, & Zivanovic, 2009), essential oil (Parris, Cooke, & Hicks, 2005), gitoxin (Muthuselvi & Dhathathreyan, 2006), and fluorouracil (Lai & Guo, 2011). Chitosan (CS), a natural polysaccharide has been considered as a versatile polymer for encapsulation and delivery of active ingredients. In order to improve its solubility in neutral pH, its derivative, carboxymethyl chitosan (CMCS), is widely used for biomedical applications. It is soluble in neutral aqueous solution, and it has been shown that negatively charged CMCS is able to form nanoparticles spontaneously with positively charged ions (Shi, Du, Yang, Zhang, & Sun, 2006). Several bioactive compounds have already been successfully encapsulated into CMCS nanoparticles to achieve controlled release and target delivery properties (Anitha, Maya, Deepa, Chennazhi, Nair, Tamura, et al., 2011; Kim, Jeong, Choi, Roh, Kang, Jang, et al., 2006). CMCS has also been modified by cholesterol to form self-assembled nanoparticles being able

to deliver anticancer drug with higher targeting efficiency and longer retention time in liver than that of pure drug solution (Wang, Jiang, Li, Liu, Zhang, Wang, et al., 2008). In addition, it is newly elucidated that negatively charged CMCS nanoparticles with particle size around 150 nm had a better in vitro cellular uptake and more efficient in vivo targeting delivery of entrapped drug to tumor (He, Hu, Yin, Tang, & Yin, 2010). In our previous studies, zein/CS complex nanoparticles were developed as delivery systems for both hydrophilic and hydrophobic nutrients (Luo, Wang, Zhang, Whent, & Yu, 2011; Luo, Zhang, Cheng, & Wang, 2010). The physico-chemical properties, including encapsulation efficiency and controlled release profile, of complex nanoparticles were greatly improved than nanoparticles prepared by the single polymer (i.e. zein or CS).

In present study, VD3 was first encapsulated into zein nanoparticles prepared by phase separation. Then, CMCS was applied to coat zein nanoparticles and hardened by calcium ions. The preparation conditions, such as zein concentration, zein/CMCS ratio, as well as CMCS/calcium ratio, were optimized to obtain nanoparticles with small particle size, high zeta potential and high encapsulation efficiency. The encapsulation of VD3 was evidenced by Diffraction Scanning Calorimetry (DSC). The in vitro release profile and stability of VD3 in nanoparticles were also studied.

4.3 Materials and Methods

4.3.1 Materials

Vitamin D3 (VD3) of 99% purity was purchased from Alfa Aesar (Ward Hill, MA). Zein sample with a minimum protein content of 97% was provided by Showa Sangyo

(Tokyo, Japan). CMCS was purchased from Nantongxingcheng Biological Product Inc., Nantong, Jiangsu Province, China), with a deacetylation degree of 96% and carboxylation degree of 65%. Phosphate buffer saline was bought from EMD Chemicals Incorporation (Gibbstown, NJ). Simulated gastric fluid (SGF) and simulated intestinal fluid with pancreatin (SIF) were purchased from RICCA Chemical Company (Arlington, TX). All other materials, including pepsin, hexane, ethyl acetate, are of analytical grade and purchased from Sigma–Aldrich Chemical Co. Ltd. (St. Louis, MO).

4.3.2 Preparation of Nanoparticles

Table 4.1. Formulations of nanoparticle complexes.

Samples	VD3 loading	Z/CMCS (m/m)	CMCS/Ca (m/m)
ZV	7.5%	N/A	N/A
A0	7.5%	1:1	N/A
A5			5:1
A10			10:1
A20			20:1
B0	7.5%	1:2	N/A
B5			5:1
B10			10:1
B20			20:1
C0	7.5%	2:1	N/A
C5			5:1
C10			10:1
C20			20:1

Z, zein, used as 2 mg/ml; CMCS, carboxymethyl chitosan; VD3, vitamin D3. ZV represents VD3 encapsulated zein nanoparticles. VD3 loading percentage was calculated as mass ratio of VD3 to zein polymer. A0-A20 represent formulations with different mass ratio of CMCS/Calcium, prepared with mass ratio zein/CMCS as 1:1. B0-B20 represent formulations with different mass ratio of CMCS/Calcium, prepared with mass ratio zein/CMCS as 1:2. C0-C20 represent formulations with different mass ratio of CMCS/Calcium, prepared with mass ratio zein/CMCS as 2:1.

VD3 (1 mg/ml) was dissolved in pure ethanol as stock solution. Zein was dissolved in 70% aqueous-ethanol solution. The nanoparticles were prepared using a phase separation

method as previously reported with some modifications (Lai et al., 2011). Briefly, 0.3 ml of VD3 solution (1 mg/ml) was added dropwise into 2 ml of zein solution (2 mg/ml) with mild stirring for 30 min. Then, the above VD3 encapsulated zein solution was rapidly poured into 5 ml of CMCS solution (0.8, 1.6, or 0.4 mg/ml), dissolved in pure water. After stirring for 30 min, 1 ml of calcium solution in different concentrations was then dropwise added into the above solution. After 30 min stirring, the obtained opaque single phase solution was then freeze dried for 48 hours. The control nanoparticles without CMCS and/or calcium were also prepared in parallel. Please refer to **Table 4.1** for detailed description of various formulations. All samples were prepared in triplicate and all procedures were performed in darkness under room temperature.

4.3.3 Fourier Transform Infrared Spectroscopy (FTIR) and Differential Scanning Calorimetry (DSC)

The chemical structure of preparation ingredients (i.e. zein and CMCS) and nanoparticles (i.e. ZV, B0, and B20) were monitored by FTIR of Jasco 4100 series with an attenuated total reflection (ATR) cell (Jasco Inc. Easton, MO). Samples were first cast-dried on an aluminum tray for 24 h, and then mounted onto ATR crystal directly. The spectra were acquired at 750-4000 cm-1 wavenumbers with a 4 cm^{-1} resolution.

DSC analysis of pure ingredients (i.e. zein, CMCS, and VD3), mixture of zein and VD3, and nanoparticles (i.e. ZV and B20) were performed using TA Q100-DSC thermal analyzer (TA Instruments, New Castle, DE), calibrated with indium. The mass ratio of zein and VD3 in the physical mixture was the same as that in nanoparticles. Each sample (5 mg) was placed onto a standard aluminum pan, crimped and heated from room temperature to 230^{o}C, with constant heating rate of 10 ^{o}C/min under continuous purging of nitrogen (20 ml/min). An empty sealed aluminum pan was applied as the baseline.

4.3.4 Morphological Observation

Morphological structures of nanoparticles were observed by a SEM (Hitachi SU-70 Pleasanton, CA). Samples were first cast-dried on an aluminum pan before cutting into an appropriate size, and then adhered to conductive carbon tapes (Electron Microscopy Sciences, Ft. Washington, PA). Subsequently, they were mounted on specimen stubs and coated with a thin (<20 nm) conductive gold and platinum layer using a sputter coater (Hummer XP, Anatech, CA). Representative SEM images were reported.

4.3.5 Particle Size and Zeta Potential

The freshly prepared nanoparticle samples were used for particle size and zeta potential measurement. Hydrodynamic diameters of different treatments were measured by a dynamic light scattering instrument (DLS, BI-200SM, Brookhaven Instruments Corp., Holtsville, NY), which was equipped with a 35mW HeNe laser beam at a wavelength of 637 nm. All DLS measurements were performed at 25ºC. The polydispersity index (PDI) reflecting the particle size distribution of nanoparticles was also reported. Electrophoretic mobility of different samples was measured by a laser Doppler velocimetry (Zetasizer Nano ZS90, Malvern, UK), using a fold capillary cuvette (Folded Capillary Cell - DTS1060, Malvern, UK). Zeta potential was obtained by converting the measured electrophoretic mobility using the Smoluchowski theory. All the measurements were performed in three replicates.

4.3.6 Encapsulation Efficiency (EE)

EE was measured according to the method of Wang Liu, Sun, Wang, and Zhang, (2005) with minor modifications. Briefly, 10 mg of lyophilized nanoparticles samples were flushed with 1 ml ethyl acetate for three times, using No. 1 Whatman filter paper. Then, the washed nanoparticle samples were vacuum-dried in a vacuum oven (VWR International, PA).

The ethyl acetate elute containing free VD3 was dried using vacuum rotary evaporator (Büchi, DE), and then VD3 was extracted by hexane and determined by an UV/VIS spectrophotometer (Beckman Coulter, DU-730, Fullerton, CA) at 264 nm. The VD3 encapsulated in lyophilized nanoparticles was also extracted based on the method described by Wang, Tian and Chen (2011), in order to calculate recovery rate . Five milliliter ethanol was added and vigorously shaken on a vortex mixer for 30 seconds and then 5 ml of hexane was added. The obtained mixture was vigorously shaken for another 30 seconds. Five milliliters of pure water was then added into the above mixture, and the tube was then sealed tightly and shaken on a Multi-Purpose Rotator/Rocker (Scientific Industries Inc., NY, USA) for 30 min. After the mixture was centrifuged at 800 x g for 5 min at 4 ^{o}C to quickly separate hexane phase and water/ethanol phase, the VD3 in hexane layer was measured as described above. The free VD3 in elute and encapsulated VD3 extracted from lyophilized nanoparticles were added up to calculated the recovery rate of VD3 measurement, which was found to be higher than 95%. The EE was calculated by the following equation：

$$EE(\%) = \frac{Total\ VD\ amount - Free\ VD\ amount}{Total\ VD\ amount} \times 100$$

$$LC(\%) = \frac{Encapsulated\ VD\ weight}{Nanoparticles\ weight} \times 100$$

4.3.7 Release Profile

The lyophilized samples after removal of free VD3 were used for *in vitro* kinetic release test in simulated gastrointestinal tract (SGI). For kinetic release test in PBS, certain amount of samples (10 mg) was resuspended in PBS (pH 7.4) containing tween 20 (Tw, 0.5%, w/v) that was to provide sink condition and increase VD3 solubility, at 37°C. At designated time intervals, samples were centrifuged at 10,000 g for 5 min to withdrawn the supernatant medium and equivalent fresh medium was added in. The released VD3 in

withdrawn medium was extracted and measured as described in EE section above. The VD3 percentage released was calculated and plotted as a function of time (up to 6.5 h). The accumulated release profiles of the nanoparticles in the SGI with digestive enzymes were obtained using the method as previously reported (Luo et al., 2011). The weighted samples (10 mg) were first incubated in 30 ml simulated gastric fluid (SGF) with 0.1% pepsin (w/v) for 0.5 h. The digestion was stopped by raising pH to 7.5 using NaOH, and then centrifuged to separate aggregates from supernatant which was collected for VD3 measurement. Subsequently, the 30 ml of simulated intestinal fluid (SIF) with 1.0% pancreatin (w/v) at 37°C was added and digested for 6 h under mild stirring. After digestion, the supernatant was collected by centrifugation and used for VD3 measurement. All measurements were performed in three replicates.

4.3.8 Photochemical-Stability Measurement

The freshly prepared samples (i.e. ZV, B0, and B20) as described in section "preparation of nanoparticles" together with VD3 dispersion in water as control, were used for VD3 stability measurement. VD3 dispersion was prepared by dissolving a small amount of VD3 in ethanol followed by dispersing into water, with the final concentration of VD3 equivalent to nanoparticle samples. Samples in transparent glass vials were placed in a light-proof cabinet, and exposed to two 352 nm UV light bulbs (15 W) for up to 9.5 hours. At exposure time intervals of 0.5, 1.0, 1.5, 3.5, 6.5, and 9.5 h, 200 µl sample was withdrawn from each treatment and then VD3 was extracted and measured according to the method described in previous sections. All measurements were performed in triplicate.

4.3.9 Statistical Analysis

All the experiments were conducted in triplicate with data reported as mean ± standard deviation. Experimental statistics were performed using the SAS software (Version

9.2, SAS Institute Inc., Cary, NC). The analysis of variance (ANOVA) Tukey's multiple comparison tests was used in analysis of differences between physicochemical properties of nanoparticles in different formulations. The significance level (P) was set at 0.05.

4.4 Results and Discussion

4.4.1 Optimization of the Formulation

Particle size and zeta potential are both paramount parameters to prepare stable nanoparticles targeting at nutritional and medical applications. The effects of preparation parameters on particle size and zeta potential in different formulations are summarized in **Table 4.2**. The particle size of VD3-encapsulated zein nanoparticles without CMCS coating was as small as 120 nm with relative small polydispersity (PDI), indicating the size distribution was uniform. After CMCS coating was applied on zein nanoparticles, the particle size varied with calcium concentrations added. Generally, the largest particle size was obtained without both CMCS and calcium (A0). The lower the calcium concentration was added, the smaller the particle size was. A20 sample (with CMCS/calcium ratio of 20:1) had the smallest particle size of 86.3 nm in all formulations ($P<0.05$). At higher concentration of CMCS, particles precipitated at CMCS/calcium ratio of 5:1 (B5) suggesting the aggregation would occur at high calcium concentration, which phenomenon was also observed previously (Shi et al., 2006). However, with same CMCS concentration, more calcium ions resulted in significant smaller PDI (A5 and C5, $P<0.05$) indicating that particle in these formulations may have more uniform particle size. The phase separation method has been considered as a reliable and simple method to produce zein nanoparticles. The preparation of zein nanoparticles was previously reported as shearing zein stock solution into water using a high speed homogenizer (Parris et al., 2005; Zhong & Jin, 2009a), with particle size around 100 nm. Although homogenization with high shearing force is an effective approach to produce

zein nanoparticles particularly when the zein concentration is high, this high-energy method generates heat during homogenization, which might cause loss of labile ingredients encapsulated as we have observed when preparing VD3-loaded zein nanoparticles. To avoid this potential disadvantage, an alternative method to produce zein nanoparticles in low concentration was adopted in this study by pouring zein stock solution into water with stirring. It was found that this low-energy method was applicable to produce zein nanoparticle with diameter of 100 nm, and similar observation was also reported previously (Lai et al., 2011).

Table 4.2. Particle size, polydispersity (PDI), zeta potential, and encapsulation efficiency (EE) of nanoparticles in different formulations.

Samples	Particle size (nm)	PDI	Zeta potential (mV)	LC (%)	EE (%)
ZV	120.2 ± 2.2bc	0.21 ± 0.02d	-26.5 ± 2.8f	3.9 ± 0.1f	52.2 ± 1.7a
A0	200.9 ± 5.9e	0.19 ± 0.01d	-26.8 ± 2.3f	2.4 ± 0.3bcd	64.1 ± 7.3ab
A5	156.6 ± 5.4d	0.07 ± 0.01ab	-13.1 ± 0.5ab	2.2 ± 0.2abc	65.1 ± 3.1ab
A10	116.7 ± 2.9b	0.16 ± 0.02d	-17.0 ± 0.8abc	2.0 ± 0.2abc	56.9 ± 6.6ab
A20	86.3 ± 2.0a	0.18 ± 0.01d	-20.5 ± 1.2cde	2.5 ± 0.1cd	69.5 ± 3.6b
B0	139.5 ± 5.8cd	0.17 ± 0.01d	-25.8 ± 0.6ef	1.8 ± 0.1ab	71.5 ± 2.5b
B5	Large aggregates				
B10	145.3 ± 6.4d	0.15 ± 0.01cd	-16.5 ± 1.9bcd	1.7 ± 0.1a	74.7 ± 5.7c
B20	109.5 ± 11.3b	0.20 ± 0.01d	-20.2 ± 1.7cde	2.1 ± 0.1abc	87.9 ± 1.8c
C0	119.1 ± 5.5bc	0.19 ± 0.02d	-27.2 ± 1.8def	3.2 ± 0.3e	63.5 ± 6.9ab
C5	200.8 ± 16.7e	0.04 ± 0.01a	-11.8 ± 0.3a	2.5 ± 0.2cd	53.1 ±3.7a
C10	113.1 ± 1.9b	0.10 ± 0.00bc	-16.3 ± 1.4abcd	3.0 ± 0.4ed	62.9 ±2.8ab
C20	109.8 ± 2.9b	0.15 ± 0.01cd	-21.0 ± 1.2cef	3.5 ± 0.2ef	72.1 ± 4.3bc

Z, zein; CMCS, carboxymethyl chitosan; VD3, vitamin D3. ZV represents VD3 encapsulated zein nanoparticles. A0-A20 represent formulations with different mass ratio of CMCS/calcium, prepared with mass ratio zein/CMCS as 1:1. B0-B20 represent formulations with different mass ratio of CMCS/Calcium, prepared with mass ratio zein/CMCS as 1:2. C0-C20 represent formulations with different mass ratio of CMCS/Calcium, prepared with mass ratio zein/CMCS as 2:1. Please refer to **Table 4.1** for detailed description of formulations. PDI, polydispersity index. Values with different letters represent significant difference within the column ($P<0.05$).

Zeta potential of VD3-encapsulated zein nanoparticles without CMCS coating was –26.5 mV, and remained the same as CMCS coating was added. As more calcium was added and crosslinked with CMCS through electrostatic interaction, zeta potential became less negative, ranging from –21.0 to –11.8 mV. It was suggested from these results that higher calcium content caused decrease of the absolute value of zeta potential, thus resulted in the polymer aggregation. It was reported that different CMCS/calcium ratio was required to form nanoparticles when the molecular weight of CMCS varied (Shi et al., 2006), showing that CMCS with molecular weight of 38.9 kDa needed only a small amount of calcium to form nanoparticles and excessive calcium would cause aggregation. It is suggested in their study that longer molecular chain was much easier to roll-up when coordinated with calcium ions, compared to shorter chains. Based on the above results, due to much higher molecular weight of CMCS (67 – 79 kDa) used in our study, it was observed that CMCS/calcium ratio of 20/1 could be an appropriate formulation, which generated nanoparticles with particle size less than 110 nm and absolute value of zeta potential higher than 20 mV.

After removal of unencapsulated or loosely attached VD3 from nanoparticles, the effects of different parameters on EE are shown in **Table 4.2**. The EE of zein nanoparticles without CMCS was around 52.2%, and increased up to 71.5% after CMCS was added to the system depending on the CMCS concentration ($P<0.05$). With addition of calcium to the system, the EE increased further up to 87.9% significantly at 20:1 CMCS/calcium and 2:1 CMCS/zein ratios ($P<0.05$). This could be ascribed to the crosslink between calcium and CMCS through electrostatic interactions, resulting in a thicker and denser coatings on the surface of zein nanoparticles and therefore increase of encapsulation efficiency. Due to the decreased surface charges of nanoparticles, too much calcium could cause aggregation of CMCS/calcium particles resulting in lower EE of VD3 (i.e. B5), compared to the formulations with lower calcium concentration (i.e. B20). LC of all samples was within the

range of 1.7 – 3.9%, almost 40 times higher than the previously reported LC of VD2 using bovine casein micelle, which is 0.05% (11). The LC of ZV and samples in C group were higher than samples in A and B groups, which were made with higher CMCS concentration at constant VD3 loading percentage. Therefore, consistently with the observation of particle size and zeta potential, the results of EE also suggested that the optimal formulation was the sample B20.

4.4.2 Physicochemical Characterization

4.4.2.1 Morphological Observation

As shown in **Fig. 4.1A**, the VD3-encapsulated zein nanoparticles without CMCS coatings shared features of a spherical shape and smooth surfaces, with uniform particle size around 100 nm. However, most of the particles were clumped and connected to each other and it was hard to see individual ones, unlike other reported studies, where the individual zein nanoparticles were clearly observed in SEM pictures (Parris et al., 2005; Zhong et al., 2009). This difference might be caused by the low-energy method used in our study instead of high-energy method using high-speed homogenizer in other studies. After zein nanoparticles were coated by CMCS, it was still unable to see individual particles clearly (**Fig. 4.1B**), which might be attributed to the highly hydrophilic CMCS coating on the surface of zein nanoparticles. Interestingly, the addition of calcium made clearer partition of nanoparticles (**Fig. 4.1C**), showing the effect of crosslinking between CMCS and calcium ions. The **Fig. 4.1D** showed the SEM image of B20 nanoparticle after one week storage under room temperature. While the particle size increased a little compared to that of the original nanoparticles (**Fig. 4.1C**), it still maintained the spherical shape and smooth surface, suggesting VD3-encapsulated B20 nanoparticles was stable over time. The freeze-dried

nanoparticles still maintained intact structure and shape after reconstitution into 25% ethanol-aqueous solution (data not shown).

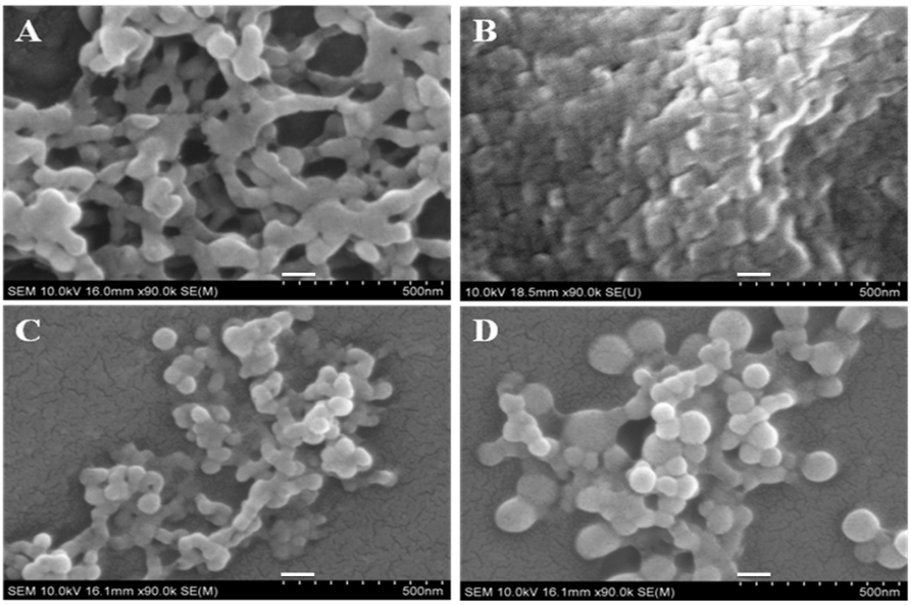

Fig. 4.1. Scanning electron microscopy (SEM) images of prepared nanoparticles. A, ZV sample, VD3 encapsulated zein nanoparticles; B, B0 sample, VD3 encapsulated zein-CMCS nanoparticle complex without calcium; C, B20 sample, VD3 encapsulated zein-CMCS nanoparticle complex with calcium; D, B20 sample after one week storage under room temperature. Please refer to **Table 4.1** for detailed information of formulations. The white bar in each image represents 100 nm.

4.4.2.2 FTIR Study

Fig. 4.2 showed the representative FT-IR spectrum of zein, CMCS and their corresponding VD3 encapsulated complex nanoparticles in different formulations (i.e. B0 and B20). In the infrared spectra, an interesting characterization peak was in the range of 3200 – 3400 cm^{-1}, indicating the hydrogen bonding. The hydrogen bonding in zein and CMCS polymer was at 3312 and 3279 cm^{-1} respectively, and they shifted to 3323 and 3291 cm^{-1} after VD3 was encapsulated, suggesting the hydrogen bonding was formed between VD3 and zein/CMCS. Therefore, the hydrogen bonding among zein, CMCS, and VD3 was considered as one of the major forces facilitating nanoparticles formation. The vibration peaks of 1500 – 1700 cm^{-1}, corresponding to amide I and II bond, had no obvious shift in all formulations. The vibration peak at 1419 cm^{-1} in CMCS could be assigned to the symmetric stretching

vibrations of carboxyl groups (Xiao, Luo, Luo, & Wang, 2011), and it shifted significantly to 1468 cm^{-1} in the B20 sample, indicating the strong electrostatic interactions between carboxyl groups in CMCS and calcium ions. Since both zein and VD3 are highly hydrophobic molecules, the hydrophobic interactions could also contribute to the formation of nanoparticles, besides the hydrogen bonds and electrostatic interactions.

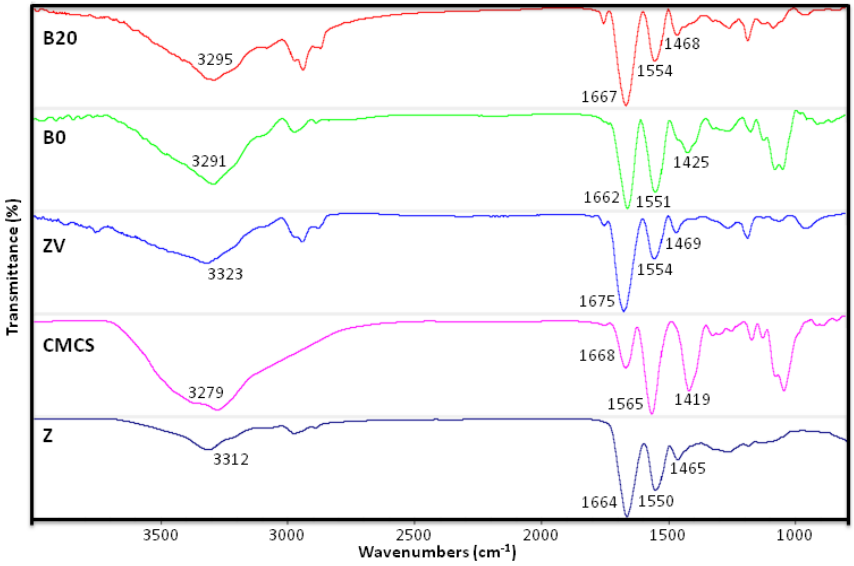

Fig. 4.2 Fourier transform infrared spectroscopy (FTIR) spectra of different samples. Z, zein powder; CMCS, carboxymethyl chitosan powder; ZV, VD3 encapsulated zein nanoparticles; B0, VD3 encapsulated zein-CMCS nanoparticle complex without calcium; B20, VD3 encapsulated zein-CMCS nanoparticle complex with calcium. Please refer to **Table 4.1** for detailed information of formulations.

4.4.2.3 Thermal Property Study

The DSC thermograms corresponding to zein, CMCS, VD3, physical mixture of zein and VD3 (i.e. sample Z+VD3), ZV, and B20 nanoparticles are shown in **Fig. 4.3**. The DSC curve of zein and CMCS exhibited broad endothermic peaks at 74.8 and 91.1 ^{o}C **(Fig. 4.3A)**, respectively. These characteristic endotherms could correspond to the evaporation of bound water from polymer molecules, and the peak for hydrophobic polymer zein was at lower temperature than hydrophilic polymer CMCS, due to the stronger affinity between CMCS and water. Similar phenomenon was also reported in our previous study (*21*). The DSC curve

of VD3 displayed a single melting peak at 88.1^{o}C (**Fig. 4.3A**). For the physical mixture of zein and VD3, both melting peak of VD3 and endothermic peak of zein had been detected (**Fig. 4.3B**). However, only endothermic peaks of zein and CMCS were detected in samples of ZV and B20 nanoparticles, respectively (**Fig. 4.3B**), giving the evidence that VD3 was molecularly dispersed in polymeric matrix and hence encapsulated in the nanoparticles. Similar observation was also reported by Lai and Guo (2011), showing that the absence of endotherm peak of drugs provided the evidence of encapsulation. Interestingly, the small characteristic peak of zein at around 180 ^{o}C was also observed in Z+VD3 and ZV nanoparticles. However, this endotherm peak is not shown in B20 nanoparticles, suggesting that zein might be molecularly dispersed and entrapped in CMCS-calcium matrix.

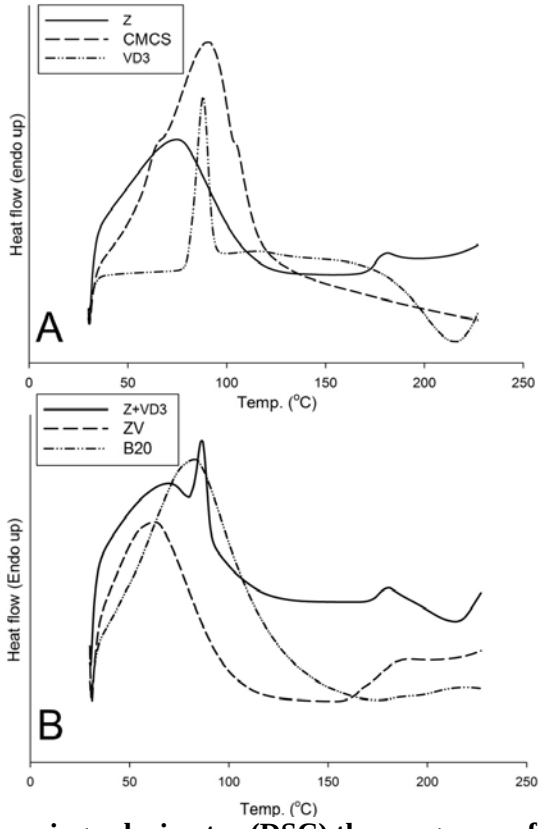

Fig. 4.3. Differential scanning calorimetry (DSC) thermograms of different samples. A, thermograms of each ingredient, i.e., zein, CMCS, VD3. B, thermograms of nanoparticle complex, i.e., ZV, VD3 encapsulated nanoparticles; Z+D, physical mixture of zein and VD3; B20, VD3 encapsulated zein-CMCS nanoparticle complex with calcium. Please refer to **Table 4.1** for detailed information of formulations.

4.4.3 Kinetic Release in PBS and Accumulative Release in SGI

Both of the kinetic release profile of nanoparticles in PBS and accumulative release profile in simulated gastricintestinal fluids with digestive enzymes were evaluated and are shown in **Fig 4.4A** and **4.4B**, respectively. In PBS medium, all formulations showed a first-order release profile, with biphasic kinetic releasing trend, i.e. a burst effect within 1.5 h followed by a sustained release for up to 7 h. ZV and B0 showed similar burst effect occurred at 1.5 h with nearly 60% VD3 released, while less than 40% VD3 was released for B20 sample. In the following sustained release phase, VD3 from B20 was released much more slowly with only about 50% of total VD3 was released after 6.5 h incubation, compared with ZV and B0, both of which had more than 80% VD3 was released. Under the SGI condition with digestive enzymes, ZV and B0 nanoparticles also performed similarly in release profile, with almost 60% being released in gastric fluid and 40% in intestinal fluid. However, release profile in SGI was significantly improved after calcium was added into the system. For the sample B20, only 30% of VD3 was released in gastric fluid and 25% of VD3 was released in intestinal fluid, indicating it had controlled release property in SGI tract. However, almost 100% of VD3 was released for the ZV and B0 nanoparticles after 6.5 h incubation.

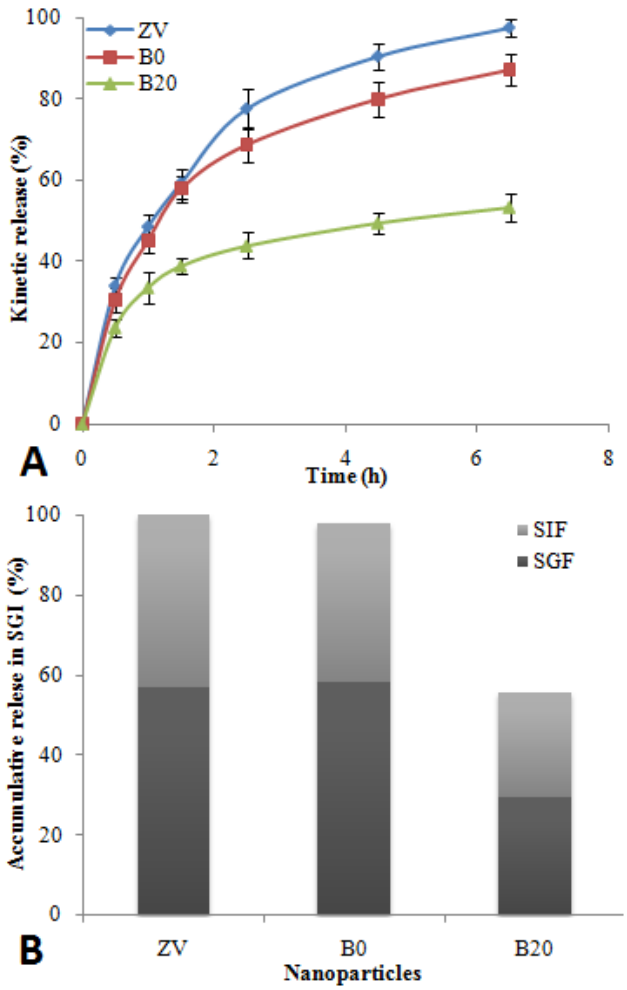

Fig. 4.4 Release profile of VD3 from nanoparticles.
(A) Kinetic release of VD3 from nanoparticles in PBS. (B) Accumulative release of nanoparticles in simulated gastrointestinal (SGI) tract (the standard error of each measurement was within 10% of the mean, n = 3). SGF, simulated gastric fluid; SIF, simulated intestinal fluid; ZV sample, VD3 encapsulated zein nanoparticles; B0 sample, VD3 encapsulated zein-CMCS nanoparticle complex without calcium; B20 sample, VD3 encapsulated zein-CMCS nanoparticle complex with calcium. Please refer to **Table 4.1** for detailed information of formulations.

The delivery system of VD3 in our study was considered as the nanoparticles with hydrophobic core and hydrophilic shell, which has been extensively studied for encapsulating hydrophobic drugs and nutrients through hydrophobic interactions (Luo et al., 2011; Li, Liu, Huang, & Xue, 2011). Based on above results, the zein nanoparticles with CMCS and calcium could provide better controlled release of VD3 in PBS medium, which mimics the

blood condition. In addition, a more significant effect in SGI tract was observed in this study, which could be explained from several aspects. First, only the nanoparticles with addition of CMCS and calcium had the morphology of clear and sphere particles, which could provide a better barrier against release of VD3 than those particles with aggregated bulk morphology. Second, calcium ions served as a crosslinker resulting in formation of dense CMCS coatings on the surface of zein nanoparticles. It was previously reported that the addition of tripolyphosphate anions to self-assembled oleoyl-carboxymethyl chitosan nanoparticles was able to slower the release of entrapped drugs (Li, Zhang, Meng, Chen, & Ren, 2011). Third, the slow release of B20 in gastric fluid might be due to the fact that although CMCS was fully soluble in water at neutral pH, it formed gels when contacting with acidic medium. Therefore, it could form CMCS gel layer, being a barrier against diffusion of VD3 and also slowed down the digestion of zein by enzymes. Compared with our previous study (Luo et al., 2011), it was suggested that the zein nanoparticles coated with CMCS could provide better controlled release in gastric fluid than that coated with native chitosan, because native chitosan is highly soluble under pH of gastric fluid and might decompose quickly. Additionally, the products of partially hydrolyzed zein in gastric fluid may act as emulsifying agents and adsorb onto oil droplets and hence increase its resistance to be degraded in intestinal fluid, resulting in slow release of VD3 in intestinal fluid (Luo et al., 2011; Subirade, Liang, Line, & Remondetto, 2010).

4.4.4 Photochemical Stability Against UV-Light

The freshly prepared samples were put in a light-proof chamber and exposed to UV light for the UV-stability measurement. As shown in **Fig. 4.5**, the control sample VD3 underwent a photochemical degradation very quickly when exposure to 352 nm UV-light. In 9.5 h, only around 30% of VD3 remained in the control. All the nanoparticle samples were able to provide great protection again UV-light induced degradation, with more than 70% of

VD3 remained in samples after 9.5 h UV-light exposure. Especially for the sample B20, around 80% of VD3 had not been degraded, showing the greatest protection among the tested samples. The photochemical stability of VD3 is one of the major hurdles for commercialization of supplement or fortified food products, such as infant formula and milk (Nelson et al., 2007). Encapsulation of labile VD3 into polymeric matrix is a proper way to provide protection against harsh environment. A previous study also demonstrated that encapsulation of vitamin D2 into casein micelles provided partial protection against UV-light induced degradation (Semo et al., 2007). One possible protection mechanism of the protein matrix against photochemical-degradation of VD3 was that protein with aromatic side groups and double bonds can absorb UV light and hence reduce the absorption of UV-light by VD3.

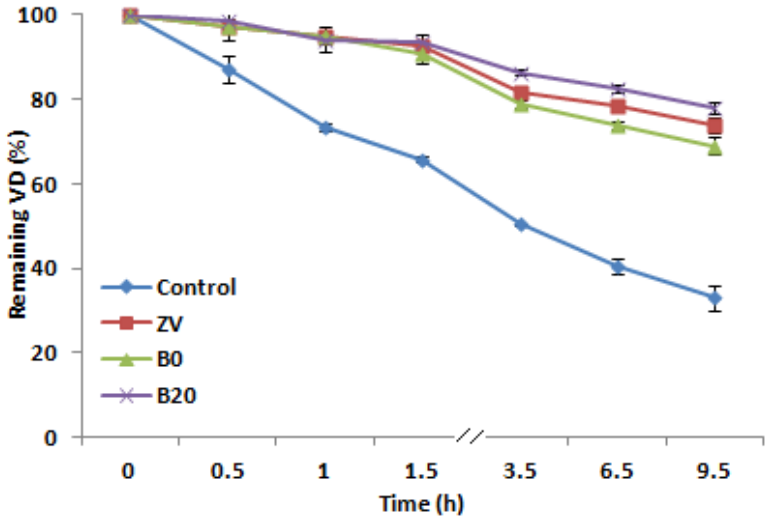

Fig. 4.5. Photochemical stability of different samples against UV-light.
Control, VD3 dispersion in water; ZV sample, VD3 encapsulated zein nanoparticles; B0 sample, VD3 encapsulated zein-CMCS nanoparticle complex without calcium; B20 sample, VD3 encapsulated zein-CMCS nanoparticle complex with calcium. Please refer to **Table 4.1** for detailed information of formulations.

4.5 Conclusion

In conclusion, zein/CMCS complex nanoparticles were successfully developed as a novel delivery system for VD3, using a low energy liquid-liquid dispersion method. Zeta

potential, particle size, and encapsulation efficiency can be modulated with different preparation parameters. The hydrogen bonding, electrostatic interaction as well as hydrophobic interaction were considered as the major forces to facilitate the formation of complex nanoparticles. In terms of their release properties in PBS solution and at SGI conditions, addition of calcium to crosslink with CMCS was found critical for the optimal performance. The photochemical stability against UV light was thought to be mainly contributed from zein protein, given the fact that no significant difference was observed between samples with and without CMCS/calcium. Thus, encapsulation of hydrophobic nutrients in zein/CMCS complex nanoparticles would achieve the controlled release property and improved the stability of labile nutrients. The bioavailability of such complex nanoparticles is currently being studied in our lab using both *in vitro* and *in vivo* approaches and results will be published in the near future.

Chapter 5: Encapsulation of Indole-3-carbinol and Diindolylmethane in Zein/Carboxymethyl Chitosan Nanoparticles with Controlled Release Property and Improved Stability

Luo, Y., Wang, T., Teng, Z., Chen, P., Sun, J., Wang, Q. Food Chemistry (Minor revision for acceptance)

5.1 Abstract

Indole-3-carbinol (I3C) and diindolylmethane (DIM) are two bioactive compounds from Cruciferous vegetables. The stabilities of these compounds are major challenges for pharmaceutical applications. In this study, zein and zein/carboxymethyl chitosan (zein/CMCS) nanoparticles have been prepared to encapsulate I3C and DIM by a liquid-liquid phase separation and ionic gelation method. The particle sizes of zein and zein/CMCS nanoparticles are around 250 and 100 nm, respectively. The zeta potentials are around -10 and -20 mV, respectively. The encapsulation efficiency of zein nanoparticles was greatly improved after being coated with CMCS. Both nanoparticle formulations provided the controlled release of I3C and DIM in PBS medium. In this study, the effects of encapsulation on the stabilities of I3C and DIM were studied under UV-light exposure and thermal (37°C) treatments. Zein and zein/CMCS nanoparticles provided similar protection for both I3C and DIM against UV-light, attributed to the contribution of zein protein. Under thermal conditions, I3C control degraded and oligomerized to form DIM and other products after 24 h. Zein/CMCS nanoparticles not only protected I3C from

degradation, but also inhibited the dimerization to DIM and other products, showing significantly better protection than zein nanoparticles. Based on our results, the encapsulation of hydrophobic bioactives in zein/CMCS nanoparticles is a promising approach to improve stability against harsh conditions, and may provide a possible way to determine the efficacy of I3C and DIM.

5.2 Introduction

Cruciferous vegetables, such as broccoli and cabbage, are well-known health-promoting vegetables because they are rich in glucosinolates, the sulfur-containing compounds. Glucosinolates can be broken down through hydrolysis into different products, among which indole-3-carbinol (I3C) is the major compound attributed to beneficial effects. I3C has been extensively studied in in vitro and in in vivo carcinogenesis models and the results consistently indicated its potency to influence carcinogenesis during initiation and promotion phases of cancer development, including cancers of lung, breast, stomach, colon, and prostate (Kim & Milner, 2005). However, the stability of I3C is the major problem for elucidating its efficacy. Under acidic conditions, I3C molecules undergo oligomerization to form a mixture of compounds, known collectively as acid condensation products (Shertzer & Senft, 2000). 3,3-Diindolylmethane (DIM) is the dimerization products of I3C, a major oligomerization product. DIM has also been proven to have potent cancer prevention effects (Abdelrahim, Newman, Vanderlaag, Samudio, & Safe, 2006; Shorey, Hagman, Williams, Ho, Dashwood, & Benninghoff, 2012; Wang, Schoene, Milner, & Kim, 2012). The in vivo bioavailability of I3C is still not clear, because the rapid acid oglimerization in the stomach after oral consumption makes it difficult to be

determined and differentiated from its oglimerization products, such as DIM. Recently, the stability of I3C in neutral cell culture media has been studied, showing that more than 50% of I3C undergoes dimerization into DIM in 24 h at 37°C conditions (Bradlow & Zeligs, 2010). Some animal studies on the efficacy of I3C were based on the oral administration by gavage to the stomach (Choi, Kim, Park, Lee, & Park; Qian, Melkamu, Upadhyaya, & Kassie, 2011), but one recent study pointed out that the clearance time for I3C was within 1 h after oral administration of I3C (250 mg/kg) in mice (Anderton, Manson, Verschoyle, Gescher, Lamb, Farmer, et al., 2004), and many other condensation products were detected. Therefore, the in vivo biological activity of I3C has been considered to be at least partially contributed by the oligomerization products during digestion in stomach. Also, I3C in vegetables or supplements degrades quickly under different processing conditions, such as heat and light (Vallejo, Tomas-Barberan, & Garcia-Viguera, 2002). Given the issues of instability of I3C under various conditions, it is difficult to predict the efficacy of a pure compound of I3C during storage or after oral consumption; and the dimerization of I3C to DIM, makes it even more difficult to determine its efficacy in terms of cancer prevention.

Encapsulation technology, as a novel approach, has drawn increasing attention for its applications in the food industry, with the aim to protect labile compounds from harsh conditions, namely, to preserve sensitive bioactive compounds, mask off-odor of some ingredients, as well as provide controlled release and target delivery properties (Arvanitoyannis, 2009; de Vos, Faas, Spasojevic, & Sikkema, 2010). Several delivery systems have been reported to improve the chemical stabilities of

natural bioactives (e.g. ascorbic acid, β- Carotene, caffeic acid, anthocyanins) to extend the shelf life and preserve the functionalities (Coimbra, Isacchi, van Bloois, Torano, Ket, Wu, et al., 2011; Han, Guenier, Salmieri, & Lacroix, 2008; Oidtmann, Schantz, Mäder, Baum, Berg, Betz, et al., 2011). Zein, the prolamine protein from corn, and chitosan, the derivative of natural polysaccharide chitin, are both food biopolymers that have been extensively investigated for their ability to encapsulate food bioactives (Dudhani & Kosaraju, 2010; Elzoghby, Samy, & Elgindy, 2012; Hu, Ting, Zeng, & Huang, 2012; Patel, Hu, Tiwari, & Velikov, 2010; Xiao & Zhong, 2011). The complex nanoparticles prepared with the combination of zein and chitosan or its derivatives have been developed in our lab as versatile delivery systems for various bioactives with wide range of hydrophobicity (Luo, Teng, & Wang, 2012; Luo, Zhang, Cheng, & Wang, 2010). For example, chitosan/tripolyphosphate nanoparticles coated with zein were used to encapsulate hydrophilic micronutrient (selenite) to improve release profile and bioactivities (Luo, Zhang, Cheng, & Wang, 2010). Carboxymethyl chitosan (CMCS) is one of the water soluble derivatives of chitosan and has been reported to form nanoparticles with calcium ions through ionic gelation for drug delivery (Shi, Du, Yang, Zhang, & Sun, 2006; Snima, Jayakumar, Unnikrishnan, Nair, & Lakshmanan, 2012). Zein nanoparticles coated with CMCS have proven to be a promising delivery system to improve release profile and enhance photo-stabilities of hydrophobic nutrients, such as vitamin D3 (Luo, Teng, & Wang, 2012).

Therefore, it is of great interest to study if the encapsulation of I3C and DIM in nanoparticles could provide a controlled release property and enhance their

stabilities from harsh environmental conditions. In the current study, I3C and DIM were encapsulated into zein nanoparticles, and then CMCS was applied to form a coating on the nanoparticles. The comparison of two delivery systems was studied, in terms of physicochemical properties of nanoparticles and their protective effects on stabilities of I3C and DIM, including thermal- and photo-stability. The effect of encapsulation on the dimerization of I3C to DIM was monitored during the stability test.

5.3 Materials and Methods

5.3.1 Materials

I3C and DIM were purchased from Sigma-Aldrich Chemical Co. Ltd. (St. Louis, MO). Zein with a minimum protein content of 97% was provided by Showa Sangyo (Tokyo, Japan). CMCS was purchased from Nantongxingcheng Biological Product Inc. (Nantong, Jiangsu Province, China), with a deacetylation degree of 96% and a carboxylation degree of 65%. Acetonitrile and tert-butyl methyl ether were of HPLC-grade and other chemicals were of analytical grade, purchased from Sigma-Aldrich.

5.3.2 Preparation of Nanoparticles

I3C (5 mg/ml) was dissolved in pure ethanol as a stock solution. Zein (5 mg/ml) was dissolved in 70% aqueous-alcohol solution. CMCS (1 mg/ml) was dissolved in pure water. Zein nanoparticles were prepared by a liquid-liquid phase separation method as reported in our previous study (Luo, Teng, & Wang, 2012). Briefly, 80 μL of I3C solution (5 mg/ml) was added into 2 mL of zein solution in a dropwise manner under mild stirring for 30 min. Then, the above zein-I3C solution was immediately poured into 5 mL of pure water or CMCS solution (containing 200 μL 0.5% Tween20), under vigorous stirring until a single phase was

formed. Then, 1 mL of calcium chloride solution (0.25 mg/ml) was added under stirring. The obtained opaque nanoparticles dispersion was freeze-dried for 48 h. The control nanoparticles were prepared by replacing CMCS and calcium solution with pure water in parallel. I3C and DIM- encapsulated zein nanoparticles were defined as Z/I and Z/D, respectively. And I3C and DIM- encapsulated zein nanoparticles with CMCS coating were defined as ZC/I and ZC/D, respectively.

5.3.3 Morphological Observation

Morphological structures of nanoparticles were observed by a scanning electron microscopy (SEM, Hitachi SU-70, Pleasanton, CA). Samples were first cast-dried on an aluminum pan and then cut to an appropriate size and adhered to conductive carbon tapes (Electron Microscopy Sciences, Fort Washington, PA). Subsequently, they were mounted on specimen stubs and coated with a thin (<20 nm) conductive gold and platinum layer using a sputter coater (Hummer XP, Anatech, Union City, CA). Representative SEM images were reported.

5.3.4 X-Ray Diffraction (XRD)

The X-ray diffraction (XRD) patterns of each individual ingredient, nanoparticles, as well as the physical mixture of zein and I3C/DIM were recorded on a Bruker D8-Advance Diffractometer (Bruker AXS Inc., Madison, WI, USA) with backgroundless sample holders. The physical mixture of zein and I3C/DIM was in the ratio of 25:1, which was the same ratio as the nanoparticles. The working parameters are as follows: voltage of 40 kV, current of 40 mA, and scanning rate of 3 min^{-1}.

5.3.5 Particle Size and Zeta Potential

The freshly prepared nanoparticle samples were used for particle size and zeta potential measurements. Hydrodynamic diameters were measured by a dynamic light

scattering instrument (DLS, BI-200SM, Brookhaven Instruments Corp., Holtsville, NY). DLS is equipped with a 35mW HeNe laser beam at a wavelength of 637 nm. The polydispersity (PDI) was also reported, representing for the distribution of particle size. All DLS measurements were performed at 25°C. Surface charge of different samples were measured by a laser Doppler velocimetry (Zetasizer Nano ZS90, Malvern, UK), using a fold capillary cuvette (Folded Capillary Cell– DTS1060, Malvern, UK). Surface charge was expressed by zeta potential, which was converted from the measured electrophoretic mobility using the Smoluchowski theory. All measurements were performed in triplicate.

5.3.6 Encapsulation Efficiency (EE)

EE was measured based on our previous method with minor modifications (Luo, Teng, & Wang, 2012). Briefly, 10 mg of lyophilized nanoparticle samples were flushed with 1 ml ethyl acetate three times, using No.1 Whatman filter paper. Then the washed samples were dried in a vacuum oven (VWR international, PA). The ethyl acetate elute containing free compounds was dried in the presence of 30 µl DMSO under a stream of nitrogen gas. The residue was then suspended in 600 µl of acetonitrile. Samples were filtered through 0.2 µm membrane and the filtrate was transferred to amber vials and analyzed by HPLC.

5.3.7 Release Profile

It is important to understand how I3C and DIM release from nanoparticles in different medium. The release profile measurements were carried out in phosphate buffer saline (PBS) medium, according to our previous method (Luo, Teng, & Wang, 2012). Briefly, certain amount of freeze-dried nanoparticles (10 mg) were incubated in 30 ml PBS (pH 7.4) containing Tween-20 (0.5%) to create sink conditions for I3C and DIM, at 37°C. At designated time intervals, 2 ml of release medium was removed and replaced with fresh PBS

containing Tween20. The removed medium was then freeze dried for 24 h, extracted, and analyzed by HPLC.

5.3.8 Effects of Encapsulation on Stabilities of I3C and DIM

The photo-stability and thermal stability of encapsulated-I3C and -DIM were evaluated as a function of time. Photo-stability was carried out under exposure of ultraviolet light (UV, 15W) for 10 h. Freshly prepared samples were subjected to a stability test. The control sample was prepared by adding the compound (I3C or DIM dissolved in ethanol) in the same amount of aqueous-alcohol system without zein or CMCS, to obtain the final concentration of the compound equivalent to nanoparticle samples. Samples in transparent glass vials were placed in a light-proof cabinet and exposed to two 352 nm UV light bulbs (15 W) for up to 10 h. At the designated time intervals, 400 µl was withdrawn from each sample and then analyzed by HPLC. For the thermal stability test, nanoparticle samples were incubated in 37°C water bath for up to 4 d. Freshly prepared samples were transferred to 15 ml centrifuge tubes with screw caps. The control samples were also prepared as described above. All the samples were placed in 37°C water bath, 400 µl was withdrawn from each sample on day 1, 2, 3 and 4, then analyzed by HPLC. All measurements were performed in triplicate.

5.3.9 High Performance Liquid Chromatography (HPLC)

For release and stability tests, the withdrawn samples were placed in a screw cap centrifuge tube and extracted according to a previously described method with a slight modification (Anderton, Jukes, Lamb, Manson, Gescher, Steward, et al., 2003). Briefly, the withdrawn samples were first freeze-dried for 24 h. The lyophilized powder of each sample was extracted three times with tert-butyl methyl ether (TBME, 1 ml) involving 5 m sonication for the first occasion and 30 s vortexing on the following two occasions. Subsequent to each

extraction, the samples were centrifuged at 6000 g for 10 m and the supernatant was transferred to a new tube. For each sample, the combined TBME layers were evaporated rapidly under nitrogen gas in the presence of 15 µl DMSO. The extracted sample in DMSO was then reconstituted in acetonitrile (300 µl) and filtered through a 0.2 µm membrane into amber vials for measurement.

HPLC analysis of extracted samples was performed on a Hewlett Packard 1100 series HPLC system (Palo Alto, CA), equipped with DAD phototiode array detector and an auto-sampler operated by a Chemstation. The column heater was set at 25 oC. The extracted standard/sample (10 µl) was injected into the HPLC system. Chromatography was achieved using a Phenomenex C18 (250 × 2 mm, 5 µm) column in tandem with a guard column. The mobile phase consisted of water (A) and acetonitrile (B). The gradient is as follows: 15% B to 60% B from 0 to 20 min; linear gradient to 75% B from 20 to 25 min; linear gradient to 85% B from 25 to 30 min, and kept at 85% B from 30 to 38 min; linear gradient to 15% B from 38 to 40 min, and then kept at 15% B for 5 min. Total run time was 45 min, and the flow rate was 0.25 ml/min. Samples were quantified by a UV detector at 280 nm.

5.4 Results and Discussion

5.4.1 Physicochemical Characterization

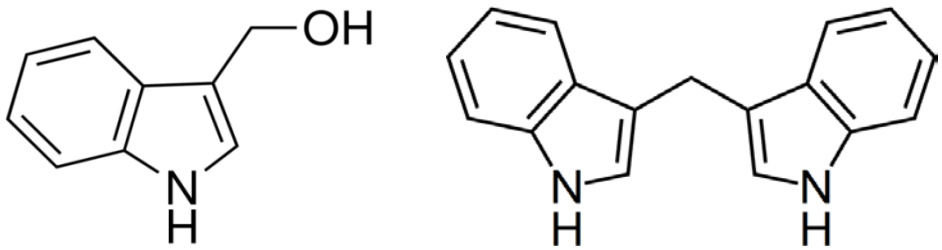

Indole-3-carbinol (I3C) Diindolylmethane (DIM)

Fig. 5.1. Chemical structures of I3C and DIM.

Protein is considered a promising biomaterial to develop nanoparticles for encapsulation, however, in many cases protein itself as a single encapsulant may not be enough to provide appropriate protection and controlled release property for encapsulated drugs or nutrients (Chen & Subirade, 2005; Gunasekaran, Ko, & Xiao, 2007). Hence, a second layer, usually a polysaccharide is usually applied to coat protein nanoparticles to improve the physicochemical properties for certain applications. Zein nanoparticles coated with CMCS have been developed in our lab as a promising approach to encapsulate fat-soluble bioactive compounds with improved stability and prolonged release property (Luo, Teng, & Wang, 2012). In the current study, zein/CMCS nanoparticles are investigated to encapsulate two labile fat-soluble phytonutrients, i.e. I3C and DIM (**Fig. 5.1**), in order to improve their stability during storage and preserve their efficacy after oral consumption. Based on our previous study, mass ratio of zein/CMCS and CMCS/calcium are determined as 1:1 and 20:1, respectively.

Table 5.1. Characterization of nanoparticles.

Samples [a]	Particle size (nm)	PDI	Zeta potential	EE
Z/I	252.8 ± 7.3	0.11 ± 0.01	-11.20 ± 0.26	63.77 ± 1.34
ZC/I	113.5 ± 2.7	0.19 ± 0.01	-19.53 ± 2.26	77.79 ± 3.79
Z/D	250.8 ± 6.4	0.04 ± 0.00	-9.98 ± 1.64	69.66 ± 1.52
ZC/D	89.1 ± 4.3	0.19 ± 0.00	-19.80 ± 0.80	78.08 ± 0.69

[a], Z/I and Z/D represent I3C- and DIM-encapsulated zein nanoparticles, respectively; ZC/I and ZC/D represent I3C- and DIM-encapsulated zein/CMCS nanoparticles. PDI, polydispersity; EE, encapsulation efficiency.

Table 5.1 summarizes the characterization of the nanoparticles, including particle size, PDI, zeta potential, as well as EE. Particle size of zein nanoparticles is around 250 nm for encapsulation of both bioactive compounds. As a result of being coated with CMCS, the particle size decreased to 113 nm for I3C and 89 nm for DIM. This difference may be in part due to the fact that DIM is more hydrophobic than I3C. DIM may interact with zein protein

via stronger hydrophobic interactions upon phase separation process resulting in nanoparticles with more compact structure. The PDI of all nanoparticle formulations were within 0.2, indicating small distribution of particle size. The zeta potential of zein nanoparticles of I3C and DIM were –11.2 mV and –9.98 mV, respectively, and dropped to around -20 mV after zein nanoparticles were coated by CMCS. The decrease of zeta potential indicated the adsorption of CMCS of the surface of zein nanoparticles. The EE of zein nanoparticles were within 60 – 70% for both compounds, but significantly increased to almost 80% after nanoparticles were coated with CMCS. This observation is similar to our previous study that CMCS coating on zein nanoparticles could improve vitamin D3 encapsulation efficiency. Several other studies also reported the beneficial effects on encapsulation efficiency by coating nanoparticles with a second polymer (Briones & Sato, 2010; Trapani, Sitterberg, Bakowsky, & Kissel, 2009).

5.4.2 Morphological Observation

As demonstrated in **Fig. 5.2**, I3C and DIM-encapsulated zein nanoparticle is successfully fabricated in our study by liquid-liquid phase separation method. Both nanoparticles shared similar features of spherical shape and smooth surface (**Fig. 5.2**, Z/I and Z/D). The CMCS coating caused the particle size of both nanoparticles to decrease and more uniform nanoparticles were formed (**Fig. 5.2**, ZC/I and ZC/D).

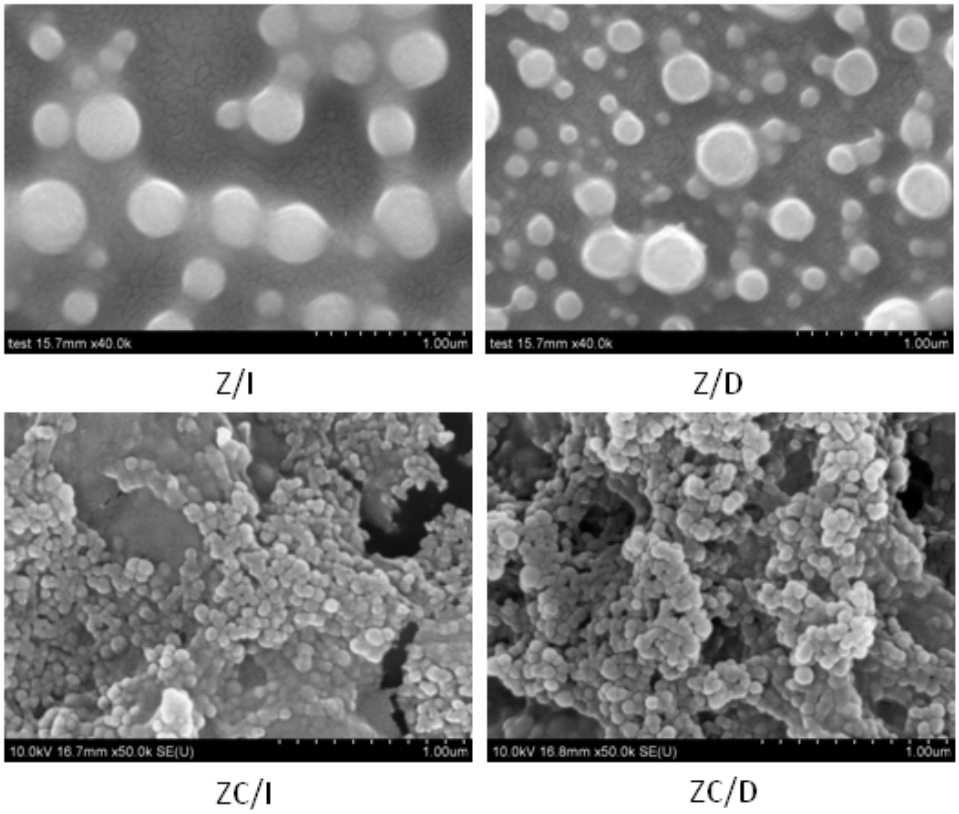

Fig. 5.2. Morphological observation with scanning electron microscopy (SEM).
Z/I and Z/D represent I3C- and DIM-encapsulated zein nanoparticles, respectively; ZC/I and ZC/D represent I3C- and DIM-encapsulated zein/CMCS nanoparticles.

5.4.3 XRD Analysis

The XRD patterns of nanoparticles, pure ingredients as well as their physical mixtures are shown in **Fig. 5.3**. The major characteristic peaks of I3C and DIM are at 11.48°, 17.16° and 13.59°, 18.70°, respectively, indicating their highly crystalline nature, which is consistent with reported literature (Maciejewska, Wolska, Niemyjska, & Żero, 2005). These characteristic peaks were also detected in the physical mixture of zein + I3C and zein + DIM samples, but the intensity of these peaks were significantly decreased due to the small mass ratio to zein protein. In contrast, zein protein showed two flatter peaks instead of sharp peaks, indicating the amorphous nature of the protein. After encapsulation, the characteristic peaks for I3C and DIM disappeared. This pattern showed that the crystalline structure of I3C and

DIM were converted into amorphous state in nanoparticles, providing additional evidence of encapsulation. This phenomenon was also reported by other studies that the disappearance of characteristic peaks of encapsulated crystal compounds after encapsulation confirmed the encapsulation process (Teng, Luo, & Wang, 2012).

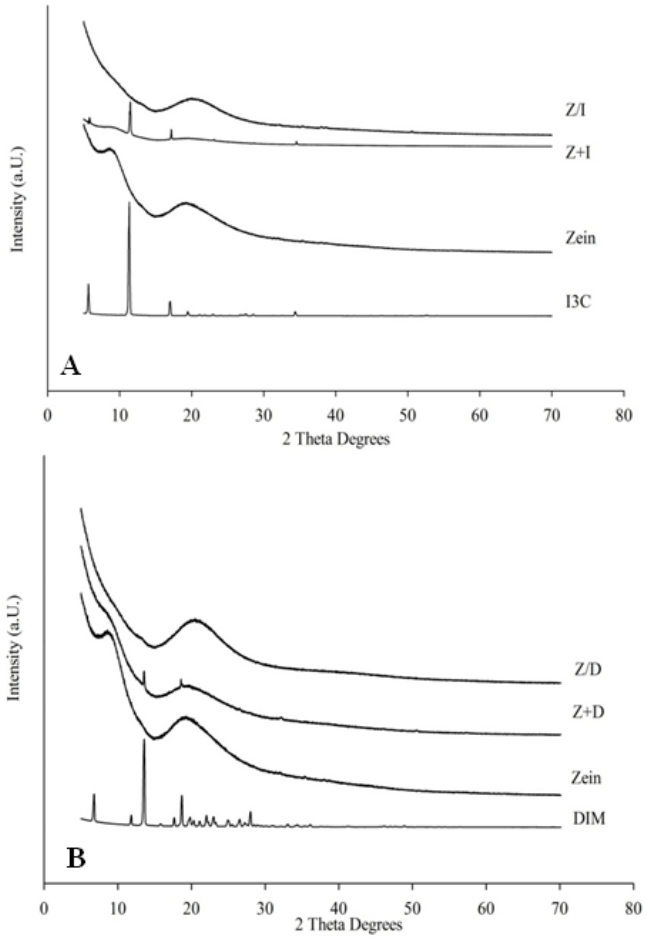

Fig. 5.3. XRD patterns of physical mixture and nanoparticles.
Z/I and Z/D represent I3C- and DIM-encapsulated zein nanoparticles, respectively; ZC/I and ZC/D represent I3C- and DIM-encapsulated zein/CMCS nanoparticles..

4.4.4 Controlled Release Profile

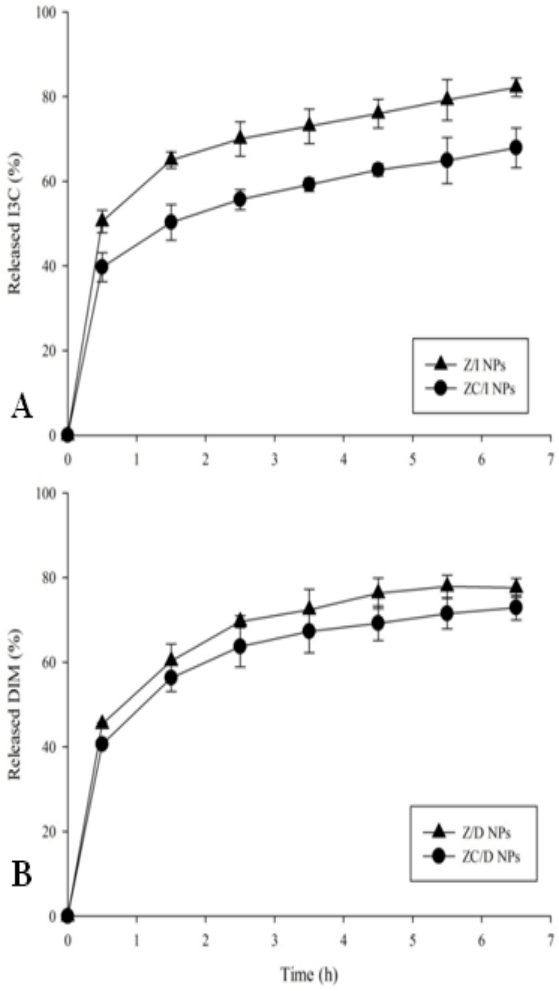

Fig. 5.4. Release profile of I3C and DIM from nanoparticles.
Z/I and Z/D represent I3C- and DIM-encapsulated zein nanoparticles, respectively; ZC/I and ZC/D represent I3C- and DIM-encapsulated zein/CMCS nanoparticles.

Fig. 5.4 shows the release profiles of I3C (A) and DIM (B) from nanoparticles in the PBS system. All formulations of nanoparticles showed a first-order release profile, consisting of biphasic trend of burst effect and sustained release. Both I3C and DIM-encapsulated nanoparticles demonstrated a similar trend, the burst effect occurred within 0.5 h; followed by sustained release for more than 6 h. For zein nanoparticles without CMCS coating, around 45-50% of the compounds released out from nanoparticles, while for CMCS coated nanoparticles the burst effect of both compounds were reduced to around 40%. The CMCS

coating also helped reduce the sustained release for 6.5 h, and this effect was more significant in I3C-encapsulated nanoparticles. The effects of various coatings on the improvement of release profile of compounds from nanoparticles have been well documented (Grenha, Remunan-Lopez, Carvalho, & Seijo, 2008; Luo, Zhang, Cheng, & Wang, 2010; Luo, Zhang, Whent, Yu, & Wang, 2011). Compared with our previous study (Luo, Teng, & Wang, 2012), however, the effect of CMCS coating on kinetic release profile was not as prominent as before. The possible reason of this phenomenon might be, in part, due to the strong hydrophobicity of the I3C and DIM and that the surfactant (Tween-20) was added during the nanoparticles preparation procedure, resulting in the increase of diffusion rate and the solubility of the encapsulated compounds into the release medium. This observation was also reported in a previous study pointing out that inclusion of Tween-20 into microspheres accelerated the release of encapsulated antimicrobial compounds (Xiao, Gommel, Davidson, & Zhong, 2011).

5.2.5 Thermal Stability

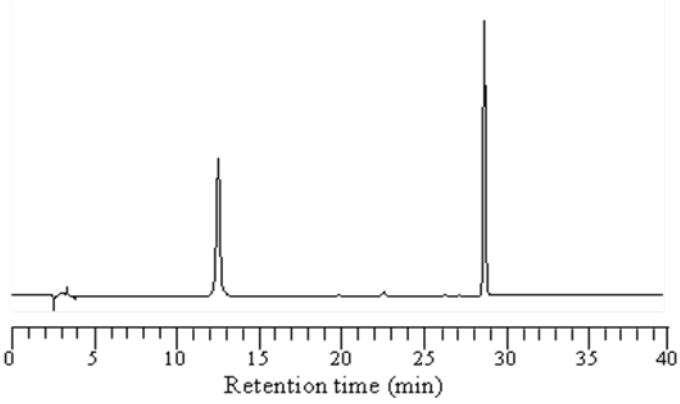

Fig. 5.5. HPLC spectra of combination of I3C and DIM standard.

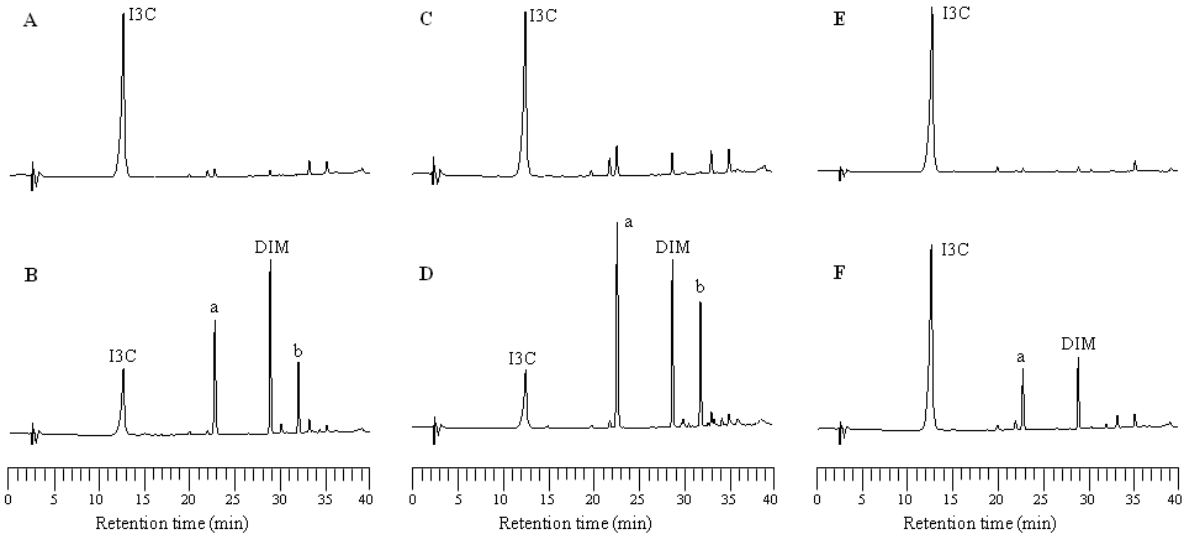

Fig. 5.6. Effects of encapsulation on thermal stability of I3C under 37°C.
A, C, E represent I3C levels in I3C control, Z/I, ZC/I samples, respectively, at the beginning of incubation (0 day); B, D, F represent I3C levels in I3C control, Z/I, ZC/I samples, respectively, after 24 h (1 day) incubation under 37°C. Z/I and ZC/I represent I3C-encapsulated zein and zein/CMCS nanoparticles, respectively. a and b represent 1-(3-hydroxymethyl)-indolyl-3-indolylmethane (HI-IM) and [2-(indol-3-ylmethyl)-indol-3-yl]indol-3-ylmethane (LTr), respectively.

The effects of encapsulation on the thermal stability of I3C and DIM were tested after incubation in 37°C water bath for 3 days. The chromatography of the standard mixture of I3C and DIM is shown in **Fig. 5.5**, with retention time around 12.5 and 28.5 min, respectively. **Fig. 5.6** shows the thermal stability of I3C after 24 h incubation. The control sample of pure I3C compound demonstrated the fastest degradation rate, followed by I3C encapsulated zein and zein/CMCS nanoparticles. From comparison of initial chromatography of I3C control and after 24 h incubation (**Fig. 5.6A and B**), it is suggested that DIM is the major dimerization product, along with other two products whose retention time are 22.5 m (peak a) and 31.8 m (peak b). According to the reference method (Anderton, et al., 2004), it could be postulated that peak a and b stand for the I3C condensation products 1-(3-hydroxymethyl)-indolyl-3-indolylmethane (HI-IM) and [2-(indol-3-ylmethyl)-indol-3-yl]indol-3-ylmethane (LTr), respectively. Zein nanoparticles provided little protection of I3C from thermal degradation (**Fig. 5.6C and D**). However, after zein nanoparticles were coated

with CMCS, the protection effect was so greatly improved that only a small amount of DIM and HI-IM were formed after 24 h incubation (**Fig. 5.6E and F**). During the thermal stability measurement, the precipitation of zein nanoparticles after 24 h incubation was clearly observed, due to the denaturation of zein protein under heat treatment. The denaturation of zein protein resulted in the collapse of nanoparticle structure and thus lost the protection of encapsulated I3C. CMCS, as a coating on zein nanoparticles, may decrease the denaturation rate of zein protein and preserve the protective effects. Chitosan nanoparticles have also been studied to encapsulate L-ascorbic acid and its stability during heat processing was greatly improved than unencapsulated L-ascorbic acid (Jang & Lee, 2008). Unlike I3C, DIM was much more stable to thermal treatment, as shown in **Fig. 5.7**. The DIM control maintained 80% of its original concentration even after 4 days of incubation in 37°C condition. The protective effects of zein and zein/CMCS nanoparticles on DIM thermal degradation showed a similar trend to that of I3C. The zein nanoparticles demonstrated very little protection on DIM degradation, but the CMCS coating on zein nanoparticles provided prominent protection of around 90% and remained intact after 4 days incubation.

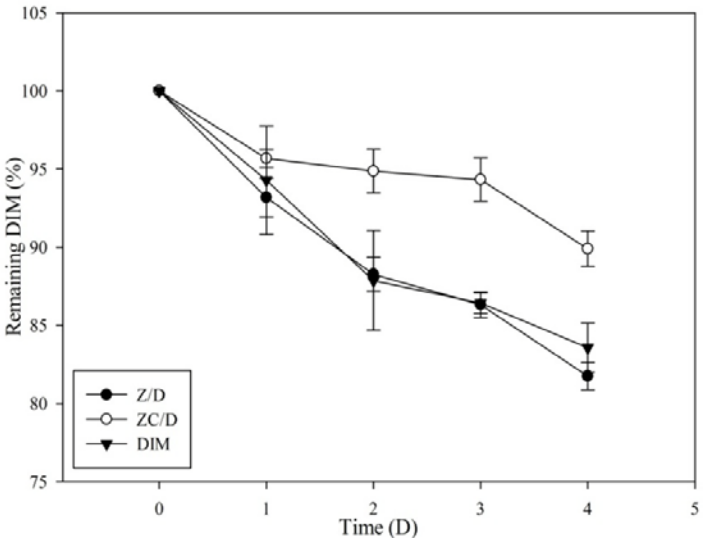

Fig. 5.7. Effects of encapsulation on thermal stability of DIM.
Z/D and ZC/D represent DIM-encapsulated zein zein/CMCS nanoparticles, respectively.

Table 5.2. I3C and DIM levels in I3C control, Z/I and ZC/I nanoparticles under 37°C incubation for 3 days.

Samples [a]	0 Day		1 Day		2 Day		3 Day	
	I3C	DIM	I3C	DIM	I3C	DIM	I3C	DIM
I3C control	49.50	-	26.97 ± 1.47	10.36 ± 0.28	9.71 ± 0.99	4.98 ± 0.07	8.30 ± 1.00	5.18 ± 0.07
Z/I NPs	49.50	-	27.60 ± 4.11	10.25 ± 1.00	6.51 ± 1.75	4.38 ± 0.79	5.53 ± 1.00	3.38 ± 0.25
ZC/I NPs	44.05	-	39.59 ± 0.84	3.06 ± 0.23	20.67 ± 0.38	3.39 ± 0.14	19.80 ± 0.38	3.88 ± 0.20

[a], Z/I and Z/D represent I3C- and DIM-encapsulated zein nanoparticles, respectively; ZC/I and ZC/D represent I3C- and DIM-encapsulated zein/CMCS nanoparticles, respectively.

Although the stabilities of I3C and DIM in acidic conditions have been extensively studied, their thermal stabilities are rarely reported in the literature. From our study, the thermal stability of I3C is much poorer than DIM at 37°C. Ciska et al. investigated the effect of boiling on the content of I3C and DIM in fermented cabbage (Ciska, Verkerk, & Honke, 2009). In their study, the content of I3C detected in both boiling water and cabbage decreased with boiling time within 30 min before reaching a plateau, due to its thermal instability; however, the DIM concentration kept increasing for 50 min. Another recent study pointed out the I3C dimerized to DIM during cell culture experiment conditions at 37°C (Bradlow & Zeligs, 2010). It has been well documented that I3C undergoes oligomerization in aqueous acidic medium, and the acid condensation products include 7 compounds (Grose & Bjeldanes, 1992). Our study shows that I3C oligomerized to three products during the thermal treatment, with DIM as the major compound. The contents of I3C and DIM in different samples during 3 days of thermal treatment were also recorded quantitatively and summarized in **Table 5.2**. After 1 day of thermal treatment, the I3C contents in I3C control and Z/I nanoparticles, only 55% of original I3C was remained and large amount of DIM (around 10.00 μg/ml for both samples) was detected. Whereas in nanoparticles with CMCS coating (ZC/I) sample, 90% of I3C was intact and minimal DIM formation was found (3.26 μg/ml). After 3 days of thermal treatment, less than 17% and 12% of I3C were detected in

control and Z/I nanoparticle samples, respectively, however, 45% of I3C was preserved in ZC/I nanoparticles.

5.4.6 Photo-Stability against UV-Light

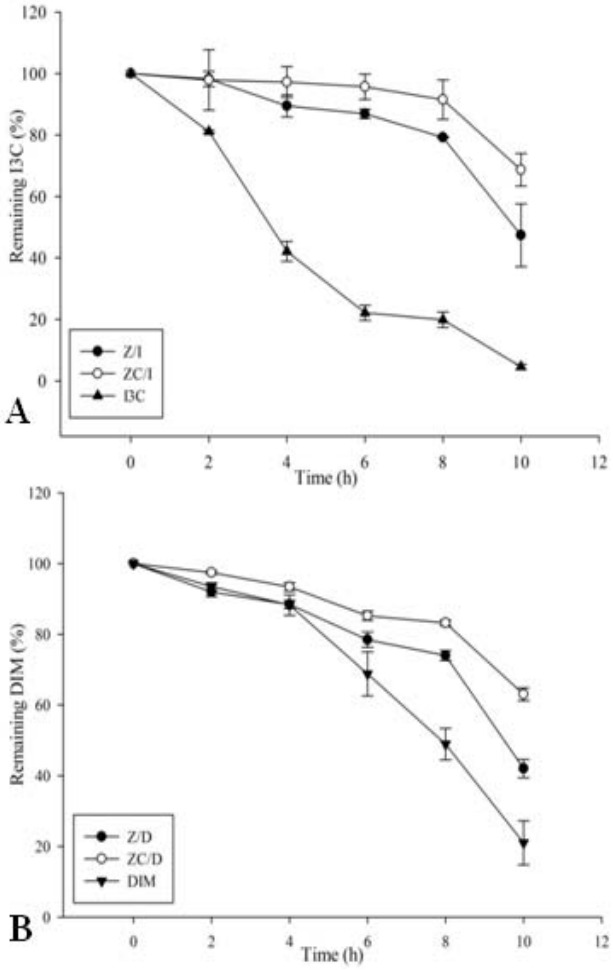

Fig. 5.8. Effects of encapsulation on photo-stability of I3C/DIM against UV.
Z/I and Z/D represent I3C- and DIM-encapsulated zein nanoparticles, respectively; ZC/I and ZC/D represent I3C- and DIM-encapsulated zein/CMCS nanoparticles, respectively.

In addition to temperature, light is another major factor causing oxidation, isomerization, and oligomerization of phytonutrients. Both I3C and DIM are the phytochemicals with aromatic rings possessing UV absorption ability which may result in their instability when exposed to UV light. The effect of encapsulation on their photo-

stabilities is shown in **Fig. 5.8**. Both I3C and DIM were extremely susceptible to UV light exposure, and I3C degraded faster than DIM. Within 6 h of UV light exposure, there was only less than 20% of I3C left in the control sample (**Fig. 5.8A**). Both of nanoparticle formulation preserved I3C content to as high as 80% for the first 6 h exposure. At the end of 10 h, I3C in control sample was not detectible, but around 50% and 70% of I3C was detected in zein and zein/CMCS nanoparticles, respectively. Compared with I3C, DIM was relatively stable given that a lag phase was observed before the rapid degradation began (**Fig. 5.8B**). At 4 h of incubation, there was more than 80% of DIM in all samples but the content decreased rapidly to less than 20% in the control sample in the following incubation. The HPLC chromatograph of UV-exposed samples indicated that I3C oglimerized to DIM, HI-IM as well as LTr but in smaller amount (data not shown) than thermal treatment. Because of the hydroxyl group in the carbinol side chain connecting to indole structure, I3C is much more reactive than DIM, resulting in the fast formation of cations and consequent photo-oxidation initiated by UV light exposure (Bloch-Mechkour, Bally, & Marcinek, 2011). Encapsulation of DIM into nanoparticles prolonged the lag phase to 8 h, with more than 75% intact. At the end of 10 h incubation, more than 40% and 60% of DIM was remained in zein and zein/CMCS nanoparticles, respectively. Therefore, encapsulation of I3C into nanoparticles provided greater protection against UV light, and slightly better protection was observed for CMCS coated zein nanoparticles. The protection against UV light was mainly contributed by zein protein containing aromatic side groups and double bonds which can absorb UV light. This observation was similar to that reported in our previous study (Luo, Teng, & Wang, 2012).

5.5 Conclusion

In summary, zein and zein/CMCS nanoparticles were successfully prepared to encapsulate hydrophobic bioactives I3C and DIM. The encapsulation was evidenced by XRD. Zein/CMCS nanoparticles showed better encapsulation efficiency and smaller particle size, than zein nanoparticles. Both nanoparticle formulations provided controlled release of the bioactive compounds. The stabilities of I3C and DIM were significantly improved after they are encapsulated in nanoparticles. Compared with zein nanoparticles, zein/CMCS nanoparticles provided better protection of I3C against degradation and dimerization under UV-light and thermal conditions. The study on the effects of encapsulation on their in vivo bioavailability is on-going research in our lab, and results will be published soon.

Chapter 6: Development of Carboxymethyl Chitosan Hydrogel Beads in Alcohol-Aqueous Binary Solvent for Nutrient Delivery Applications

Luo, Y., Teng, Z., Wang, X., Wang, Q. 2013. Food Hydrocolloids (Accepted)

6.1 Abstract

Carboxymethyl chitosan (CMCS) hydrogel beads were normally prepared from a composite formulation with other polymers, such as alginate. In present study, a novel method was developed to prepare CMCS, as a single compound, to form hydrogel beads in an alcohol-aqueous binary solvent. The morphology and shape of the CMCS hydrogel beads were highly dependent on alcohol concentration of the binary solvent. The most spherical hydrogel beads were prepared with 3% calcium dissolving in 30% alcohol solution. The chemical crosslinking agent, glutaraldehyde, was required to maintain the hydrogel integrity and morphology. The effects of drying processes on the swelling ratio and release profile of prepared CMCS hydrogel beads in simulated gastrointestinal conditions were studied. Some underlying mechanisms for CMCS hydrogel beads formation in binary solvents were also discussed. Vitamin D3 was encapsulated into the CMCS hydrogel beads to explore delivery applications for hydrophobic nutrient. The CMCS hydrogel beads prepared in 30% alcohol-aqueous binary solvent may be considered as a promising delivery system for hydrophobic nutrients or drugs.

6.2 Introduction

Hydrogels are the networks of hydrophilic polymeric chains that can hold a significant amount of water, from 10% to thousand times of their dry weight (Hoffman,

2002). Hydrogel may be physically crosslinked between polymeric polyelectrolytes and multivalent ions or chemically crosslinked by crosslinking agents, such as glutaraldehyde. Hydrogels fabricated from natural polymers are the biomaterials of particular interests in biomedical applications, such as drug and cell carriers, and tissue engineering matrices.

Chitosan (CS) is the N-deacetylated product of chitin, a natural biopolymer from exoskeleton of crustacean, insects, and fungi. CS and its derivatives have been extensively studied for their drug delivery applications in various forms (Dash, Chiellini, Ottenbrite, & Chiellini, 2011), including nano-/microparticles (Dass, Contreras, Dunstan, & Choong, 2007; Luo, Zhang, Cheng, & Wang, 2010), nanofibers (Uygun, Kiristi, Oksuz, Manolache, & Ulusoy, 2011), films (Kithva, Grondahl, Martin, & Trau, 2010), membranes (Liu, et al., 2012), and hydrogel beads (Torelli-Souza, Cavalcante Bastos, Nunes, Camara, & Amorim, 2012). The major concern of its applications is the solubility problem that CS only dissolves in acidic medium with pH lower than 6. CS hydrogel beads have been prepared by electrostatic crosslinking between CS and tripolyphosphate (TPP). The challenge of CS/TPP hydrogel beads for oral drug delivery is that it may dissociate quickly under gastric conditions with low pH, therefore chemically crosslinking and/or secondary coating were generally applied to achieve controlled release of encapsulated drugs (Durkut, Elçin, & Elçin, 2006; Jain, Jain, Gupta, & Ahirwar, 2007).

Carboxymethyl chitosan (CMCS) is one of the most investigated water-soluble derivatives of CS for biomedical applications (Mouryaa, Inamdara, & Tiwari, 2010). The drug delivery systems prepared from CMCS-based formulations have received increasing attention in recent years (Chen, Tian, & Du, 2004; El-Sherbiny, 2010; Luo, Teng, & Wang, 2012; Snima, Jayakumar, Unnikrishnan, Nair, & Lakshmanan, 2012). Because of the carboxymethylation, CMCS possesses negative charges when dissolved in water, the CMCS hydrogels are generally prepared by physically crosslinking with calcium and/or

polyelectrolyte biopolymers, or by chemically crosslinked with chemical agents. CMCS hydrogels were generally formed through cylindrical mould (Chen, et al., 2004) or cast drying (Chen, Wu, Mi, Lin, Yu, & Sung, 2004; Guo & Gao, 2007), in the form of a piece of gel. However, preparation and application of CMCS hydrogel in the form of beads are rarely reported. Unlike hydrogel formed in certain mould, the hydrogel beads are normally formed simultaneously via crosslinking between biopolymer molecules and crosslinker agents, no further cutting or shaping procedure is required. The chain rigidity and inefficient chain entanglement of CMCS in aqueous solution have been reported during the preparation of CMCS nano fiber (Du & Hsieh, 2008). A study on the CMCS-alginate hydrogel beads pointed out that the beads were formed when CMCS was crosslinked with calcium in the presence of alginate, otherwise an irregular shape of gel would form (Lin, Liang, Chung, Chen, & Sung, 2005). Although the CMCS-calcium hydrogel beads can be prepared when the CMCS with low molecular weight (2.5×10^4 Da) was used, the loading capacity and encapsulation efficiency of these beads were low unless they were further coated with CS (Z. H. Liu, Jiao, & Zhang, 2007). This report indicated that CMCS with low molecular weight has a shorter chain and less charged groups, which may be easier to be entangled.

The objective of current study is to investigate the formation of CMCS hydrogel beads crosslinked with calcium in different alcohol-aqueous binary solvents. The shape of the beads will be further fixed by adding glutaraldehyde as a chemical crosslinking agent. The potentials of CMCS hydrogel beads are also explored for nutrient delivery applications.

6.3 Materials and Methods

6.3.1 Materials

Chitosan with deacetylation degree of 77% with medium molecular weight was purchased from Sigma-Aldrich. Calcium chloride, 25% Glutaraldehyde (GA), vitamin D3 (VD), and other reagents were of analytical grade and purchased from Sigma-Aldrich.

6.3.2 Preparation of CMCS

CMCS was prepared according to a previously published literature (Chen & Park, 2003). Sodium hydroxide (27.2 g) was first dissolved in 40 ml water, and to which 160 ml of isopropanol was added. Then, 20 g chitosan was dispersed into the solution and kept at 50°C for 1 h under mild stirring. After that, 30 g of monochloroacetic acid dissolved in 40 ml of isopropanol was added to the mixture dropwise and reacted at 50°C for 4 h. The reaction solution was then filtered, and washed with 80% alcohol until the filtrate solution was neutral. The resulting solid was dried overnight in an oven at 60°C to obtain CMCS.

6.3.3 Characterization of Prepared CMCS

The molecular weight of CMCS was determined by viscosity measurement (Brookfield) and calculated according to classic Mark–Houwink equation $[\eta] = 7.92\times10^{-5}$ M (Sun, Zhou, Mao, & Zhu, 2007). The degree substitution (DS) was determined by potentiometric titration (Vaghani, Patel, & Satish, 2012). Briefly, 0.1 g of CMCS was dissolved in 100 ml of 0.05 M HCl with mild stirring and the pH was adjusted to 2.0 by 0.1 M NaOH. The CMCS solution was then titrated with 0.1 M NaOH by 0.5 ml increment up to 26 ml, until the final pH of CMCS solution reached 12.0. The conductivity was monitored by using a Conductivity Meter (AP85 Series, Accumet). The titration curve was plotted to calculate DS shown in equation 1 as follows. The chemical structures of CS and CMCS were monitored by Fourier transform infrared spectroscopy (FTIR, Jasco 4100 series with an

attenuated total reflection cell) (Jasco Inc., Easton, MO, USA). Dried powder of sample was placed onto ATR crystal directly. The spectra were acquired at 750 – 4000 cm^{-1} wavenumbers with a 4 cm^{-1} resolution.

$$DS = \frac{(V_2 - V_1)}{(V_3 - V_2)} \times DD \qquad \text{Eq. 1}$$

where DS is the degree of substitution of CMCS and DD is the degree of deacetylation of original chitosan. V_1, V_2, V_3 were the consumed volume of NaOH in different linear section of the titration curve, as designated at **Fig. 6.2**.

6.3.4 Zeta Potential of CMCS Solution in Binary System

The zeta potential of CMCS in different binary solution was also investigated. CMCS (3%) was dissolved in distilled water as stock solution. Then, 200 µl of CMCS stock solution was diluted by 1.8 ml of water and alcohol to obtain different CMCS binary solutions, ranging from 10% to 90% alcohol concentrations. The freshly prepared samples were subjected to zeta potential measurement using a laser Doppler velocimetry (Zetasizer Nano ZS90, Malvern, UK). All measurements were performed in triplicate.

6.3.5 Preparation of Crosslinked CMCS Hydrogel Beads

The CMCS hydrogel beads in this study were prepared by a reported method (Lin, et al., 2005) with modifications. The 3% calcium solution was dissolved in different alcohol-aqueous binary solutions, with alcohol concentration ranging from 0% - 90%. Then, 2 ml of 3% CMCS solution was added dropwise into 10 ml of the above calcium binary solution through a pipette tip (1000 µl) with gently stirring. Hydrogel beads were formed instantaneously. The beads were cured in binary solution for 1 h, followed by the addition of 20 µl of 25% glutaraldehyde. The final concentration of glutaraldehyde in crosslinking solution was 0.05%, and the beads were crosslinked for another 1 h. The formed beads were

then rinsed with 10 ml distilled water four times to remove unreacted calcium chloride and glutaraldehyde, and subsequently dried under room temperature for 48 h. The freeze drying method was also studied to explore the effect of drying process on prepared CMCS hydrogel beads. Briefly, the freshly prepared beads were collected and pre-dried under -80ºC overnight and then freeze-dried (Labconco) for 24 h.

6.3.6 Morphological Observation

The surface morphology of prepared hydrogel beads were examined by a scanning electron microscopy (SEM, Hitachi SU-70, Pleasanton, CA). Samples were dried and mounted on metal stub and then coated with gold using gold sputter coater machine (Hummer XP, Anatech, Union City, CA, USA). Representative SEM images were reported.

6.3.7 Swelling Property

The dried hydrogel beads were carefully weighed and placed into 10 mL simulated gastric fluid (pH 1.2, without pepsin) for 2 h, and then transferred into 10 mL simulated intestinal fluid (pH 7.4, without pancreatin) for 4 h. At designated time intervals, the swelling medium was carefully decanted and the hydrogel beads were carefully weighted after blotted with a piece of paper towel to remove the excess water on the surface. The swelling ratio was determined from the following expression:

$$\text{Swelling ratio} = (W_s - W_d) / W_d,$$

Where W_s is the weight of swollen hydrogel beads, and W_d is the weight of dried hydrogel beads.

6.3.8 Delivery Potential of Hydrophobic Nutrient

To evaluate the drug delivery applications of CMCS hydrogel beads, VD was used as a model nutrient and encapsulated into the beads. Briefly, VD of 10 mg/ml was dissolved in ethanol as stock solution. Then VD ethanol solution (0.25 ml) was mixed with CMCS (10 ml) under mild stirring until homogeneous solution was obtained. Then, the hydrogel beads were

prepared as described aforementioned at 30% alcohol-aqueous binary solution. After the beads were formed, the crosslinking solution was collected for the VD measurement to calculate encapsulation efficiency (EE). The 5 mL of the crosslinking solution was collected for measurement of VD, respectively. EE was calculated as follow:

$$\text{EE}\,(\%) = \frac{\text{Total drug} - \text{drug in crosslinking solution}}{\text{Total drug}} \times 100\%$$

UV-visible spectrophotometer was applied to determine VD concentration. Five milliliter of withdrawn sample was freeze-dried for 48 h. The lyophilized samples were then extracted with 2 ml of hexane for two times, with 2 min of sonification for the first time and 20 s vortexing for second time. Subsequent to each extraction, samples were centrifuged at 6000 g for 10 min, and the supernatant was collected. The combined hexane layer was then measured using a UV-visible spectrophotometer at 264 nm (Beckman Coulter, DU-730, Fullerton, CA).

6.3.9 Release of Nutrient from CMCS Hydrogel Beads

The release profile of encapsulated VD was evaluated in simulated gastrointestinal fluid at 37°C. Fifty milligrams of dried hydrogel beads were incubated in 30 ml of simulated gastric fluid (pH 1.2) for 2 h, then transferred to 30 ml of simulated intestinal fluid (pH 7.4) for 4 h. At designated time intervals, certain amount of release medium was withdrawn and replaced with fresh medium. The VD content in the withdrawn release medium was determined as described in section 6.3.8.

6.4 Results and Discussion

6.4.1 Characterization of Prepared CMCS

Carboxymethylation is one of the most investigated methods to modify chitosan with aims to expand its biomedical applications with improved water solubility. In order to characterize the prepared CMCS, both FTIR and conductimetric titration were used to monitor its molecular structure and carboxymethylation efficiency, respectively. The molecular weight of prepared CMCS was 1.39×10^5 Da, estimated by Mark–Houwink Eq 1. The chemical structures of CS and CMCS were monitored and compared by FT-IR, as shown in **Fig. 6.1**. The spectrum of CS showed characteristic peak of amino group, as observed at 1664 cm-1. In contrast, the spectrum of CMCS showed a characteristic peak of carboxylic acid salt (—COO^- stretch), as observed at 1602 cm^{-1}. The presence of this peak indicated successful addition of carboxymethyl groups onto CS chains. Another vibration area of interest was between 1000 and 1100 cm^{-1}, indicating the C–O stretch. The peaks of 1044 and 1047 cm^{-1} were assigned to primary hydroxyl group (–CH_2–OH in primary alcohols), and peaks of 1069and 1078 cm^{-1} were assigned to secondary hydroxyl group (–CH–OH in cyclic alcohols), in CS and CMCS spectrum, respectively. Since the secondary hydroxyl was not affected during carboxymethylation, it can act as an internal control. The change of the intensity ratio of secondary and primary hydroxyl groups was indicative to the carboxymethylation on primary hydroxyl group (Chen, et al., 2004). This ratio in CS was 1.09 and changed to 0.94 in CMCS after modification, providing further evidence that carboxymethyl group was substituted to –CH_2–OH at C6 position.

The conductimetric titration curve is shown in **Fig. 6.2**. The titration typically consists of four linear portions. The first portion (0 – V1) corresponded to the volume of NaOH used to neutralize the excess amount of HCl; the second portion (V1 – V2) related to the volume of NaOH used to react with carboxymethyl groups on CMCS; the third portion

(V2 – V3) was contributed to the volume of NaOH used to react with NH_3+, which was proportional to the deacytelation degree of the native CS; the forth portion indicated the excess amount of NaOH. As per equation 1, the calculated DS was 0.67 for the prepared CMCS. Similar results were also reported in previous literature (Vaghani, et al., 2012).

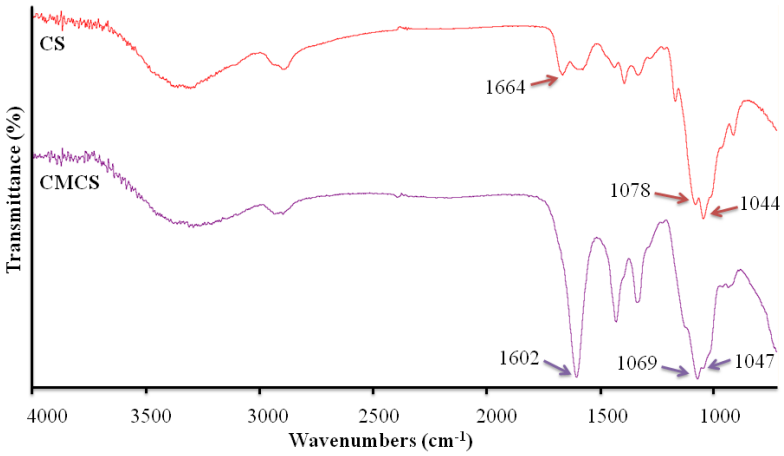

Fig. 6.1. FT-IR spectra of CS and CMCS.

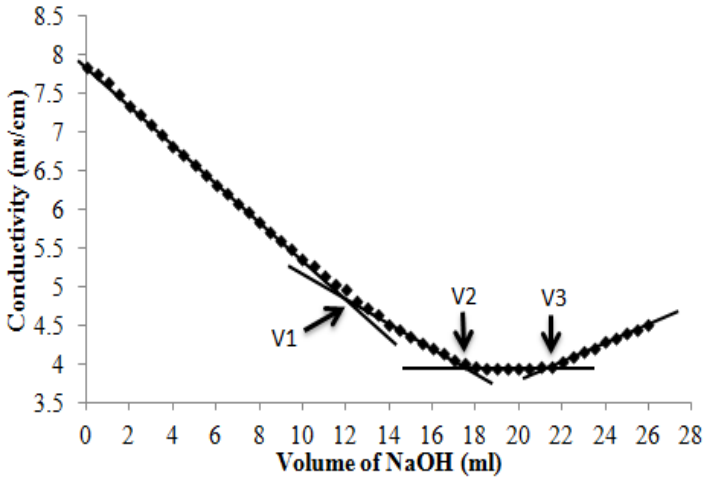

Fig. 6.2. Conductimetric titration curve of CMCS

6.4.2 Formation of CMCS Hydrogel Beads in Binary Solution

Since the previous literature pointed out that CMCS itself cannot form hydrogel beads in the calcium aqueous solution (Lin, et al., 2005), it may be of great interests to test whether the CMCS hydrogel beads can be formed in a binary solution. Herein, the effects of alcohol-aqueous binary solution were investigated in present study. **Fig. 6.3** shows the digital photo of hydrogel beads prepared in different alcohol-aqueous binary calcium solutions. It is clearly observed that homogeneous and spherical beads were formed when the alcohol concentration was less than 50%. Rough and irregular-shaped beads were formed when the alcohol concentration was 50% and higher. Hydrogel beads are generally formed by trapping certain amount of water via molecular entanglements and/or secondary forces including ionic, H-bonding, and hydrophobic forces. Therefore, factors that affect these driving forces, such as solvent composition, temperature, and solids concentration, will also affect beads formation during the gelling process (Hoffman, 2002). Based on our results, solvent composition played an important role in CMCS hydrogel beads formation. This is explained in the following three aspects. First, the H-bonding between water and alcohol increased when the alcohol concentration increased in the solution, resulting in disruption of the H-bonding between CMCS chains and water. Second, the increase of alcohol concentration increased the surface hydrophobicity of CMCS molecules, which might create stronger intermolecular and hydrophobic interactions, and hence facilitated the entanglement of CMCS chains and the formation of hydrogel beads. Third, if the alcohol concentration was higher than 50%, it turned out that water concentration might be too low for CMCS to hold sufficient amount of water inside its network to form spherical beads, and therefore the beads with irregular shape and rough surface were observed.

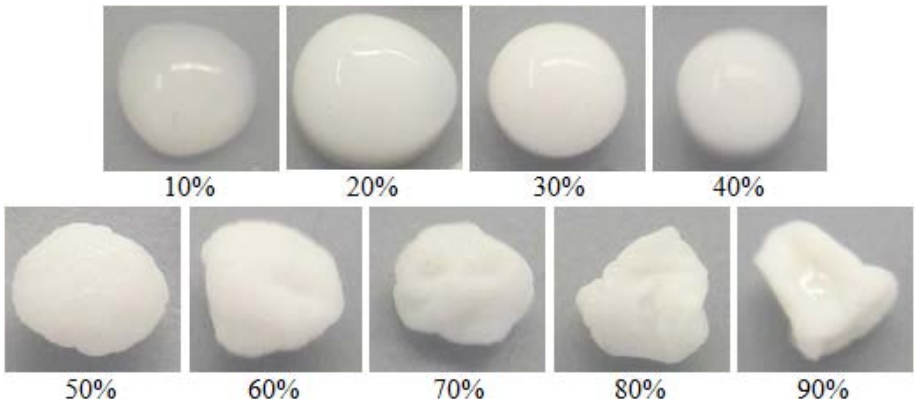

Fig. 6.3. Digital photos of CMCS hydrogel beads prepared in different alcohol-aqueous binary solutions.
The percentage below each photo represents the alcohol concentration for preparation of each bead.

After the CMCS hydrogel beads were formed, it was cured in calcium alcohol-aqueous solution for 1 h before drying and some beads were further crosslinked with gluraraldehyde for 1 h. **Fig. 6.4** showed the digital photos of CMCS hydrogel beads with and without chemical crosslinking. The formed hydrogel beads were spherical at the time of preparation (**Fig. 6.4a**), however, after the beads were removed from calcium binary solution for drying, they redissolved very quickly within 0.5 h in the water (**Fig. 6.4b**). This observation indicated that the physically crosslinked CMCS hydrogel beads cannot maintain its network upon leaving the crosslinking solution, which may be partly due to the evaporation of alcohol from the CMCS hydrogel matrix. The decrease of alcohol concentration may reinforce the H-bonding between CMCS molecules and water, resulting in the disrupture of CMCS network. Therefore, the chemical crosslinking agent is needed to fix the structure and maintain the spherical shape. As shown in **Fig. 6.4c**, the beads crosslinked with calcium and glutaraldehyde maintained the spherical structure after drying. Glutaraldehyde reacted with amino groups on the CMCS chains to form amide bond. Therefore, although the alcohol was evaporated during drying process, the covalent bonds may provide adequate support to hold water and maintain the spherical structure of the beads.

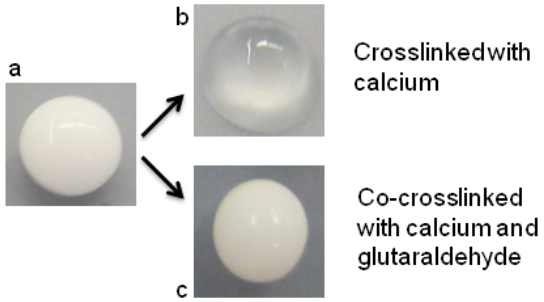

Fig. 6.4. Digital photos of CMCS hydrogels beads crosslinked with different crosslinking reagents.
a, bead immediately removed from 3% calcium in 30% alcohol-aqueous solution; b, bead a after dried at room temperature for 0.5 h; c, bead crosslinked with glutaraldehyde and dried at room temperature for 0.5 h.

6.4.3 Morphological Observation

The digital photographs and SEM images of hydrogel beads dried under different conditions are compared in **Fig. 6.5**. The digital photographs revealed that the hydrogel beads dried at room temperature were yellow in color with diameter of 1.08 mm (**Fig. 6.5A**), while the beads dried by lyophilization were white with diameter of 1.72 mm (**Fig. 6.5D**). This difference in size and color may be due to the fact that the crosslinking agent, glutaraldehyde, continuously reacted with CMCS during the drying process at room temperature whereas this reaction was inhibited by low temperature during lyophilization. At low magnification (**Fig. 6.5B**), a slight depression was observed at the center on one side of the surface of beads dried at room temperature , which was probably due to the surface shrinkage during drying. The lyophilization process, on the other hand, resulted in a very smooth surface without any depression (**Fig. 6.5D**). Similar observations were also noticed in the case of preparation of zinc-pectin-chitosan beads (Das, Chaudhury, & Ng, 2011) and calcium-pectinate beads (Bourgeois, et al., 2008) dried at room temperature. The SEM image at high magnification exhibited rugged and rough surface for the room temperature dried beads (**Fig. 6.5C**), but smooth surface for the lyophilized beads (**Fig. 6.5F**).

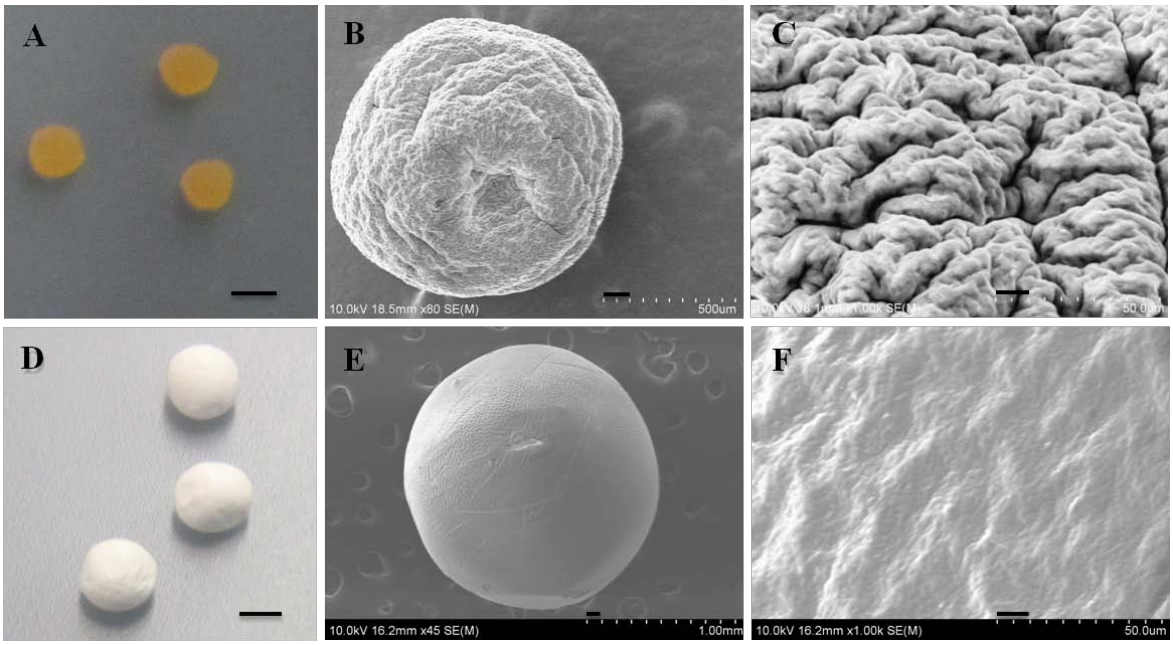

Fig. 6.5. Photographs of CMCS hydrogel beads prepared at 30% alcohol-aqueous binary solution.
A and D, digital photograph of hydrogel beads dried at room temperature and lyophilization, respectively, the scale bar represents 1 mm; B, C and E, F, the scanning electron microscopy (SEM) images of one bead, dried at room temperature and lyophilization, respectively. The scale bar represents 100 μm; B, morphology of the surface, the scale bars in B and E represent 100 μm, and the scale bars in C and F represent 10 μm.

6.4.4 Zeta Potential

With the aim to investigate the underlying mechanism of how binary solvents affected the gelling properties of CMCS, surface charge of CMCS molecules in different binary solvent were measured. As shown in **Fig. 6.6**, the CMCS hydrogel beads carried high negative charges when dissolved in distilled water, showing the zeta potential of –55 mV. As the alcohol concentration increased from 10 to 90%, the absolute value of zeta potential of CMCS decreased gradually to nearly zero, showing the –4.8 and –5.4 mV in 80% and 90% alcohol-aqueous solution, respectively. Surface charge of polymer chains may serve as a paramount parameter contributing to gelling property. The high surface charge on CMCS chains may provide strong repulsion forces resulting in long persistent length and hence stiff chains. Boucard and colleagues (Boucard, et al., 2007) pointed out that as the increase of

alcohol concentration and decrease of water content, CS had less and less charge fraction, which made CS more solvophobic and resulted in gel formation. Another fact supporting for this observation is that the dielectric constant of water is close to 80, much higher than alcohol which is only 24. Therefore, significant decrease of ionic dissociation of CMCS molecules was expected upon increasing alcohol concentration in a binary solvent. This phenomenon was also evidenced in our study. In terms of the CMCS hydrogel beads formation with most spherical morphology, 30 – 40% alcohol-aqueous binary composition may be the optimal solvent with zeta potential ranging between –28 and –21 mV.

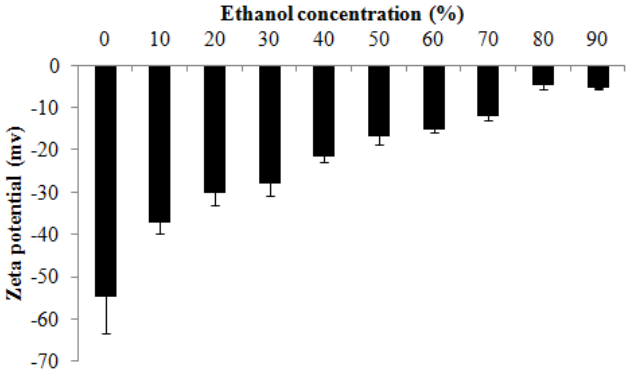

Fig. 6.6. Zeta potential of CMCS in different alcohol-aqueous binary solvents.

5.4.5 Swelling Properties

To explore the drug delivery potentials of prepared CMCS hydrogel beads, the swelling properties in response to physiological conditions were studied. **Fig. 6.7** shows the swelling ratio of CMCS hydrogel beads in simulated gastrointestinal fluid at 37°C. For CMCS beads dried at room temperature, a burst swelling of 2 times of dry weight was observed in the first hour in simulated gastric fluid, followed by a slight swelling. After the CMCS hydrogel beads were transferred into simulated intestinal fluid, their weight kept increasing at a very low speed for the following 4 h, even for the next 24 h (data now shown). The final swelling ratio of CMCS was 2.7 times after 6 h and up to 3 times after 24 h. A

similar swelling pattern with a significantly higher swelling ratio was observed for the lyophilized CMCS hydrogel beads, i.e. a burst swelling of 10 times of its dry weight in gastric fluid within 1 h followed by sustained swelling. The swelling ratio of lyophilized beads was more than 12 after 24 h. The swelling is a process of hydration. Therefore, the hydrophilicity and amount of charged groups of the beads will have great effect on their swelling property. The swelling in gastric fluid may be attributed to the repulsion forces from protonated NH_3+ groups as well as the disruption of Ca^{2+}–COO- interaction caused by the protonation of COO- groups at acidic condition. These two factors led to the migration of water into the dried beads together with the release of unassociated Ca^{2+} from the hydrogel beads to the gastric fluid. When the beads were transferred to simulated intestinal fluid (pH 7.4), the carboxylic group on CMCS was deprotonated and carried negative charges, while the Ca^{2+} –COO^- interaction was weakened because of the release of Ca^{2+}. Therefore, the CMCS molecules became more negatively charged, resulting in stronger electrostatic repulsion and thus facilitating the swelling of the beads (Lin, et al., 2005). The different swelling ratio for room-temperature dried and lyophilized beads may be due to the size of dried beads. As shown in **Fig. 6.7A** and **D**, the size of lyophilized beads was 1.7 folds greater than room temperature dried beads, and the larger size may facilitate water molecules to migrate into the beads network.

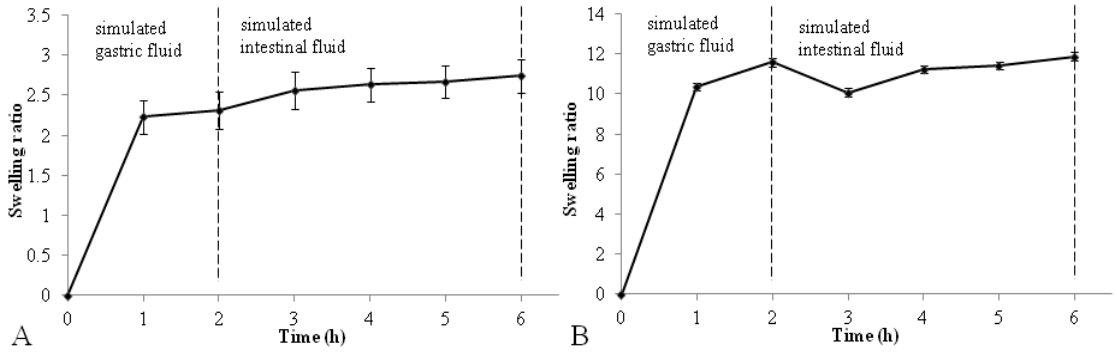

Fig. 6.7. Swelling properties and release profile of CMCS in simulated gastrointestinal conditions.
A, room temperature dried CMCS hydrogel beads; B, lyophilized CMCS hydrogel beads.

Several factors may affect the swelling properties, including molecular weight and surface charge of the polymer(s) used, crosslinking method (physical or chemical), swelling medium. A previous literature investigating the hydrogel beads prepared from CMCS of low molecular weight, pointed out the maximum swelling ratio of CMCS beads were around 20 times in pH 7.4 tris/HCl buffer for 10 h. Because the medium molecular weight of CMCS in our study possessed stiffer chains and stronger electrostatic repulsion between chains, and the use of chemical crosslinker during the preparation, the swelling capability of prepared CMCS beads was demonstrated to be strictly limited. The polymeric matrix composition also affected the swelling capability, i.e., matrix of two or three polymers may show a better swelling property than using single polymer. For instance, the hydrogel beads with composition of alginate and CMCS showed swelling ratio of 32 in 6 h, showing a significant improvement than the beads of alginate itself, the swelling ratio of which was only 5 (Lin, et al., 2005). Similar to previous literature (Vaghani, et al., 2012), the small swelling ratio of prepared CMCS hydrogel beads was due to the chemical crosslinking agent, glutaraldehyde, which created covalent bonds and formed a tight and irreversible network between CMCS chains.

6.4.6 Drug Delivery Applications

The drug delivery applications of prepared CMCS hydrogel beads were investigated. The CMCS hydrogel beads were formed due to the reinforcing of hydrophobicity and disrupting of H-bonding of CMCS chains in alcohol-aqueous binary solvents, therefore, it might be an ideal delivery system for hydrophobic nutrients and drugs. Vitamin D (VD) was tested as the model nutrient, to study the delivery capability of prepared CMCS hydrogel beads. The encapsulation efficiency (EE) of VD was 96.9±0.9%, which is higher than other polymeric delivery systems for VD (Li, Liu, Huang, & Xue, 2011; Luo, et al., 2012; Shi &

Tan, 2002). The high EE may be partly due to the strong hydrophobic interactions between VD and CMCS, and their co-precipitation in crosslinking solution. As shown in **Fig. 6.8**, the kinetic release of VD demonstrated two similar biphasic profiles in simulated gastric fluid and intestinal fluid. Under gastric condition, a burst effect was observed within the first hour with 20% of VD released, and then a slow sustained release in the following hours for the CMCS hydrogel beads dried at room temperature. This phenomenon was corresponded to the burst swelling ratio (**Fig. 6.7**), resulting in the burst release of peripherally encapsulated VD from the swollen matrix. As the pH raised to 7.4 from 1.2 by transferring beads to intestinal condition, CMCS chains may become more expanded due to the electrostatic repulsion. A sustained release was observed in the following hours. For the lyophilized CMCS hydrogel beads, a similar release profile with milder burst effect was observed that only 12% of VD was released in the first hour of incubation in simulated gastric fluid. The accumulated release of VD from CMCS hydrogel beads after 6 h in simulated gastrointestinal fluid was 41%, which was much slower than other CMCS-based hydrogel beads (Lin, et al., 2005; Vaghani, et al., 2012). While a previous study pointed out that the lyophilization drying may accelerate the release rate of hydrophilic protein drug by producing beads with higher porosity, our study revealed that the release rate of hydrophobic drug/nutrient may become slower after lyophilization, partly due to the stronger hydrophobic interaction between polymer and drug during freeze-drying process (Sriamornsak, 1999). The particle size may also contribute to the release profile. The CMCS beads dried at room temperature had smaller particle size and higher surface to volume ratio which may result in a faster release of encapsulated VD.

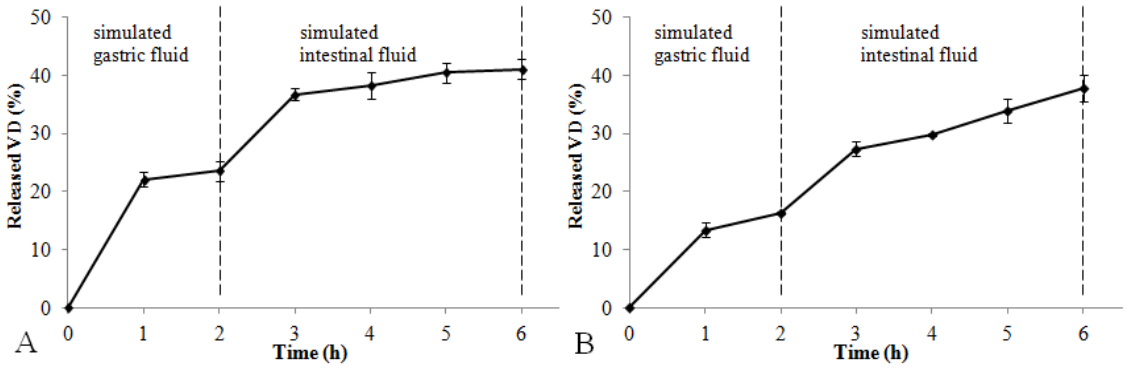

Fig. 6.8. Release profile of VD from CMCS hydrogel beads in simulated gastrointestinal condition.
A, room temperature dried CMCS hydrogel beads; B, lyophilized CMCS hydrogel beads.

6.4.7 Schematic illustration

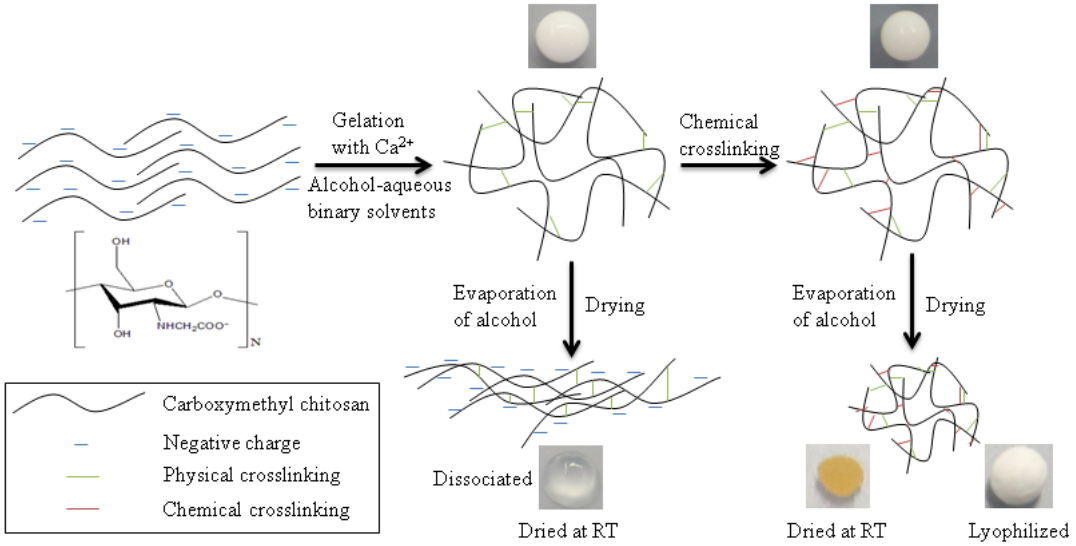

Fig. 6.9. Schematic illustration of the development of CMCS hydrogel beads.

The schematic illustration of the CMCS hydogel beads in alcohol-aqueous binary solvents was summarized in **Fig. 6.9**. The CMCS was first dissolved into distilled water. Because the carboxyl groups on its chains were highly charged in water, strong repulsion forces resulted in the chain rigidity and little entanglement. By dripping the CMCS solution

into alcohol-aqueous binary solvents containing calcium ions, the surface charge of CMCS decreased significantly due to low dielectric constant of alcohol. Meanwhile the carboxyl groups were crosslinked by calcium, resulting in more entanglements and less repulsion forces of CMCS chains. As a result, the hydrogel beads were spontaneously formed. Upon leaving the gelation medium for drying, however, the calcium crosslinked hydrogel beads were unable to maintain its network, due to the evaporation of alcohol from the hydrogel matrix and consequently reinforced the H-bonding and strong repulsive forces. When the hydrogel beads were further crosslinked chemically by glutaraldehyde, the covalent bonds provided adequate support to hold water and maintain the spherical structure of the beads after drying. Different drying methods resulted in different morphology of the beads.

6.5 Conclusion

The CMCS hydrogel beads were successfully prepared in alcohol-aqueous binary solvents, and 30% alcohol concentration turned out to be the optimal solvent to obtain the most spherical beads with smooth surface. The driving forces to form CMCS beads were attributed to the reduced surface charge and interchain H-bonding, enhanced hydrophobicity as well as increased chain entanglement in alcohol-aqueous binary solvent. The prepared CMCS hydrogel beads are believed to possess high potential as a drug delivery system for hydrophobic drugs or nutrients, with high encapsulation efficiency and sustained release profile in simulated gastrointestinal condition. The CMCS hydrogel beads prepared in current study may also be considered for many other applications, including enzyme immobilization and protein encapsulation.

Chapter 7: Cellular Evaluation of Zein Nanoparticles using Caco-2 Cells

7.1 Abstract

Zein nanoparticles can be easily produced by liquid-liquid phase separation, while the cellular evaluations were quite limited due to the poor redispersibility after drying. Caseinate stabilized zein nanoparticles have been recently developed with better redispersibility in salt solutions. In this study, zein-caseinate nanoparticles were prepared with different zein/caseinate mass ratios. The prepared nanoparticles demonstrated good stabilities to maintain particle size (120-140 nm) in cell culture medium and buffer solutions at 37°C. The nanoparticles showed no cytoxicity in Caco-2 cells for 72 h. Coumarin 6 was encapsulated into zein nanoparticles for cell uptake study. Caseinate in zein nanoparticle formulations favored cell uptake in a concentration-dependent manner over time. The cell uptake of zein nanoparticles indicated an energy dependent endocytosis process. The fluorescent microscopy clearly showed the internalization of the zein nanoparticles. Transport of zein nanoparticles were also tested using Caco-2 cell monolayers, showing that caseinate improved zein nanoparticles transport and 60% of nanoparticles were accumulated on cell monolayers. These results for the first time clearly demonstrated the cell uptake and transport of zein nanoparticles and discussed the possible mechanisms, and may shed some light on the cellular evaluations of hydrophobic protein nanoparticles.

7.2 Introduction

It has become clear that cellular evaluation of polymeric delivery systems plays a critical role to explore their potential efficacy and understand specific mechanisms in certain biological conditions. Although in food science area, most of the delivery systems are

prepared with biodegradable and biocompatible polymeric materials, it is not unusual to encounter toxic or side effects of nanoparticle made from GRAS biomaterials, when the in vitro cellular evaluation is performed. For instance, the CS nanoparticles of small particle size (<30 nm) could be internalized by Caco-2 cells to inflict extensive damage to the intracellular organells (Loh, Saunders, & Lim, 2012), as well as be toxic in a dose-dependent manner in human hepatocytes (Loh, Yeoh, Saunders, & Lim, 2010). CS nanoparticles of larger sizes (400 nm) have also been recently shown to be toxic at low concentrations (Liang, Li, Fang, Yang, An, Zhao, et al., 2011).

Zein, as a natural corn protein, has been extensively studied for its delivery application in encapsulation and controlled release of hydrophobic drugs/nutraceuticals. However, due to its unique solubility, the cellular evaluation studies on zein nanoparticles are not fully explored. The zein can only be dissolved in 60-85% aqueous-alcohol binary solutions, and the liquid-liquid phase separation method was usually adopted to prepare zein nanoparticles by sheering zein solution into distilled water (Zhong & Jin, 2009a). While extensive studies have been done to investigate the fabrication parameters and encapsulation of different drugs, the in vivo and in vitro evaluation of efficacy and toxicity of zein nanoparticles are limited. A recent study reported that the zein nanoparticle suspensions can provide target delivery to liver and prolonged blood residence time of the encapsulated drug by intravenous injection (Lai & Guo, 2011). In our previous trials, after zein nanoparticles were freeze dried the nanoparticles powders cannot be redispersed in water or buffer solutions, and even diluting zein dispersion (before freeze-drying) into different buffers would also destabilize zein nanoparticles. Recently, Patel and colleagues prepared sodium caseinate stabilized zein colloidal nanoparticles, which retained good stability against a wide range ionic strength (15 mM−1.5 M NaCl) and good redispersibility after drying (Patel, Bouwens, & Velikov, 2010). Sodium caseinate is a milk protein consisting of several soluble

caseins (αs1, αs2, β, and κ) with various portions of both hydrophobic and hydrophilic groups. It has been widely used in food industry as a nutritional ingredient and a functional component serving as emulsifier and stabilizer (Dickinson, 1997).

Therefore, it may be interested to explore the cellular evaluation of caseinate stabilized zein nanoparticles, in order to shed some light on cytotoxicity and cell uptake of zein nanoparticles. In present study, in addition to cell viability and cell uptake of nanoparticles by Caco-2 cell, the Caco-2 cell monolayer was also used to investigate epithelial transport of zein nanoparticles. The possible mechanisms of cell uptake and transport were also discussed.

7.3 Materials and Methods

7.3.1 Materials

Zein sample with a minimum protein content of 97% was provided by Showa Sangyo (Tokyo, Japan). Sodium caseinate (CAS), coumarin-6 of 98% purity were purchased from Sigma-Aldrich. Dulbecco's modified Eagle medium (DMEM), fetal bovine serum (FBS), 100 × nonessential amino acids, 100× penicillin and streptomycin, 0.25% trypsin (w/v) with EDTA, and 1 M 4-(2-hydroxyethyl)-1-piperazineethanesulfonic acid (HEPES), phosphate buffer saline were all purchased from Life Technologies. Transwell permeable polycarbonate inserts (0.4 μm) and 12-well cell culture plates were obtained from Corning.

7.3.2 Preparation of Nanoparticles

Zein nanoparticles were prepared by liquid-liquid phase separation method, and sodium caseinate was used as a stabilizer. Briefly, zein (10 mg/ml) was first dissolved in 70% aqueous-alcohol solution, and was dissolved in distilled water as stock solution. The 5 ml of zein solution was rapidly poured into 12.5 ml of CAS solution with vigorously stirring for 30 min, the zein nanoparticles were spontaneously formed by phase separation. The

nanoparticles with three different zein to CAS mass ratios were prepared, namely 1:0.5, 1:1,1:2 and defined as sample A, B, and C, respectively. Then, ethanol was removed under nitrogen stream. The nanoparticle suspensions were centrifuged at 2,000 g for 10 min to separate out a few aggregates. The nanoparticle suspensions were freeze-dried for 48 h to obtain dry powders.

7.3.3 Particle Size and Zeta Potential

Hydrodynamic diameter of selenite-loaded CS/TPP nanoparticles was measured by a dynamic light scattering instrument (DLS, BI-200SM, Brookhaven Instruments Corporation, Holtsville, NY, USA). DLS is equipped with a 35 mW HeNe laser beam at a wavelength of 637 nm. All DLS measurements were performed at 25°C. Surface charges of the nanoparticles were measured by a laser Doppler velocimetry (Zetasizer Nano ZS90, Malvern, UK), using a fold capillary cuvette (Folded Capillary Cell-DTS1060, Malvern, UK). The freshly prepared nanoparticle suspensions were used for particle size and surface charge measurement. All measurements were conducted in triplicate.

7.3.4 Stability of Nanoparticles

Stabilities of nanoparticles were investigated in different conditions. The freshly prepared nanoparticles were subjected to freeze drying process for 48 h to obtain dry powders. The nanoparticle powders were redispersed into different conditions to test stabilities, namely, distilled water, HBSS, DMEM. The nanoparticles in different conditions were then incubated at 37°C and the particle size was measured as a function of time.

7.3.5 Cell Culture

Caco-2 cell was generously provided by Dr. Liangli (Lucy) Yu, Department of Nutrition and Food Science, University of Maryland. Caco-2 cells were cultivated in DMEM supplemented with 10% FBS and 1% penicillin-streptomycin at 37°C in humidified

environment with 5% CO_2. The medium was changed every other day and the cells were subcultured after reaching 80-90% confluence. Caco-2 cells between 10-15 passages were used in this study.

7.3.6 Cytoxicity of Nanoparticles

The freeze-dried nanoparticles powders were dissolved in DMEM to different concentrations, i.e. 0.2, 0.5 and 1.0 mg/ml. Caco-2 cells were seeded in 96-well microplates (Corning, USA) at seeding density of 2×10^4 cells/well. Cells were incubated for 24 h to allow cell attachment. Then, cells were treated with DMEM containing different samples. Each treatment had six replicates. At designated time intervals (24, 48 and 72 h), the medium was removed and cells were washed with PBS three times to remove free nanoparticles. Then, 100 μL of DMEM containing MTT (10 μL, 5 mg/ml in PBS) was added into each well. After incubation for 4 h, the culture solution was carefully aspirated and residue was left in the wells. Subsequently, 100 μL of DMSO was added to each well to solubilize the formazan crystals formed. The absorbance at 550 nm was measured by a multilabel microplate reader (Victor X3, PerkinElmer 2030, MA, USA). The cell viability was calculated by the absorbance percentage of nanoparticles treated cells versus blank cells (treated with cell culture medium only).

7.3.7 Cell Uptake of Nanoparticles

To investigate the cell uptake of nanoparticles, coumarin-6, as a fluorescent marker, was encapsulated into the nanoparticles, and both quantitative and qualitative studies were carried out according to previous literature (Zhang & Feng, 2006). The zein solution containing 0.02% coumarin 6 (dissolved in 80% ethanol solution) was used in preparation of fluorescent nanoparticles, all other conditions remained the same. The cell uptake experiment, both quantitative and qualitative studies were carried out as described below.

7.3.7.1 Quantitative Study

Caco-2 cells were seeded in 96-well black plates (BD Falcon, NJ, USA) and incubated until a confluent monolayer was formed. Then, the cell culture medium was replaced with transport buffer (HBSS supplemented with 25 mM HEPES, pH 7.4) pre-warmed at 37°C for equilibration for 20 min. The cell uptake was initiated by incubating cells with 200 μL of different samples dissolved in HBSS at various concentrations for 0.5 – 4 h. At designated intervals of every 30 min, cell monolayer was washed with PBS three times to remove free nanoparticles. Cells were then treated with100 μl of lyse buffer (0.5% Triton X-100 in 0.2N NaOH solution) to permeabilize cell membrane and expose the internalized nanoparticles. The fluorescent intensity was then measured with excitation at 485 nm / emission at 535 nm. The uptake efficiency was expressed as the percentage of fluorescent intensity in cells versus the original intensity present in feed medium (Yinwin & Feng, 2005).

7.3.7.2 Qualitative Study

Caco-2 cell were seeded on Lab-Teks chambered cover glasses (Nalge Nunc International, Naperville, IL, USA), and incubated until cells were about 80% confluence. Prior to uptake test, the growth medium were replaced with transport medium, HBSS buffered with 25 mM HEPES (pH 7.4) and equilibrated for 20 min at 37°C. Then, nanoparticles dissolved in HBSS (1 mg/ml) was added into the wells and incubated for 4 h. At the end, cells were washed thrice with cold PBS to remove free nanoparticles. Cells were then fixed by 70% ethanol for 15 min under –20°C and subsequently nuclei were stained by DAPI. GFP channel was used for green fluorescence of coumarin 6, and DAPI channel for red fluorescence of DAPI. Fluorescent images were taken after deconvolution using AxioVision Release 4.7.2.0 coupled to a Zeiss Axio Observer Z1m fluorescence microscope (Zeiss, Thornwood, NY, USA).

7.3.8 Transport of Nanoparticles via Caco-2 Cell Monolayer

The maintenance of caco-2 cell monolayer was followed by the published protocol (Hubatsch, Ragnarsson, & Artursson, 2007). Briefly, Caco-2 cells were seeded on the tissue-culture-treated polycarbonate filter (diameter 12 mm, growth area 1.1 cm^2) in Costar Transwell 12 wells/plate (Corning Costar Corp., NY, USA) at a seeding density of 3 × 105 cells/cm^2. The medium was replaced every 48 h for the first 6 days and every 24 h thereafter. The cultures were used for the transport experiments 21 – 29 days after seeding. The Transepithelial electrical resistance (TEER) values of the Caco-2 cell monolayer was monitored using EVEO2 with Edohm chamber (World Precision Instrument, FL). The TEER values in the range of 600 – 800 Ω/cm^2 were used. The TEER value of the monolayer was measured at every half hour during 2 h transport study. To initiate the transport experiments, the culture media in the donor and acceptor compartments were carefully aspirated, and the cells were rinsed twice with pre-warmed transport media (HBSS supplemented 25 mM HEPES, pH 7.4). Following a 30 min equilibration with the transport media at 37°C, the cells were incubated for 2 h for transport study. For apical-to-basolateral transport (a-b), 1.2 ml of transport media was added in the basolateral part and 0.4 ml of nanoparticles dissolved in HBSS-HEPES solution (1 mg/ml). At designated time intervals, 0.6 ml of basolateral transport media was withdrawn for fluorescent intensity measurement, and replenished with fresh 0.6 ml transport media. For basolateral-to-apical transport (b-a), 1.2 ml of nanoparticles dissolved in HBSS-HEPES solution (1 mg/ml) was added in the basolateral part and 0.4 ml of transport media was added into apical part. At designated time intervals, 0.2 ml of apical transport media was withdrawn for fluorescent intensity measurement, and replenished with equal volume of fresh HBSS-HEPES solution. To determine the coumarin 6 recovery rate of the transport study, at the end of the experiment, the media from both apical and basolateral compartments were collected for fluorescent intensity measurement to determine the

concentration of coumarin 6. The apparent permeability coefficient (P_{app}) was calculated as follows:

$$P_{app} = \frac{\partial Q}{AC_0 \partial t}$$

where $\partial Q/\partial t$ is the permeability rate, A is the surface area of the membrane filter, and C_0 is the initial concentration in donor compartment (apical compartment in A-B transport study, basolateral compartment in B-A transport study).

7.3.9 Inhibition Study

To evaluate the specific mechanism of nanoparticles involved in uptake process, cell uptake studies were performed under three different blocking conditions (He, Hu, Yin, Tang, & Yin, 2010). For the first condition, Caco-2 cells were incubated with nanoparticles at 4°C for 4 h. For the other two conditions, Caco-2 cells were pre-incubated with the metabolic inhibitor sodium azide (10 μM) and endocytosis inhibitor colchicines (5 μg/ml) for 30 min before adding nanoparticles, and then incubated for 4 h at 37°C for cell uptake experiment. The positive control was the cells incubated without inhibitors. The results were expressed as the inhibition percentage versus control.

7.3.10 Statistical Analysis

All the experiments were conducted in triplicate with data reported as mean ± standard deviation. Experimental statistics were performed using the SAS software (Version 9.2, SAS Institute Inc., Cary, NC, USA). The analysis of variance (ANOVA) Tukey's multiple comparison tests was performed to compare the significant difference. The significance level (P) was set at 0.05.

7.4 Results and Discussion

7.4.1 Stability of Nanoparticles

It is of great significance to evaluate the dispersibilities and stabilities of nanoparticles in different media at 37°C. The nanoparticles were prepared at three different zein to caseiante mass ratios, namely, 1:0.5 (A), 1:1 (B), 1:2 (C). The caseinate stabilized zein nanoparticles were highly negatively charged with the zeta potential around –30 mV, indicating the high stability of the colloidal system. After freeze drying for 48 h, the nanoparticle powders of different formulations were obtained, which were then redispersed into three media, water, DMEM, HBSS-HEPES. DMEM is a culture medium of most mammalian cell lines. HBSS-HEPES is a buffer solution generally used for cell uptake and monolayer transport study. In order to accurately perform the cellular evaluation of the nanoparticles, the nanoparticles should be stable and maintain its particle size during the incubation at 37°C during the period of cell experiments. The stabilities results are shown in **Fig. 7.1**. The freeze dried powder in all formulations possessed good redispersibility in three solutions (1 mg/ml). The opaque nano-suspensions without any large aggregates were easily obtained after gentle vortex. When the samples were incubated in 37°C, during the first hour, the particle size of all nanoparticles remained as the same as the original size before freeze drying, i.e. 120-130 nm. After that, the particle size increase slightly by 5-10 nm. The dispersibility of nanoparticles in DMEM resulted in greater augment of particle size of all formulations. The particle sizes were 150-160 nm in DMEM before the 37°C incubation, but increased to 225 nm for the A nanoparticles, which contains the least caseinate amount. For the B and C nanoparticles, only a slight increase by 5-10 nm was observed. The larger particle size of dispersion in DMEM may be due to its high glucose content, which may interact with protein nanoparticles to form larger particles. Better stabilities of particle size were observed in the nanoparticle formulations with more caseinate content.

Sodium caseinate has been studied in previous literature that the minimum of zein /caseinate ratio 1:0.3 was required to avoid large aggregates during preparation and provide good stability during storage in phosphate buffer (Patel, Bouwens, & Velikov, 2010). In our study, zein/caseiante ratio of 1:0.5 was sufficient to provide good stability at three tested medium at 37°C for 48 h. Since no large aggregates nanoparticle formulations were formed for 37°C incubation for 48 h, they were all suitable to incubate with cells while maintained stable particle size. As a amphiphilic stabilizer, caseinate was able to adsorb to the surface of zein nanoparticles due to the strong hydrophobic interactions. Additionally, caseinate also carries a large portion of negatively charged groups, therefore, it provides electrosteric stabilization of zein nanoparticles against aggregation.

7.4.2 Cytotoxicity of Nanoparticles

The cell viability of Caco-2 cells was tested for each nanoparticle formulation at three concentrations, 0.1, 0.5, 1.0 mg/ml. **Fig. 7.2** demonstrated that all caseinate stabilized nanoparticles showed no toxic effect on cell viability at all concentrations, up to 72 h incubation. Our results agree with the previous literature that zein showed a higher cyto-compatibility compared with many other biomaterials. The same study also pointed out that the cell adhesion rate of zein film was even higher than that on collagen film (Sun, Dong, Lin, Yang, & Wang, 2005).

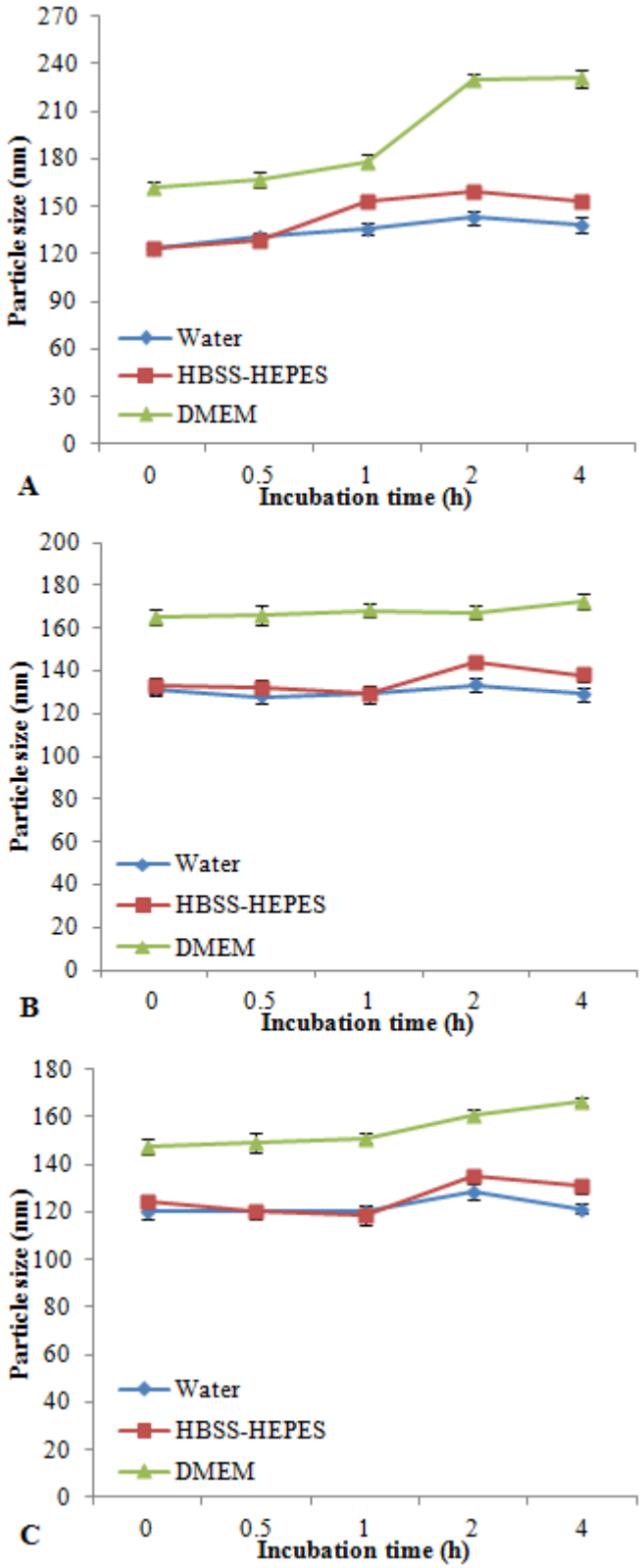

Fig. 7.1. Particle size in different medium at 37°C. A, nanoparticles of zein/caseinate 1:0.5; B, nanoparticles of zein/caseinate 1:1; C, nanoparticles of zein/caseinate 1:2.

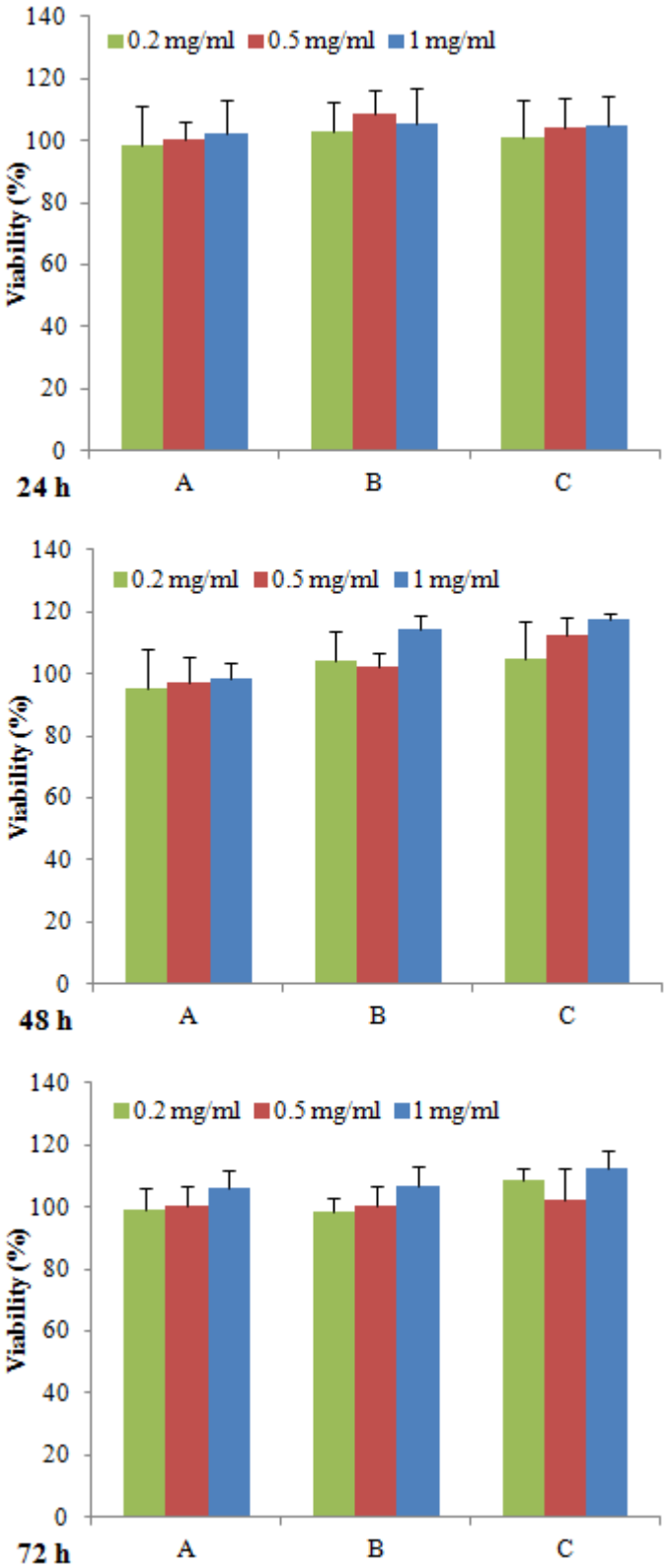

Fig. 7.2. Cell cytotoxicity of zein nanoparticles. A, nanoparticles of zein/caseinate 1:0.5; B, nanoparticles of zein/caseinate 1:1; C, nanoparticles of zein/caseinate 1:2.

7.4.3 Cell Uptake

To investigate the cell uptake of zein nanoparticles, coumarin 6 was selected as a fluorescent marker. Coumarin 6 is one of the most common and suitable fluorescent marker to study cell uptake of nanoparticles by many researchers (Liu, Wang, Sun, Feng, Zhou, Yang, et al., 2010; Zhang, Tan, & Feng, 2012). It has relative high fluorescent intensity and interacts with polymeric nanoparticles via strong hydrophobic interactions. It has also been reported that free coumarin 6 cannot be directly internalized by Caco-2 cells (Dong & Feng, 2005). Therefore, the fluorescence detected represents the uptake of coumarin 6 encapsulated nanoparticles.

7.4.3.1 Quantitative Study

The cell uptake of zein nanoparticles was measured by the fluorescence intensity of coumarin 6 in Caco-2 cells as a function of nanoparticle concentration and incubation time, as shown in **Fig. 7.3.** Among three formulations, the nanoparticles A showed the minimal uptake by Caco-2 cells. During the 4 h of incubation, the cell uptake of all nanoparticle formulations increased gradually. The uptake increased from 5% to 10% during the first hour, but the increase rate of nanoparticles A was much gentler than nanoparticles B and C after 1 h incubation. The uptake of nanoparticles was also concentration dependent, showing that the nanoparticles with higher concentration had a significant higher uptake. The accumulative uptake of nanoparticles A was 16.0% for the concentration of 1 mg/ml, while the accumulative uptake of nanoparticles B and C reached 37.2% and 39.8%, respectively, at the same concentration.

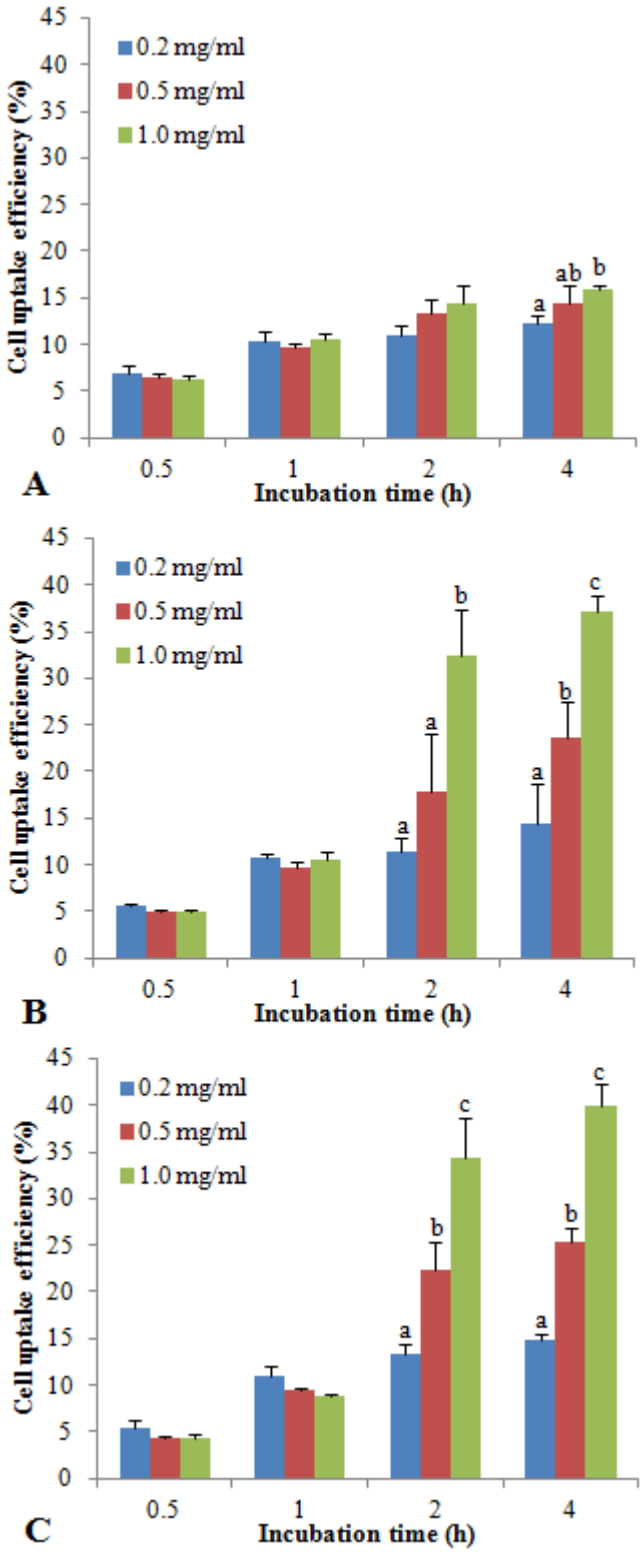

Fig. 7.3. Cell uptake of zein nanoparticles at different concentrations. A, nanoparticles of zein/caseinate 1:0.5; B, nanoparticles of zein/caseinate 1:1; C, nanoparticles of zein/caseinate 1:2. The values sharing different letter within the same time point were significantly different.

Based on our results, it can be concluded that the sodium caseinate enhanced the cell uptake of zein nanoparticles in a dose-dependent manner. Caseinate is a common emulsifier and stabilizer to produce stable nano-emulsions or nanoparticles, in order to increase the solubility of hydrophobic nutrients. For instance, sodium caseinate has been used to produce the nanodispersion of a poorly soluble carotenoid pigment, and it was found that caseinate enhanced the diffusivity of the nanoparticles and facilitated the cell uptake by human colonic epithelial cells (Anarjan, Tan, Ling, Lye, Malmiri, Nehdi, et al., 2011). Another recent study pointed out that the dietary proteins, especially casein and zein, signicantly improved the cell uptake of heme iron by Caco-2 cells (Villarroel, Flores, Pizarro, de Romana, & Arredondo, 2011), suggesting that certain peptides from zein and casein are necessary to activate uptake mechanisms in the enterocyte. Another possible mechanism of the enhanced uptake effect of caseinate on zein nanoparticles may be that the adsorption of caseinate on zein surface could lower the interfacial tension and hence improve the interaction between zein nanoparticles and cell membranes. The higher ratio of caseinate in nanoparticle formulation resulted in higher surface charge. The surface carboxyl groups have also been reported to play an important role in cell uptake of nanoparticles, and the higher surface charge will result in a higher efficiency of cell uptake (Dausend, Musyanovych, Dass, Walther, Schrezenmeier, Landfester, et al., 2008; He, Hu, Yin, Tang, & Yin, 2010).

The cell uptake of polymeric nanoparticles with particle size smaller than 150 nm has been previously characterized as endocytotic internalization (Conner & Schmid, 2003). In order to investigate the possible mechanisms involved in cell uptake of zein nanoparticles, three blocking conditions against endocytosis were tested on Caco-2 cell uptake, as shown in **Fig. 7.4**. The cell uptake of all nanoparticles was significantly inhibited at 4°C, the inhibition percentage was more than 85%. Both sodium azide and colchicine also significantly inhibited cell uptake of nanoparticles, although the inhibition percentage was not as high as that at 4°C

condition. The remarkable inhibition of cell uptake at 4°C was due to the low metabolic activity and poor membrane fluidity, and the 10-15% cell uptake may be attributed to physical adhesion or binding of nanoparticles to the cell membrane (He, Hu, Yin, Tang, & Yin, 2010; Liu, et al., 2010). Sodium azide is a metabolic inhibitor that blocks cellular ATP synthesis. The decrease of cell uptake, but not completely inhibition, of nanoparticles could be the utilization of exogenous ATP by cells (Gratton, Ropp, Pohlhaus, Luft, Madden, Napier, et al., 2008). The inhibition by 4°C condition and sodium azide suggested that the cell uptake of zein nanoparticles was through an active endocytosis, an energy-dependent process. During endocytotic internalization, it has been reported that actin polymerization and rearrangement were required in the clathrin- and caveolae- mediated process (Harush-Frenkel, Rozentur, Benita, & Altschuler, 2008; He, Hu, Yin, Tang, & Yin, 2010). Therefore, the actin polymerization inhibitor, colchicine, was also tested and again observed to reduce cell uptake nanoparticles significantly. This may indicate that the receptor-mediated endocytosis was involved in the cell uptake process. The detailed mechanisms involved in the entry route and pathway of cell uptake of zein nanoparticles required further investigation.

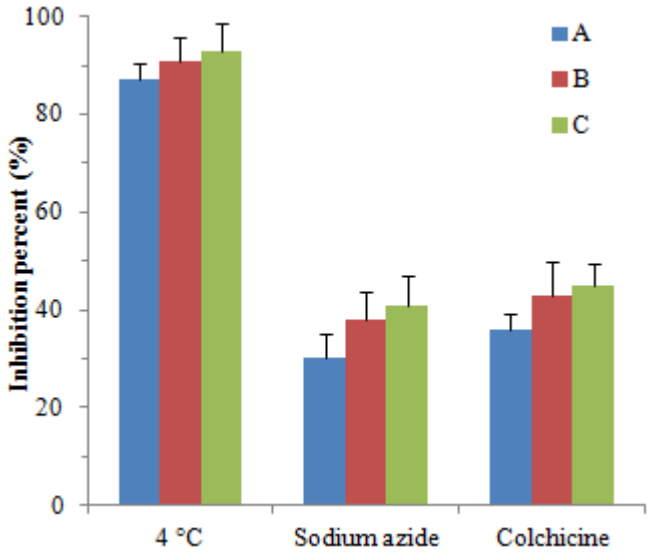

Fig. 7.4. Cell uptake inhibition percentage of zein nanoparticles under different blocking conditions. A, nanoparticles of zein/caseinate 1:0.5; B, nanoparticles of zein/caseinate 1:1; C, nanoparticles of zein/caseinate 1:2.

7.4.3.2 Qualitative Study

The qualitative study was carried out using a fluorescent microscopy to visualize the cell uptake of zein nanoparticles. As shown in **Fig. 7.5**, the zein nanoparticles were internalized into Caco-2 cells, strongly supporting the aforementioned quantitative measurement of cell uptake. Negligible fluorescence was detected in free coumarin 6 control (figure not shown), which was consistent with previous report that coumarin 6 cannot be directly be internalized by Caco-2 cell (Yin Win & Feng, 2005). Therefore, the coumarin 6 detected was due to the internalization of nanoparticles. Zein nanoparticles were found throughout the cytoplasm surrounding the nucleus. The fluorescence intensity was different in three nanoparticles, showing the strongest intensity in nanoparticles C, which had highest ratio of caseinate. This observation was consistent with quantitative study in previous section and confirmed that caseinate favored the cell uptake of zein nanoparticles.

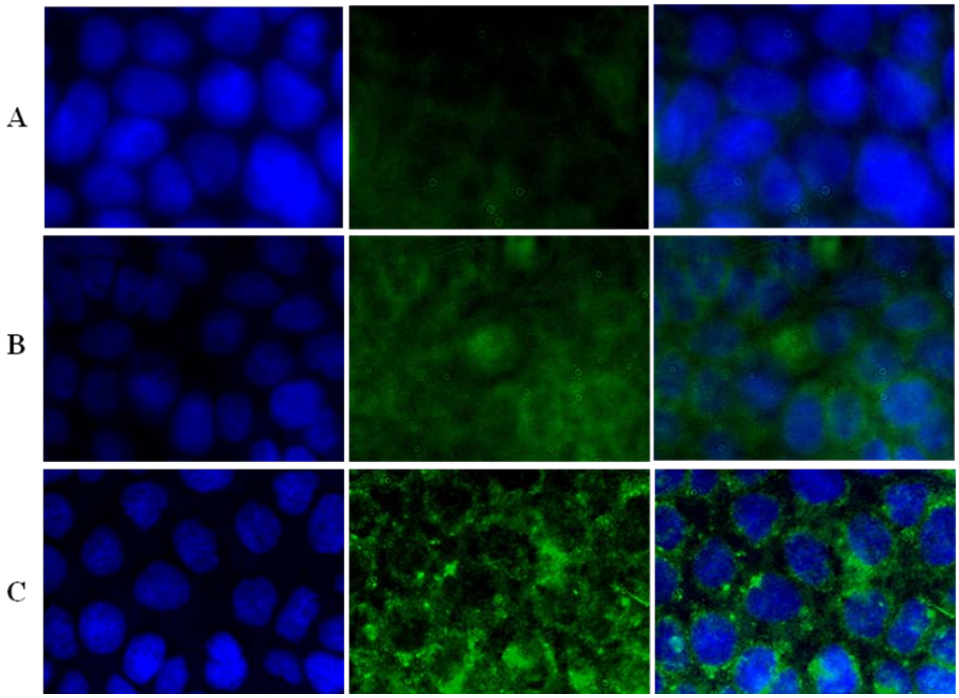

Fig. 7.5. Fluorescent microscopic images for Caco-2 cells after 4 h incubation with zein nanoparticles in different formulations. The first column showed cell nuclei stained DAPI (blue); the second column showed cytoplasm filled with coumarin 6-encapsulated nanoparticles (green); the third column was the merged images. A, nanoparticles of zein/caseinate 1:0.5; B, nanoparticles of zein/caseinate 1:1; C, nanoparticles of zein/caseinate 1:2.

7.4.4 Transport Study

Based on the cell uptake study, nanoparticles of 1 mg/ml had the highest uptake efficiency and hence were selected for permeability study using Caco-2 cell monolayer. Both A-B and B-A transport were evaluated for three nanoparticle formulations, as shown in **Fig. 7.6.** For a-b transport, the P_{app} for nanoparticles A and B were 0.24 $\times 10^{-6}$ and 0.25 $\times 10^{-6}$ cm/s, respectively. However, P_{app} of nanoparticle C was remarkably increased to 0.32 $\times 10^{-6}$ cm/s, significantly different from nanoparticles A and B. Similar trends was observed for B-A transport that nanoparticles C had an enhanced permeability rate. The higher ratio of caseinate in nanoparticle favored the transport of zein nanoparticles. The higher b-a permeability of nanoparticles than a-b direction may be, in part, due to the tighter junction of Caco-2 cells monolayer in the apical membrane than basolateral membrane, as also observed in other literatures (El-Sayed, Ginski, Rhodes, & Ghandehari, 2002; Pisal, Yellepeddi, Kumar, Kaushik, Hildreth, Guan, et al., 2008).

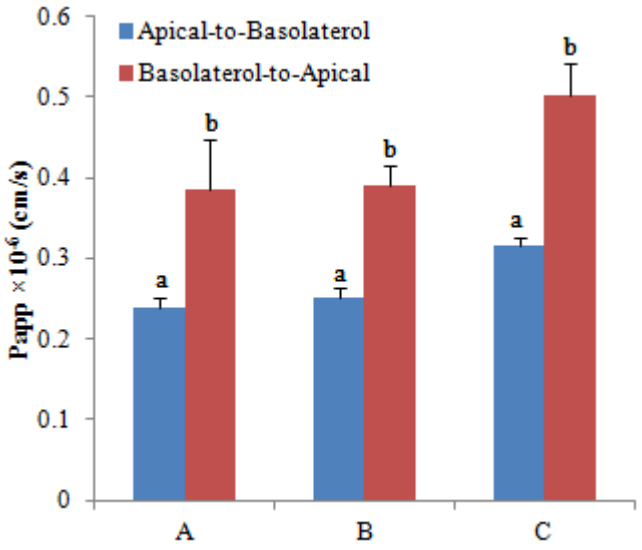

Fig. 7.6. Transport of nanoparticles through Caco-2 cell monolayer. A, nanoparticles of zein/caseinate 1:0.5; B, nanoparticles of zein/caseinate 1:1; C, nanoparticles of zein/caseinate 1:2. The values sharing different letter within one sample were significantly different.

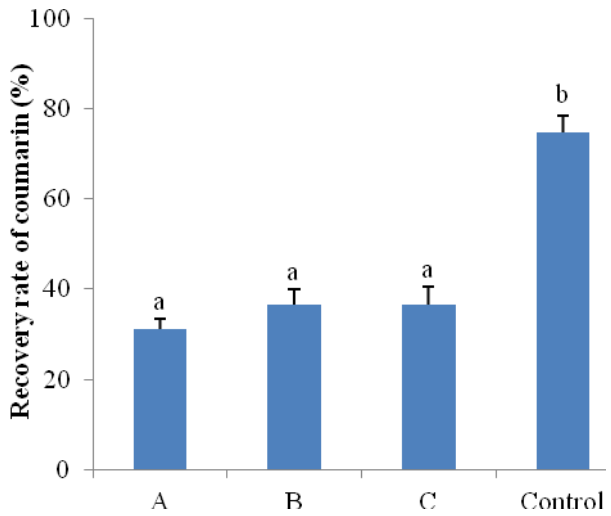

Fig. 7.7. Recovery rate of coumarin 6 from Caco-2 cell monolayer transport study (Apical to basolateral). A, nanoparticles of zein/caseinate 1:0.5; B, nanoparticles of zein/caseinate 1:1; C, nanoparticles of zein/caseinate 1:2. The values sharing the different letter were signicantly different.

To further investigate the tranepithelial tranposrt of zein nanoparticles, the mass balance was checked after the transport study. As shown in **Fig. 7.7**, the coumarin 6 control (free compound dissolved in DMSO and diluted with HBSS) showed a 75% recovery rate, indicating mass balance of free coumarin was good. However, for the coumarin 6 encapsulated in nanoparticles, the recovery rate was much lower, 31%, 36%, and 36% for nanoparticles A, B, and C, respectively. This observation suggested that some of the zein nanoparticles were accumulated in the cells, which might indicate the endocytosis and transcellular transposrt of zein nanoparticles. Further, the TEER values were monitored throughout the 2 h transport study. The TEER values were not altered significantly in all nanoparticle formulations, compared with the control (data not shown). Because the Caco-2 cell monolayers were characterized to carry negative surface charges due to glycoproteins on its surface, the negative charged nanoparticles may only have limited capability to open tight junctions of the monolayers. Hafner and coworkers also reported that negatively charged lecithin nanoparticles had the least effect on tight junction openings, compared with chitosan

coated nanoparticles which carried positive surface charge (Hafner, Lovrić, Voinovich, & Filipović-Grčić, 2009).

7.5 Conclusion

The caseinate stabilized zein nanoparticles were prepared in different zain/caseianate mass ratios, and the effects of caseinate on the stabilities, cytotoxicity, cell uptake, epithelial transport were investigated on Caco-2 cells. Three formulations showed similar good stabilities to maintain particles size in cell culture medium and buffer solutions at 37°C. Zein-caseinate nanoparticles showed no cytotoxicity for 72 h. The caseinate content in zein nanoparticles favored the cell uptake by concentration- and time- dependent manner. The cell uptake of nanoparticles was also visualized by fluorescent microscopy, showing that zein nanoparticles were seen throughout the cytoplasm surrounding the nucleus. The Caco-2 cell monolayers transport study demonstrated that zein-caseinate nanoparticles transported via transcellular pathway by endocytosis and some of the nanoparticles accumulated in the monolayers.

References

Abdelrahim, M., Newman, K., Vanderlaag, K., Samudio, I., & Safe, S. (2006). 3,3'-Diindolylmethane (DIM) and its derivatives induce apoptosis in pancreatic cancer cells through endoplasmic reticulum stress-dependent upregulation of DR5. Carcinogenesis, 27(4), 717-728.

Agriculture, U. S. D. o. (2010). Dietary Guilines for Americans. www.dietaryguilines.gov, Chapter 4.

Anarjan, N., Tan, C. P., Ling, T. C., Lye, K. L., Malmiri, H. J., Nehdi, I. A., Cheah, Y. K., Mirhosseini, H., & Baharin, B. S. (2011). Effect of organic-phase solvents on physicochemical properties and cellular uptake of astaxanthin nanodispersions. Journal of Agricultural and Food Chemistry, 59(16), 8733-8741.

Anderson, T. J., & Lamsal, B. P. (2011). Review: zein extraction from corn, corn products, and coproducts and modifications for various applications: A Review. Cereal Chemistry, 88(2), 159-173.

Anderton, M. J., Jukes, R., Lamb, J. H., Manson, M. M., Gescher, A., Steward, W. P., & Williams, M. L. (2003). Liquid chromatographic assay for the simultaneous determination of indole-3-carbinol and its acid condensation products in plasma. Journal of Chromatography B, 787(2), 281-291.

Anderton, M. J., Manson, M. M., Verschoyle, R. D., Gescher, A., Lamb, J. H., Farmer, P. B., Steward, W. P., & Williams, M. L. (2004). Pharmacokinetics and tissue disposition of indole-3-carbinol and its acid condensation products after oral administration to mice. Clin Cancer Res, 10(15), 5233-5241.

Anitha, A., Maya, S., Deepa, N., Chennazhi, K. P., Nair, S. V., Tamura, H., & Jayakumar, R. (2011). Efficient water soluble O-carboxymethyl chitosan nanocarrier for the delivery of curcumin to cancer cells. Carbohydrate Polymers, 83(2), 452-461.

Arvanitoyannis, I. S. (2009). Encapsulation and controlled release technologies in food systems. International Journal of Food Science & Technology, 44(7), 1462-1463.

Baysal, T., Ersus, S., & Apaydın, E. (2009). The effect of corn zein edible film coating on quality of intermediate moisture tomatoes. GIDA-Journal of Food, 34(6), 359-366.

Berger, J., Reist, M., Mayer, J. M., Felt, O., Peppas, N. A., & Gurny, R. (2004). Structure and interactions in covalently and ionically crosslinked chitosan hydrogels for biomedical applications. European Journal of Pharmaceutics and Biopharmaceutics, 57(1), 19-34.

Bhattarai, N., Gunn, J., & Zhang, M. (2010). Chitosan-based hydrogels for controlled, localized drug delivery. Advanced Drug Delivery Reviews, 62(1), 83-99.

Björkhem-Bergman, L., Jönsson, K., Eriksson, L. C., Olsson, J.M., Lehman, S., Paul, C., & Björnstedt, M. (2002). Drug-resistant human lung cancer cells are more sensitive to selenium cytotoxicity: Effects on thioredoxin reductase and glutathione reductase. Biochemical Pharmacology, 63, 1875-1884.

Bloch-Mechkour, A., Bally, T., & Marcinek, A. (2011). Dimer radical cations of indole and indole-3-carbinol: localized and delocalized radical cations of diindolylmethane. Journal of Physical Chemistry A, 115(26), 7700-7708.

Boucard, N., David, L., Rochas, C., Montembault, A., Viton, C., & Domard, A. (2007). Polyelectrolyte microstructure in chitosan aqueous and alcohol solutions. Biomacromolecules, 8(4), 1209-1217.

Bourgeois, S., Tsapis, N., Honnas, H., Andremont, A., Shakweh, M., Besnard, M., & Fattal, E. (2008). Colonic delivery of β-lactamases does not affect amoxicillin pharmacokinetics in rats. Journal of Pharmaceutical Sciences, 97(5), 1853-1863.

Bradlow, H. L., & Zeligs, M. A. (2010). Diindolylmethane (DIM) Spontaneously forms from indole-3-carbinol (I3C) during cell culture experiments. In Vivo, 24(4), 387-391.

Brigelius-Flohe, R., & Traber, M. G. (1999). Vitamin E: function and metabolism. Faseb Journal, 13(10), 1145-1155.

Briones, A. V., & Sato, T. (2010). Encapsulation of glucose oxidase (GOD) in polyelectrolyte complexes of chitosan–carrageenan. Reactive and Functional Polymers, 70(1), 19-27.

Campaniello, D., Bevilacqua, A., Sinigaglia, M., & Corbo, M. (2008). Chitosan: antimicrobial activity and potential applications for preserving minimally processed strawberries. Food Microbiology, 25(8), 992-1000.

Chang, D. S., Cho, H. R., Gao, H. Y., & Choe, W. K. (1989). A development of food preservation with the waste of crab processing. Bullletin of the Korean Fisheries Society, 22, 70-78.

Chang, Y. M., Chang, C. T., Huang, T. C., Chen, S. M., Lee, J. A., & Chung, Y. C. (2011). Effects of low molecular weight chitosans on aristolochic acid-induced renal lesions in mice. Food Chemistry, 129(4), 1751-1758.

Chen, L. Y., Tian, Z. G., & Du, Y. M. (2004). Synthesis and pH sensitivity of carboxymethyl chitosan-based polyampholyte hydrogels for protein carrier matrices. Biomaterials, 25(17), 3725-3732.

Chen, L., & Subirade, M. (2005). Chitosan/β-lactoglobulin core-shell nanoparticles as nutraceutical carriers. Biomaterials, 26(30), 6041-6053.

Chen, L., Remondetto, G. E., & Subirade, M. (2006). Food protein-based materials as nutraceutical delivery systems. Trends in Food Science & Technology, 17(5), 272-283.

Chen, L., Tian, Z., & Du, Y. (2004). Synthesis and pH sensitivity of carboxymethyl chitosan-based polyampholyte hydrogels for protein carrier matrices. Biomaterials, 25(17), 3725-3732.

Chen, S. C., Wu, Y. C., Mi, F. L., Lin, Y. H., Yu, L. C., & Sung, H. W. (2004). A novel pH-sensitive hydrogel composed of N,O-carboxymethyl chitosan and alginate cross-linked by genipin for protein drug delivery. Journal of Controlled Release, 96(2), 285-300.

Chen, X. G., & Park, H. J. (2003). Chemical characteristics of O-carboxymethyl chitosans related to the preparation conditions. Carbohydrate Polymers, 53(4), 355-359.

Cheng, W. H. (2009). Impact of inorganic nutrients on maintenance of genomic stability. Environmental and Molecular Mutagenesis, 50, 349-360.

Choi, Y., Kim, Y., Park, S., Lee, K. W., & Park, T. Indole-3-carbinol prevents diet-induced obesity through modulation of multiple genes related to adipogenesis, thermogenesis or inflammation in the visceral adipose tissue of mice. The Journal of Nutritional Biochemistry(0).

Chung, M. J., Park, J. K., & Park, Y. I. (2012). Anti-inflammatory effects of low-molecular weight chitosan oligosaccharides in IgE–antigen complex-stimulated RBL-2H3 cells and asthma model mice. International immunopharmacology.

Ciska, E., Verkerk, R., & Honke, J. (2009). Effect of boiling on the content of ascorbigen, indole-3-carbinol, indole-3-acetonitrile, and 3,3 '-diindolylmethane in fermented cabbage. Journal of Agricultural and Food Chemistry, 57(6), 2334-2338.

Coimbra, M., Isacchi, B., van Bloois, L., Torano, J. S., Ket, A., Wu, X., Broere, F., Metselaar, J. M., Rijcken, C. J. F., Storm, G., Bilia, R., & Schiffelers, R. M. (2011). Improving solubility and chemical stability of natural compounds for medicinal use by incorporation into liposomes. International Journal of Pharmaceutics, 416(2), 433-442.

Conner, S. D., & Schmid, S. L. (2003). Regulated portals of entry into the cell. Nature, 422(6927), 37-44.

Cooper, C., Dubin, P., Kayitmazer, A., & Turksen, S. (2005). Polyelectrolyte–protein complexes. Current opinion in colloid & interface science, 10(1), 52-78.

Dael, P. V., Davidsson L., Munoz-Box, R., Fay, L. B., & Barclay, D. (2001). Selenium absorption and retention from a selenite- or selenate-fortified milk-based formula in men measured by a stable-isotope technique. British Journal of Nutrition, 85, 157-163.

Dai, Y. N., Li, P., Zhang, J. P., Wang, A. Q., & Wei, Q. (2008). Swelling characteristics and drug delivery properties of nifedipineloaded pH sensitive alginate –chitosan hydrogel beads. Journal of Biomedical Materials Research Part B: Applied Biomaterials, 86(2), 493-500.

Dash, M., Chiellini, F., Ottenbrite, R. M., & Chiellini, E. (2011). Chitosan—A versatile semi-synthetic polymer in biomedical applications. Progress in Polymer Science, 36(8), 981-1014.

Dass, C. R., Contreras, K. G., Dunstan, D. E., & Choong, P. F. M. (2007). Chitosan microparticles encapsulating PEDF plasmid demonstrate efficacy in an orthotopic metastatic model of osteosarcoma. Biomaterials, 28(19), 3026-3033.

Dausend, J., Musyanovych, A., Dass, M., Walther, P., Schrezenmeier, H., Landfester, K., & Mailänder, V. (2008). Uptake mechanism of oppositely charged fluorescent nanoparticles in HeLa cells. Macromolecular Bioscience, 8(12), 1135-1143.

de Vos, P., Faas, M. M., Spasojevic, M., & Sikkema, J. (2010). Encapsulation for preservation of functionality and targeted delivery of bioactive food components. International Dairy Journal, 20(4), 292-302.

Delaurent, C., Siouffi, A. M., & Pèpe, G. (1998). Cyclodextrin inclusion complexes with vitamin D3: investigation of the solid complex characterization. Chem. Anal. (Warsaw), 43(601), 6.

Desai, K. G. H., & Park, H. J. (2005). Recent developments in microencapsulation of food ingredients. Drying Technology, 23(7), 1361-1394.

Desai, M. P., Labhasetwar, V., Amidon, G. L., & Levy, R. J. (1996). Gastrointestinal uptake of biodegradable microparticles: effect of particle size. Pharmaceutical Research, 13(12), 1838-1845.

Desai, M. P., Labhasetwar, V., Walter, E., Levy, R. J., & Amidon, G. L. (1997). The mechanism of uptake of biodegradable microparticles in Caco-2 cells is size dependent. Pharmaceutical Research, 14(11), 1568-1573.

Di Martino, A., Sittinger, M., & Risbud, M. V. (2005). Chitosan: a versatile biopolymer for orthopaedic tissue-engineering. Biomaterials, 26(30), 5983-5990.

Dickinson, E. (1997). Properties of Emulsions Stabilized with Milk Proteins: Overview of Some Recent Developments. Journal of Dairy Science, 80(10), 2607-2619.

Dong, Y., & Feng, S.-S. (2005). Poly(d,l-lactide-co-glycolide)/montmorillonite nanoparticles for oral delivery of anticancer drugs. Biomaterials, 26(30), 6068-6076.

Du, J., & Hsieh, Y. L. (2008). Nanofibrous membranes from aqueous electrospinning of carboxymethyl chitosan. Nanotechnology, 19(12).

Duan, J. H., Zhang, Y. D., Han, S. W., Chen, Y. X., Li, B., Liao, M. M., Chen, W., Deng, X. M., Zhao, J. F., & Huang, B. Y. (2010). Synthesis and in vitro/in vivo anti-cancer evaluation of curcumin-loaded chitosan/poly(butyl cyanoacrylate) nanoparticles. International Journal of Pharmaceutics, 400(1-2), 211-220.

Duclairoir, C., Orecchioni, A. M., Depraetere, P., & Nakache, E. (2002). alpha-Tocopherol encapsulation and in vitro release from wheat gliadin nanoparticles. Journal of Microencapsulation, 19(1), 53-60.

Dudhani, A. R., & Kosaraju, S. L. (2010). Bioadhesive chitosan nanoparticles: Preparation and characterization. Carbohydrate Polymers, 81(2), 243-251.

Dung, T. H., Lee, S. R., Han, S. D., Kim, S. J., Ju, Y. M., Kim, M. S., & Yoo, H. (2007). Chitosan-TPP nanoparticle as a release system of antisense oligonucleotide in the oral environment. Journal of Nanoscience and Nanotechnology, 7(11), 3695-3699.

Durkut, S., Elçin, Y. M., & Elçin, A. E. (2006). Biodegradation of Chitosan-Tripolyphosphate Beads: In Vitro and In Vivo Studies. Artificial Cells, Blood Substitutes and Biotechnology, 34(2), 263-276.

El-Sayed, M., Ginski, M., Rhodes, C., & Ghandehari, H. (2002). Transepithelial transport of poly(amidoamine) dendrimers across Caco-2 cell monolayers. Journal of Controlled Release, 81(3), 355-365.

El-Sherbiny, I. M. (2010). Enhanced pH-responsive carrier system based on alginate and chemically modified carboxymethyl chitosan for oral delivery of protein drugs: Preparation and in-vitro assessment. Carbohydrate Polymers, 80(4), 1125-1136.

Elzatahry, A., Eldin, M., Soliman, E., & Hassan, E. (2009). Evaluation of alginate–chitosan bioadhesive beads as a drug delivery system for the controlled release of theophylline. Journal of Applied Polymer Science, 111(5), 2452-2459.

Elzoghby, A. O., Samy, W. M., & Elgindy, N. A. (2012). Protein-based nanocarriers as promising drug and gene delivery systems. Journal of Controlled Release, 161(1), 38-49.

Esumi, K., Takei, N., & Yoshimura, T. (2003). Antioxidant-potentiality of gold-chitosan nanocomposites. Colloids and Surfaces B: Biointerfaces, 32, 117-123.

Ferguson, L. R., Philpott, M., & Karunasinghe, N. (2006). Oxidative DNA damage and repair: significance and biomarkers. Journal of Nutrition, 136, 2687S-2689S.

Fernandez, A., Torres-Giner, S., & Lagaron, J. M. (2009). Novel route to stabilization of bioactive antioxidants by encapsulation in electrospun fibers of zein prolamine. Food Hydrocolloids, 23(5), 1427-1432.

Fernandez-Saiz, P., Lagaron, J., & Ocio, M. (2009). Optimization of the biocide properties of chitosan for its application in the design of active films of interest in the food area. Food Hydrocolloids, 23(3), 913-921.

Gan, Q., & Wang, T. (2007). Chitosan nanoparticle as protein delivery carrier: Systematic examination of fabrication conditions for efficient loading and release. Colloids and Surfaces B: Biointerfaces, 59(1), 24-34.

Gan, Q., & Wang, T. (2007). Chitosan nanoparticle as protein delivery carrier: systematic examination of fabrication conditions for efficient loading and release. Colloids and Surfaces B: Biointerfaces, 59(1), 24-34.

Gan, Q., Wang, T., Cochrane, C., & McCarron, P. (2005). Modulation of surface charge, particle size and morphological properties of chitosan-TPP nanoparticles intended for gene delivery. Colloids and Surfaces B: Biointerfaces, 44, 65-73.

Ginter, E., & Simko, V. (2009). Vitamin D deficiency, atherosclerosis and cancer. Bratislava Medical Journal-Bratislavske Lekarske Listy, 110(12), 751-756.

Gonnet, M., Lethuaut, L., & Boury, F. (2010). New trends in encapsulation of liposoluble vitamins. Journal of Controlled Release, 146(3), 276-290.

Gratton, S. E. A., Ropp, P. A., Pohlhaus, P. D., Luft, J. C., Madden, V. J., Napier, M. E., & DeSimone, J. M. (2008). The effect of particle design on cellular internalization pathways. Proceedings of the National Academy of Sciences of the United States of America, 105(33), 11613-11618.

Grenha, A., Remunan-Lopez, C., Carvalho, E. L. S., & Seijo, B. (2008). Microspheres containing lipid/chitosan nanoparticles complexes for pulmonary delivery of therapeutic proteins. European Journal of Pharmaceutics and Biopharmaceutics, 69(1), 83-93.

Grenha, A., Seijo, B., & Remuñán-López, C. (2005). Microencapsulated chitosan nanoparticles for lung protein delivery. European journal of pharmaceutical sciences, 25(4), 427-437.

Grose, K. R., & Bjeldanes, L. F. (1992). Oligomerization of Indole-3-Carbinol in Aqueous Acid. Chemical Research in Toxicology, 5(2), 188-193.

Gunasekaran, S., Ko, S., & Xiao, L. (2007). Use of whey proteins for encapsulation and controlled delivery applications. Journal of Food Engineering, 83(1), 31-40.

Guo, B. L., & Gao, Q. Y. (2007). Preparation and properties of a pH/temperature-responsive carboxymethyl chitosan/poly(N-isopropylacrylamide)semi-IPN hydrogel for oral delivery of drugs. Carbohydrate Research, 342(16), 2416-2422.

Hafner, A., Lovrić, J., Voinovich, D., & Filipović-Grčić, J. (2009). Melatonin-loaded lecithin/chitosan nanoparticles: Physicochemical characterisation and permeability through Caco-2 cell monolayers. International Journal of Pharmaceutics, 381(2), 205-213.

Hamman, J. H. (2010). Chitosan based polyelectrolyte complexes as potential carrier materials in drug delivery systems. Marine drugs, 8(4), 1305-1322.

Han, J., Guenier, A.-S., Salmieri, S., & Lacroix, M. (2008). Alginate and Chitosan Functionalization for Micronutrient Encapsulation. Journal of Agricultural and Food Chemistry, 56(7), 2528-2535.

Harush-Frenkel, O., Rozentur, E., Benita, S., & Altschuler, Y. (2008). Surface charge of nanoparticles determines their endocytic and transcytotic pathway in polarized MDCK cells. Biomacromolecules, 9(2), 435-443.

Hatanaka, J., Chikamori, H., Sato, H., Uchida, S., Debari, K., Onoue, S., & Yamada, S. (2010). Physicochemical and pharmacological characterization of [alpha]-tocopherol-loaded nano-emulsion system. International Journal of Pharmaceutics, 396(1-2), 188-193.

He, C., Hu, Y., Yin, L., Tang, C., & Yin, C. (2010). Effects of particle size and surface charge on cellular uptake and biodistribution of polymeric nanoparticles. Biomaterials, 31(13), 3657-3666.

Hejazi, R., & Amiji, M. (2003). Chitosan-based gastrointestinal delivery systems. Journal of Controlled Release, 89(2), 151-165.

Herrera, E., & Barbas, C. (2001). Vitamin E: action, metabolism and perspectives. Journal of Physiology and Biochemistry, 57(2), 43-56.

Hirano, S., Itakura, C., Seino, H., Akiyama, Y., Nonaka, I., Kanbara, N., & Kawakami, T. (1990). Chitosan as an ingredient for domestic animal feeds. Journal of agricultural and food chemistry, 38(5), 1214-1217.

Hoffman, A. S. (2002). Hydrogels for biomedical applications. Advanced Drug Delivery Reviews, 54(1), 3-12.

Hu, B., Pan, C. L., Sun, Y., Hou, Z. Y., Ye, H., Hu, B., & Zeng, X. X. (2008). Optimization of fabrication parameters to produce chitosan-tripolyphosphate nanoparticles for delivery of tea catechins. Journal of Agricultural and Food Chemistry, 56(16), 7451-7458.

Hu, B., Ting, Y., Zeng, X., & Huang, Q. (2012). Cellular uptake and cytotoxicity of chitosan–caseinophosphopeptides nanocomplexes loaded with epigallocatechin gallate. Carbohydrate Polymers, 89(2), 362-370.

Huang, Q. R., Yu, H. L., & Ru, Q. M. (2010). Bioavailability and delivery of nutraceuticals using nanotechnology. Journal of Food Science, 75(1), R50-R57.

Hubatsch, I., Ragnarsson, E. G. E., & Artursson, P. (2007). Determination of drug permeability and prediction of drug absorption in Caco-2 monolayers. Nature Protocols, 2(9), 2111-2119.

Hurtado-López, P., & Murdan, S. (2006). Zein microspheres as drug/antigen carriers: A study of their degradation and erosion, in the presence and absence of enzymes. Journal of microencapsulation, 23(3), 303-314.

Il'ina, A., & Varlamov, V. (2005). Chitosan-based polyelectrolyte complexes: a review. Applied Biochemistry and Microbiology, 41(1), 5-11.

Jain, S., Jain, A., Gupta, Y., & Ahirwar, M. (2007). Design and development of hydrogel beads for targeted drug delivery to the colon. AAPS PharmSciTech, 8(3), E34-E41.

Janes, M., Kooshesh, S., & Johnson, M. (2006). Control of Listeria monocytogenes on the surface of refrigerated, ready-to-aat chicken coated with edible zein film coatings containing nisin and/or calcium propionate. Journal of food science, 67(7), 2754-2757.

Jang, K. I., & Lee, H. G. (2008). Stability of chitosan nanoparticles for l-ascorbic acid during heat treatment in aqueous solution. Journal of Agricultural and Food Chemistry, 56(6), 1936-1941.

Jiang, Q., & Yang, Y. (2011). Water-stable electrospun zein fibers for potential drug delivery. Journal of Biomaterials Science, Polymer Edition, 22(10), 1393-1408.

Jiang, T., Feng, L., & Zheng, X. (2011). Effect of chitosan coating enriched with thyme oil on postharvest quality and shelf life of shiitake mushroom (Lentinus edodes). Journal of agricultural and food chemistry, 60(1), 188-196.

Jin, M., Davidson, P. M., Zivanovic, S., & Zhong, Q. (2009). Production of corn zein microparticles with loaded lysozyme directly extracted from hen egg white using spray drying: extraction studies. Food Chemistry, 115(2), 509-514.

Kean, T., & Thanou, M. (2010). Biodegradation, biodistribution and toxicity of chitosan. Advanced Drug Delivery Reviews, 62(1), 3-11.

Khlifi, S., EI Hachimi, Y., Khalil, A., Es-Safi, N., & EI Abbouyi, A. (2005). In vitro antioxidant effect of Globularia alypum L. hydromethanolic extract. Indian Journal of Pharmacology, 37(4), 227-237.

Kim, D. G., Jeong, Y. I., Choi, C., Roh, S. H., Kang, S. K., Jang, M. K., & Nah, J. W. (2006). Retinol-encapsulated low molecular water-soluble chitosan nanoparticles. International journal of pharmaceutics, 319(1), 130-138.

Kim, Y. J., Chae, S. Y., Jin, C. H., Sivasubramanian, M., Son, S., Choi, K. Y., Jo, D. G., Kim, K., Kwon, I. C., Lee, K. C., & Park, J. H. (2010). Ionic complex systems based on hyaluronic acid and PEGylated TNF-related apoptosis-inducing ligand for treatment of rheumatoid arthritis. Biomaterials, 31(34), 9057-9064.

Kim, Y. S., & Milner, J. A. (2005). Targets for indole-3-carbinol in cancer prevention. Journal of Nutritional Biochemistry, 16(2), 65-73.

Kithva, P., Grondahl, L., Martin, D., & Trau, M. (2010). Biomimetic synthesis and tensile properties of nanostructured high volume fraction hydroxyapatite and chitosan biocomposite films. Journal of Materials Chemistry, 20(2), 381-389.

Kittur, F. S., Prashanth, K. V. H., Sankar, K. U., & Tharanathan, R. N. (2002). Characterization of chitin, chitosan and their carboxymethyl derivatives by differential scanning calorimetry. Carbohydrate Polymers, 49(2), 185-193.

Klaypradit, W., & Huang, Y. W. (2008). Fish oil encapsulation with chitosan using ultrasonic atomizer. Lwt-Food Science and Technology, 41(6), 1133-1139.

Ko, J. A., Park, H. J., Hwang, S. J., Park, J. B., & Lee, J.S. (2002). Preparation and characterization of chitosan microparticles intended for controlled drug delivery. International Journal of Pharmacology, 249, 165-174.

Kockisch, S., Rees, G. D., Young, S. A., Tsibouklis, J., & Smart, J. D. (2003). Polymeric microspheres for drug delivery to the oral cavity: an in vitro evaluation of mucoadhesive potential. Journal of pharmaceutical sciences, 92(8), 1614-1623.

Korean Drug and Food Administration (KFDA).(1995). Food additives code. Seoul, Korea: KFDA.

Krajewska, B. (2004). Application of chitin-and chitosan-based materials for enzyme immobilizations: a review. Enzyme and microbial technology, 35(2), 126-139.

Lai, L. F., & Guo, H. X. (2011). Preparation of new 5-fluorouracil-loaded zein nanoparticles for liver targeting. International Journal of Pharmaceutics, 404(1-2), 317-323.

Lau, E. T. L., Johnson, S. K., Mikkelsen, D., Halley, P. J., & Steadman, K. J. (2012). Preparation and in vitro release of zein microparticles loaded with prednisolone for oral delivery. Journal of microencapsulation(0), 1-7.

Lawrie, G., Keen, I., Drew, B., Chandler-Temple, A., Rintoul, L., & Fredericks, P. (2007). Grøndahl, L. Interactions between alginate and chitosan biopolymers characterized using FTIR and XPS. Biomacromolecules, 8, 2533-2541.

Li, Q. A., Liu, C. G., Huang, Z. H., & Xue, F. F. (2011). Preparation and characterization of nanoparticles based on hydrophobic alginate derivative as carriers for sustained release of vitamin D-3. Journal of Agricultural and Food Chemistry, 59(5), 1962-1967.

Li, Y. Y., Zhang, S. S., Meng, X. J., Chen, X. G., & Ren, G. D. (2011). The preparation and characterization of a novel amphiphilic oleoyl-carboxymethyl chitosan self-assembled nanoparticles. Carbohydrate Polymers, 83(1), 130-136.

Li, Y., Lim, L. T., & Kakuda, Y. (2009). Electrospun Zein Fibers as Carriers to Stabilize (-)-Epigallocatechin Gallate. Journal of food science, 74(3), C233-C240.

Liang, J., Li, F., Fang, Y., Yang, W., An, X., Zhao, L., Xin, Z., Cao, L., & Hu, Q. (2011). Synthesis, characterization and cytotoxicity studies of chitosan-coated tea polyphenols nanoparticles. Colloids and Surfaces B: Biointerfaces, 82(2), 297-301.

Liang, L., Line, V. L. S., Remondetto, G. E., & Subirade, M. (2010). In vitro release of alpha-tocopherol from emulsion-loaded beta-lactoglobulin gels. International Dairy Journal, 20(3), 176-181.

Lin, Y. H., Liang, H. F., Chung, C. K., Chen, M. C., & Sung, H. W. (2005). Physically crosslinked alginate/N,O-carboxymethyl chitosan hydrogels with calcium for oral delivery of protein drugs. Biomaterials, 26(14), 2105-2113.

Liu, A., Song, W., Cao, D., Liu, X., & Jia, Y. (2008). Growth inhibition and apoptosis of human leukemia K562 cells induced by seleno-short-chain chitosan. Methods and Findings Experimental and Clinical Pharmacology, 30(3), 181-186.

Liu, N., & Park, H. J. (2009). Chitosan-coated nanoliposome as vitamin E carrier. Journal of Microencapsulation, 26(3), 235-242.

Liu, X. M., Sun, Q. S., Wang, H. J., Zhang, L., & Wang, J. Y. (2005). Microspheres of corn protein, zein, for an ivermectin drug delivery system. Biomaterials, 26(1), 109-115.

Liu, X., Sun, Q., Wang, H., Zhang, L., & Wang, J. Y. (2005). Microspheres of corn protein, zein, for an ivermectin drug delivery system. Biomaterials, 26(1), 109-115.

Liu, Y. Z., Wu, Z. X., Chen, X., Shao, Z. Z., Wang, H. T., & Zhao, D. Y. (2012). A hierarchical adsorption material by incorporating mesoporous carbon into macroporous chitosan membranes. Journal of Materials Chemistry, 22(24), 11908-11911.

Liu, Y., Wang, P. F., Sun, C., Feng, N. P., Zhou, W. X., Yang, Y., Tan, R., Chen, Z. Q., Wu, S., & Zhao, J. H. (2010). Wheat germ agglutinin-grafted lipid nanoparticles: Preparation and in vitro evaluation of the association with Caco-2 monolayers. International Journal of Pharmaceutics, 397(1-2), 155-163.

Liu, Z. H., Jiao, Y. P., & Zhang, Z. Y. (2007). Calcium-carboxymethyl chitosan hydrogel beads for protein drug delivery system. Journal of Applied Polymer Science, 103(5), 3164-3168.

Liu, Z., Jiao, Y., Wang, Y., Zhou, C., & Zhang, Z. (2008). Polysaccharides-based nanoparticles as drug delivery systems. Advanced Drug Delivery Reviews, 60(15), 1650-1662.

Loh, J. W., Saunders, M., & Lim, L.-Y. (2012). Cytotoxicity of monodispersed chitosan nanoparticles against the Caco-2 cells. Toxicology and Applied Pharmacology, 262(3), 273-282.

Loh, J. W., Yeoh, G., Saunders, M., & Lim, L.-Y. (2010). Uptake and cytotoxicity of chitosan nanoparticles in human liver cells. Toxicology and Applied Pharmacology, 249(2), 148-157.

Looker, A. C., Pfeiffer, C. M., Lacher, D. A., Schleicher, R. L., Picciano, M. F., & Yetley, E. A. (2008). Serum 25-hydroxyvitamin D status of the US population: 1988-1994 compared with 2000-2004. Am J Clin Nutr, 88(6), 1519-1527.

Luo, Y. C., Teng, Z., & Wang, Q. (2012). Development of zein nanoparticles coated with carboxymethyl chitosan for encapsulation and controlled release of vitamin D3. Journal of Agricultural and Food Chemistry, 60(3), 836-843.

Luo, Y. C., Zhang, B. C., Cheng, W.-H., & Wang, Q. (2010). Preparation, characterization and evaluation of selenite-loaded chitosan/TPP nanoparticles with or without zein coating. Carbohydrate Polymers, 82(3), 942-951.

Luo, Y. C., Zhang, B. C., Whent, M., Yu, L., & Wang, Q. (2011). Preparation and characterization of zein/chitosan complex for encapsulation of alpha-tocopherol, and its in vitro controlled release study. Colloids and Surfaces B-Biointerfaces, 85(2), 145-152.

Maciejewska, D., Wolska, I., Niemyjska, M., & Żero, P. (2005). Structure in solid state of 3,3′-diindolylmethane derivatives, potent cytotoxic agents against human tumor cells, followed X-ray diffraction and 13C CP/MAS NMR analyses. Journal of Molecular Structure, 753(1–3), 53-60.

Mastromatteo, M., Barbuzzi, G., Conte, A., & Del Nobile, M. (2009). Controlled release of thymol from zein based film. Innovative Food Science & Emerging Technologies, 10(2), 222-227.

Meng, X., Li, P., Wei, Q., & Zhang, H. X. (2011). pH sensitive alginate-chitosan hydrogel beads for carvedilol delivery. Pharmaceutical development and technology, 16(1), 22-28.

Miquel, E., Alegría, A., Barberá, R., Farré, R., & Clemente, G. (2004). Stability of tocopherols in adapted milk-based infant formulas during storage. International dairy journal, 14(11), 1003-1011.

Miyoshi, T., Toyohara, K., & Minematsu, H. (2005). Preparation of ultrafine fibrous zein membranes via electrospinning. Polymer international, 54(8), 1187-1190.

Moak, M. A., & Christensen, M. J. (2001). Promotion of lipid oxidation by selenate and selenite and indicators of lipid peroxidation in the rat. Biological Trace Element Research, 79, 257-269.

Moraru, C. I., Panchapakesan, C. P., Huang, Q., Takhistov, P., Liu, S., & Kokini, J. L. (2003). Nanotechnology: a new frontier in food science. Food Technology, 57(12), 24-29.

Mouryaa, V. K., Inamdara, N. N., & Tiwari, A. (2010). Carboxymethyl chitosan and its applications. Advanced Materals Letters, 1(1), 11-33.

Mun, S., Decker, E. A., & McClements, D. J. (2006). Effect of molecular weight and degree of deacetylation of chitosan on the formation of oil-in-water emulsions stabilized by

surfactant–chitosan membranes. Journal of colloid and interface science, 296(2), 581-590.

Muthu, M. S., Kulkarni, S. A., Xiong, J., & Feng, S.-S. (2011). Vitamin E TPGS coated liposomes enhanced cellular uptake and cytotoxicity of docetaxel in brain cancer cells. International Journal of Pharmaceutics, 421(2), 332-340.

Muthuselvi, L., & Dhathathreyan, A. (2006). Simple coacervates of zein to encapsulate Gitoxin. Colloids and Surfaces B: Biointerfaces, 51(1), 39-43.

Naghibzadeh, M., Amani, A., Amini, M., Esmaeilzadeh, E., Mottaghi-Dastjerdi, N., & Faramarzi, M. A. (2010). An Insight into the Interactions between alpha-Tocopherol and Chitosan in Ultrasound-Prepared Nanoparticles. Journal of Nanomaterials, -.

Navarro-Alarcon, M., & Cabrera-Vique, C. (2008). Selenium in food and the human body: A review. Science of the Total Environment. 400, 115-141.

Navas-Acien, A., Bleys, J., & Guallar, E. (2008). Seleniumintake and cardiovascular risk: what is new? Current Opinion Lipidology, 19, 43-49.

Nelson, E. D., Ballard, J. M., Zhu, L. M., & Seburg, R. A. (2007). Degradation of vitamin D-3 in a stressed formulation: The identification of esters of vitamin D-3 formed by a transesterification with triglycerides. Journal of Pharmaceutical and Biomedical Analysis, 43(1), 142-150.

Neo, Y. P., Ray, S., Easteal, A. J., Nikolaidis, M. G., & Quek, S. Y. (2012). Influence of solution and processing parameters towards the fabrication of electrospun zein fibers with sub-micron diameter. Journal of Food Engineering, 109(4), 645-651.

Neo, Y. P., Ray, S., Jin, J., Gizdavic-Nikolaidis, M., Nieuwoudt, M. K., Liu, D., & Quek, S. Y. (2012). Encapsulation of food grade antioxidant in natural biopolymer by electrospinning technique: a physicochemical study based on zein-gallic acid system. Food Chemistry.

No, H., Meyers, S., Prinyawiwatkul, W., & Xu, Z. (2007). Applications of chitosan for improvement of quality and shelf life of foods: a review. Journal of food science, 72(5), R87-R100.

Oidtmann, J., Schantz, M., Mäder, K., Baum, M., Berg, S., Betz, M., Kulozik, U., Leick, S., Rehage, H., Schwarz, K., & Richling, E. (2011). Preparation and comparative release characteristics of three anthocyanin encapsulation systems. Journal of Agricultural and Food Chemistry, 60(3), 844-851.

Parris, N., Cooke, P. H., & Hicks, K. B. (2005). Encapsulation of essential oils in zein nanospherical particles. Journal of agricultural and food chemistry, 53(12), 4788-4792.

Parveen, S., Mitra, M., Krishnakumar, S., & Sahoo, S. K. (2010). Enhanced antiproliferative activity of carboplatin-loaded chitosan-alginate nanoparticles in a retinoblastoma cell line. Acta Biomaterialia, 6(8), 3120-3131.

Patel, A. R., Bouwens, E. C. M., & Velikov, K. P. (2010). Sodium caseinate stabilized zein colloidal particles. Journal of Agricultural and Food Chemistry, 58(23), 12497-12503.

Patel, A., Hu, Y. C., Tiwari, J. K., & Velikov, K. P. (2010). Synthesis and characterisation of zein-curcumin colloidal particles. Soft Matter, 6(24), 6192-6199.

Paula, H. C. B., Sombra, F. M., Cavalcante, R. d. F., Abreu, F. O. M. S., & de Paula, R. C. M. (2011). Preparation and characterization of chitosan/cashew gum beads loaded with Lippia sidoides essential oil. Materials Science and Engineering: C, 31(2), 173-178.

Picciano, M. F. (2010). Vitamin D status and health. Critical Reviews in Food Science and Nutrition, 50, 24-25.

Picker-Freyer, K. M., & Brink, D. (2006). Evaluation of powder and tableting properties of chitosan. AAPS PharmSciTech, 7, E1-E10.

Pisal, D. S., Yellepeddi, V. K., Kumar, A., Kaushik, R. S., Hildreth, M. B., Guan, X., & Palakurthi, S. (2008). Permeability of surface-modified polyamidoamine (PAMAM)

dendrimers across Caco-2 cell monolayers. International Journal of Pharmaceutics, 350(1–2), 113-121.

Pittas, A. G., Chung, M., Trikalinos, T., Mitri, J., Brendel, M., Patel, K., Lichtenstein, A. H., Lau, J., & Balk, E. M. (2010). Systematic review: vitamin D and cardiometabolic outcomes. Annals of Internal Medicine, 152(5), 307-W101.

Podaralla, S., & Perumal, O. (2010). Preparation of zein nanoparticles by pH controlled nanoprecipitation. Journal of biomedical nanotechnology, 6(4), 312-317.

Qian, X., Melkamu, T., Upadhyaya, P., & Kassie, F. (2011). Indole-3-carbinol inhibited tobacco smoke carcinogen-induced lung adenocarcinoma in A/J mice when administered during the post-initiation or progression phase of lung tumorigenesis. Cancer Letters, 311(1), 57-65.

Qin, C. Q., Xiao, L., Du, Y. M., & Gao, X. H. (2002). Antitumor activity of chitosan hydrogen selenites. Chinese Chemical Letter, 13(3), 213-214.

Quispe-Condori, S., Saldaña, M. D. A., & Temelli, F. (2011). Microencapsulation of flax oil with zein using spray and freeze drying. LWT-Food Science and Technology, 44(9), 1880-1887.

Rabea, E. I., Badawy, M. E. T., Stevens, C. V., Smagghe, G., & Steurbaut, W. (2003). Chitosan as antimicrobial agent: applications and mode of action. Biomacromolecules, 4(6), 1457-1465.

Rakotonirainy, A., Wang, Q., & Padua, G. (2001). Evaluation of zein films as modified atmosphere packaging for fresh broccoli. Journal of food science, 66(8), 1108-1111.

Rao, M., Chawla, S., Chander, R., & Sharma, A. (2011). Antioxidant potential of Maillard reaction products formed by irradiation of chitosan–glucose solution. Carbohydrate Polymers, 83(2), 714-719.

Ray, A. L, Semba, R. D., Walston, J., Ferrucci, L., Cappola, A. R., Ricks, M. O., Xue, Q. L., & Fried, L. P. (2006). Low serum selenium and total carotenoids predict mortality among older women living in the community: the women's health and aging studies. Journal of Nutrition, 136, 172-176.

Sabliov, C. M., Fronczek, C., Astete, C. E., Khachaturyan, M., Khachatryan, L., & Leonardi, C. (2009). Effects of temperature and UV light on degradation of alpha-tocopherol in free and dissolved form. Journal of the American Oil Chemists Society, 86(9), 895-902.

Saether, H. V., Holme, H. K., Maurstald, G., Smidsrod, O., & Stokke, B. T. (2008). Polyelectrolyte complex formation using alginate and chitosan. Carbohydrate Polymers, 74(4), 813-821.

Sahoo, D., Sahoo, S., Mohanty, P., Sasmal, S., & Nayak, P. L. (2009). Chitosan: a new versatile bio-polymer for various applications. Designed Monomers and Polymers, 12(5), 377-404.

Semo, E., Kesselman, E., Danino, D., & Livney, Y. D. (2007). Casein micelle as a natural nano-capsular vehicle for nutraceuticals. Food Hydrocolloids, 21(5-6), 936-942.

Shah, S., Pal, A., Kaushik, V., & Devi, S. (2009). Preparation and characterization of venlafaxine hydrochloride-loaded chitosan nanoparticles and in vitro release of drug. Journal of Applied Polymer Science, 112(5), 2876-2887.

Shea, T. B., Ortiz, D., Nicolosi, R. J., Kumar, R., & Watterson, A. C. (2005). Nanosphere-mediated delivery of vitamin E increases its efficacy against oxidative stress resulting from exposure to amyloid beta. Journal of Alzheimers Disease, 7(4), 297-301.

Shertzer, H. G., & Senft, A. P. (2000). The micronutrient indole-3-carbinol: implications for disease and chemoprevention. Drug Metabol Drug Interact, 17(1-4), 159-188.

Shi, K., Kokini, J. L., & Huang, Q. (2009). Engineering zein films with controlled surface morphology and hydrophilicity. Journal of Agricultural and Food Chemistry, 57(6), 2186-2192.

Shi, X. W., Du, Y. M., Yang, J. H., Zhang, B. Z., & Sun, L. P. (2006). Effect of degree of substitution and molecular weight of carboxymethyl chitosan nanoparticles on doxorubicin delivery. Journal of Applied Polymer Science, 100(6), 4689-4696.

Shi, X. Y., & Tan, T. W. (2002). Preparation of chitosan/ethylcellulose complex microcapsule and its application in controlled release of vitamin D-2. Biomaterials, 23(23), 4469-4473.

Shi, X., Du, Y., Yang, J., Zhang, B., & Sun, L. (2006). Effect of degree of substitution and molecular weight of carboxymethyl chitosan nanoparticles on doxorubicin delivery. Journal of Applied Polymer Science, 100(6), 4689-4696.

Shi, X.-Y., & Tan, T.-W. (2002). Preparation of chitosan/ethylcellulose complex microcapsule and its application in controlled release of Vitamin D2. Biomaterials, 23(23), 4469-4473.

Shimizu, R., Ueno, H., Okuno, T., Sakazaki, F., & Nakamuro, K. (2009). Effect of sodium selenite supplementation on glucose intolerance and pancreatic oxidative stress in type 2 diabetic mice under different selenium status. Journal of Health Science, 55, 271-280.

Shimoda, J., Onishi, H., & Machida, Y. (2001). Bioadhesive characteristics of chitosan microspheres to the mucosa of rat small intestine. Drug Development and Industrial Pharmacy, 27(6), 567-576.

Shorey, L. E., Hagman, A. M., Williams, D. E., Ho, E., Dashwood, R. H., & Benninghoff, A. D. (2012). 3,3'-Diindolylmethane induces G1 arrest and apoptosis in human acute T-cell lymphoblastic leukemia cells. PLoS One, 7(4), e34975.

Shukla, R., & Cheryan, M. (2001). Zein: the industrial protein from corn. Industrial Crops and Products, 13(3), 171-192.

Simon, E., Paul, J. L., Atger, V., Simon, A., & Moatti, N. (1998). Erythrocyte antioxidant status in asymptomatic hypercholesterolemic men. Atherosclerosis, 138(2), 375-381.

Simpson, B., Gagne, N., Ashie, I., & Noroozi, E. (1997). Utilization of chitosan for preservation of raw shrimp (Pandalus borealis). Food Biotechnology, 11(1), 25-44.

Sinha, V. R., Singla, A. K., Wadlhawan, S., Kaushik, R., & Kumria, R. (2004). Chitosan microspheres as a potential carrier for drugs. International Journal of Pharmaceutics, 274, 1-33.

Siripatrawan, U., & Noipha, S. (2012). Active film from chitosan incorporating green tea extract for shelf life extension of pork sausages. Food Hydrocolloids, 27(1), 102-108.

Snima, K. S., Jayakumar, R., Unnikrishnan, A. G., Nair, S. V., & Lakshmanan, V. K. (2012). O-Carboxymethyl chitosan nanoparticles for metformin delivery to pancreatic cancer cells. Carbohydrate Polymers, 89(3), 1003-1007.

Somchue, W., Sermsri, W., Shiowatana, J., & Siripinyanond, A. (2009). Encapsulation of alpha-tocopherol in protein-based delivery particles. Food Research International, 42(8), 909-914.

Song, T. Y., Yao, C., & Li, X. S. (2010). Electrospinning of zein/chitosan composite fibrous membranes. Chinese Journal of Polymer Science, 28(2), 171-179.

Song, Y.-B., Lee, J.-S., & Lee, H. G. (2009). [alpha]-Tocopherol-loaded Ca-pectinate microcapsules: Optimization, in vitro release, and bioavailability. Colloids and Surfaces B: Biointerfaces, 73(2), 394-398.

Sriamornsak, P. (1999). Effect of calcium concentration, hardening agent and drying condition on release characteristics of oral proteins from calcium pectinate gel beads. European Journal of Pharmaceutical Sciences, 8(3), 221-227.

Subirade, M., Liang, L., Line, V. L. S., & Remondetto, G. E. (2010). In vitro release of alpha-tocopherol from emulsion-loaded beta-lactoglobulin gels. International Dairy Journal, 20(3), 176-181.

Sun, P., Li, P., Li, Y. M., Wei, Q., & Tian, L. H. (2011). A pH-sensitive chitosan-tripolyphosphate hydrogel beads for controlled glipizide delivery. Journal of Biomedical Materials Research Part B: Applied Biomaterials, 97(1), 175-183.

Sun, Q. S., Dong, J., Lin, Z. X., Yang, B., & Wang, J. Y. (2005). Comparison of cytocompatibility of zein film with other biomaterials and its degradability in vitro. Biopolymers, 78(5), 268-274.

Sun, T., Zhou, D., Mao, F., & Zhu, Y. (2007). Preparation of low-molecular-weight carboxymethyl chitosan and their superoxide anion scavenging activity. European Polymer Journal, 43(2), 652-656.

Teng, Z., Luo, Y., & Wang, Q. (2012). Nanoparticles Synthesized from Soy Protein: Preparation, Characterization, and Application for Nutraceutical Encapsulation. Journal of Agricultural and Food Chemistry, 60(10), 2712-2720.

Thein-Han, W., Kitiyanant, Y., & Misra, R. (2008). Chitosan as scaffold matrix for tissue engineering. Materials Science and Technology, 24(9), 1062-1075.

Thomson, C. D. (2004). Assessment of requirements for selenium and adequacy of selenium status: a review. European Journal of Clinical Nutrition, 58, 391-402.

Tian, F., Li, B., Ji, B. P., Yang, J. H., Zhang, G. Z., Chen, Y., & Luo, Y. C. (2009). Antioxidant and antimicrobial activities of consecutive extracts from Galla chinensis: The polarity affects the bioactivities. Food Chemistry, 113, 173-179.

Torelli-Souza, R. R., Cavalcante Bastos, L. A., Nunes, H. G. L., Camara, C. A., & Amorim, R. V. S. (2012). Sustained release of an antitumoral drug from alginate-chitosan hydrogel

beads and its potential use as colonic drug delivery. Journal of Applied Polymer Science, 126(S1), E409-E418.

Torres-Giner, S., Gimenez, E., & Lagaron, J. (2008). Characterization of the morphology and thermal properties of zein prolamine nanostructures obtained by electrospinning. Food Hydrocolloids, 22(4), 601-614.

Torres-Giner, S., Ocio, M. J., & Lagaron, J. M. (2009). Novel antimicrobial ultrathin structures of zein/chitosan blends obtained by electrospinning. Carbohydrate Polymers, 77(2), 261-266.

Trapani, A., Sitterberg, J., Bakowsky, U., & Kissel, T. (2009). The potential of glycol chitosan nanoparticles as carrier for low water soluble drugs. International Journal of Pharmaceutics, 375(1–2), 97-106.

Tucker, J. M., & Townsend, D. M. (2005). Alpha-tocopherol: roles in prevention and therapy of human disease. Biomedicine & Pharmacotherapy, 59(7), 380-387.

Uygun, A., Kiristi, M., Oksuz, L., Manolache, S., & Ulusoy, S. (2011). RF hydrazine plasma modification of chitosan for antibacterial activity and nanofiber applications. Carbohydrate Research, 346(2), 259-265.

Vaghani, S. S., Patel, M. M., & Satish, C. S. (2012). Synthesis and characterization of pH-sensitive hydrogel composed of carboxymethyl chitosan for colon targeted delivery of ornidazole. Carbohydrate Research, 347(1), 76-82.

Valencia-Chamorro, S. A., Palou, L., del Río, M. A., & Pérez-Gago, M. B. (2011). Antimicrobial Edible Films and Coatings for Fresh and Minimally Processed Fruits and Vegetables: A Review. Critical Reviews in Food Science and Nutrition, 51(9), 872-900.

Vallejo, F., Tomas-Barberan, F. A., & Garcia-Viguera, C. (2002). Glucosinolates and vitamin C content in edible parts of broccoli florets after domestic cooking. European Food Research and Technology, 215(4), 310-316.

Veiga, N., Rivero-Huguet, M., & Huertas, R. (2008). An improved spectrofluorometric determination of selenium in biological materials after microwave digestion. Atomic Spectroscopy. 29(2), 63-68.

Villarroel, P., Flores, S., Pizarro, F., de Romana, D. L., & Arredondo, M. (2011). Effect of dietary protein on heme iron uptake by Caco-2 cells. European Journal of Nutrition, 50(8), 637-643.

Wang, G., & Uludag, H. (2008). Recent developments in nanoparticle-based drug delivery and targeting systems with emphasis on protein-based nanoparticles. Expert Opinion on Drug Delivery, 5(5), 499-515.

Wang, J. Y., Liu, X. M., Sun, Q. S., Wang, H. J., & Zhang, L. (2005). Microspheres of corn protein, zein, for an ivermectin drug delivery system. Biomaterials, 26(1), 109-115.

Wang, Q., Yin, L., & Padua, G. W. (2008). Effect of hydrophilic and lipophilic compounds on zein microstructures. Food Biophysics, 3, 174-181.

Wang, R. X., Tian, Z. G., & Chen, L. Y. (2011). Nano-encapsulations liberated from barley protein microparticles for oral delivery of bioactive compounds. International Journal of Pharmaceutics, 406(1-2), 153-162.

Wang, S. L., Yao, H. H., Guo, L. L., Dong, L., Li, S. G., Gu, Y. P., & Qin, Z. H. (2009). Selection of optimal sites for TGFB1 gene silencing by chitosan–TPP nanoparticle-mediated delivery of shRNA. Cancer genetics and cytogenetics, 190(1), 8-14.

Wang, T. T. Y., Schoene, N. W., Milner, J. A., & Kim, Y. S. (2012). Broccoli-derived phytochemicals indole-3-carbinol and 3,3'-diindolylmethane exerts concentration-dependent pleiotropic effects on prostate cancer cells: Comparison with other cancer preventive phytochemicals. Molecular Carcinogenesis, 51(3), 244-256.

Wang, Y., Jiang, Q., Li, R., Liu, L., Zhang, Q., & Zhao, J. (2008). Self-assembled nanoparticles of cholesterol-modified O-carboxymethyl chitosan as a novel carrier for paclitaxel. Nanotechnology, 19(14), 145101.

Weiner, M. L. (1992). An overview of the regulatory status and of the safety of chitin and chitosan as food and pharmaceutical ingredients. In C. J. Brine, P. A. Sandfor & J. P. Zikakis (Eds.), Advances in Chitin and Chitosan, (pp. 663). London: Elsevier Applied Science.

Wu, Y., Luo, Y., & Wang, Q. (2012). Antioxidant and antimicrobial properties of essential oils encapsulated in zein nanoparticles prepared by liquid-liquid dispersion method. LWT-Food Science and Technology.

Wu, Y., Yang, W. L., Wang, C. C., Hu, J. H., & Fu, S. K. (2005). Chitosan nanoparticles as a novel delivery system for ammonium glycyrrhizinate. International Journal of Pharmacology, 295, 235-245.

Xia, W., Liu, P., Zhang, J., & Chen, J. (2011). Biological activities of chitosan and chitooligosaccharides. Food Hydrocolloids, 25(2), 170-179.

Xiang, N., Zhao, R., & Zhong, W. X. (2009). Sodium selenite induces apoptosis by generation of superoxide via the mitochondrial-dependent pathway in human prostate cancer cells. Cancer Chemotherapy and Pharmacology, 63, 351-362.

Xiao, D., & Zhong, Q. (2011). In vitro release kinetics of nisin as affected by Tween 20 and glycerol co-encapsulated in spray-dried zein capsules. Journal of Food Engineering, 106(1), 65-73.

Xiao, D., Davidson, P. M., & Zhong, Q. (2011). Spray-dried zein capsules with coencapsulated nisin and thymol as antimicrobial delivery system for enhanced antilisterial properties. Journal of agricultural and food chemistry, 59(13), 7393-7404.

Xiao, D., Gommel, C., Davidson, P. M., & Zhong, Q. X. (2011). Intrinsic Tween 20 Improves Release and Antilisterial Properties of Co-encapsulated Nisin and Thymol. Journal of Agricultural and Food Chemistry, 59(17), 9572-9580.

Xiao, Z., Luo, Y., & Wang, Q. (2011). Combined effects of sodium chlorite dip treatment and chitosan coatings on the quality of fresh-cut d'Anjou pears. Postharvest Biology and Technology.

Yang, J. M., Zha, L., Yu, D. G., & Liu, J. (2012). Coaxial electrospinning with acetic acid for preparing ferulic acid/zein composite fibers with improved drug release profiles. Colloids and Surfaces B: Biointerfaces.

Yang, J., Chen, J., Pan, D., Wan, Y., & Wang, Z. (2012). pH-sensitive interpenetrating network hydrogels based on chitosan derivatives and alginate for oral drug delivery. Carbohydrate Polymers.

Yang, R., Yang, S. G., Shim, W. S., Cui, F., Cheng, G., Kim, I. W., Kim, D. D., Chung, S. J., & Shim, C. K. (2009). Lung-specific delivery of paclitaxel by chitosan-modified PLGA nanoparticles via transient formation of microaggregates. Journal of Pharmaceutical Science, 98(3), 970-984

Yao, C., Li, X., & Song, T. (2006). Electrospinning and crosslinking of zein nanofiber mats. Journal of Applied Polymer Science, 103(1), 380-385.

Yen, M. T., Yang, J. H., & Mau, J. L. (2007). Antioxidant properties of fungal chitosan from shiitake stipes. LWT-Food Science and Technology, 40, 225-261.

Yen, M. T., Yang, J. H., Mau, J. L. (2008). Antioxidant properties of chitosan from crab shells. Carbohydrate Polymer, 74, 840-844.

Yinwin, K., & Feng, S.-S. (2005). Effects of particle size and surface coating on cellular uptake of polymeric nanoparticles for oral delivery of anticancer drugs. Biomaterials, 26(15), 2713-2722.

Yoksan, R., Jirawutthiwongchai, J., & Arpo, K. (2010). Encapsulation of ascorbyl palmitate in chitosan nanoparticles by oil-in-water emulsion and ionic gelation processes. Colloids and Surfaces B: Biointerfaces, 76(1), 292-297.

Yoo, S. H., Song, Y. B., Chang, P. S., & Lee, H. G. (2006). Microencapsulation of alpha-tocopherol using sodium alginate and its controlled release properties. International Journal of Biological Macromolecules, 38(1), 25-30.

Zachara, B. A., Gromadzinska, J., Wasowizc, W., & Zbrog, Z. (2006). Red blood cell and plasma peroxidase activities and selenium concentration in patients with chronic kidney disease: A review. Acta Biochimca Polonica, 53(4), 663-677.

Zhang, B. C., Luo, Y. C., & Wang, Q. (2011). Effect of acid and base treatments on structural, rheological, and antioxidant properties of alpha-zein. Food Chemistry, 124(1), 210-220.

Zhang, J., Zhang, W., Mamadouba, B., & Xia, W. (2012). A comparative study on hypolipidemic activities of high and low molecular weight chitosan in rats. International Journal of Biological Macromolecules.

Zhang, S., Luo, Y. C., Zeng, H., Wang, Q., Tian, F., Song, J., & Zeng, W. H. (2011b). Encapsulation of selenium in chitosan nanoparticles improves selenium availability and protects cells from selenium-induced DNA damage response. Journal of Nutritional Biochemistry, Accepted on Sept 23, 2010.

Zhang, Y. Y., Yang, Y., Tang, K., Hu, X., & Zou, G. L. (2008). Physicochemical characterization and antioxidant activity of quercetin-loaded chitosan nanoparticles. Journal of Applied Polymer Science, 107(2), 891-897.

Zhang, Z., & Feng, S.-S. (2006). The drug encapsulation efficiency, in vitro drug release, cellular uptake and cytotoxicity of paclitaxel-loaded poly(lactide)–tocopheryl polyethylene glycol succinate nanoparticles. Biomaterials, 27(21), 4025-4033.

Zhang, Z., Tan, S., & Feng, S.-S. (2012). Vitamin E TPGS as a molecular biomaterial for drug delivery. Biomaterials, 33(19), 4889-4906.

Zheng, L. Y., & Zhu, J. F. (2003). Study on antimicrobial activity of chitosan with different molecular weights. Carbohydrate Polymers, 54(4), 527-530.

Zhong, Q. X., & Jin, M. F. (2009a). Zein nanoparticles produced by liquid-liquid dispersion. Food Hydrocolloids, 23(8), 2380-2387.

Zhong, Q. X., Tian, H. L., & Zivanovic, S. (2009). Encapsulation of fish oil in solid zein particles by liquid-liquid dispersion. Journal of Food Processing and Preservation, 33(2), 255-270.

Zhong, Q., & Jin, M. (2009a). Nanoscalar structures of spray-dried zein microcapsules and in vitro release kinetics of the encapsulated lysozyme as affected by formulations. Journal of agricultural and food chemistry, 57(9), 3886-3894.

Zhong, Q., & Jin, M. (2009b). Zein nanoparticles produced by liquid–liquid dispersion. Food Hydrocolloids, 23(8), 2380-2387.

Zhou, S. B., Deng, X. M., & Li, X. H. (2001). Investigation on a novel core-coated microspheres protein delivery system. Journal of Controlled Release, 75, 27-36.

Zou, T., Li, Z., Percival, S. S., Bonard, S., & Gu, L. (2011). Fabrication, characterization, and cytotoxicity evaluation of cranberry procyanidins-zein nanoparticles. Food Hydrocolloids.